**Title**
Scattering Versus Intrinsic Attenuation in the Near Surface: Measurements from Permanent Down-hole Geophones



**Author**
Mangriotis, Maria-Daphne

**Publication Date**
2009

Peer reviewed|Thesis/dissertation

# Scattering Versus Intrinsic Attenuation in the Near Surface: Measurements from Permanent Down-hole Geophones

By

Maria-Daphne Mangriotis

A dissertation submitted in partial satisfaction of the

requirements for the degree of

Doctor of Philosophy

in

Engineering - Civil and Environmental Engineering

in the

Graduate Division

of the

University of California, Berkeley

Committee in charge:

Professor James W. Rector III, Chair

Professor Steven D. Glaser

Professor John C. Neu

Fall 2009

The dissertation of Maria-Daphne Mangriotis titled Scattering Versus Intrinsic Attenuation in the Near Surface: Measurements from Permanent Down-hole Geophones, is approved:

Chair _____ Date _____

_____ Date _____

_____ Date _____

University of California, Berkeley

Scattering Versus Intrinsic Attenuation in the Near Surface:
Measurements from Permanent Down-hole Geophones


by
Maria-Daphne Mangriotis

Abstract

Scattering Versus Intrinsic Attenuation in the Near Surface:

Measurements from Permanent Down-hole Geophones

by

Maria-Daphne Mangriotis

Doctor of Philosophy in Civil and Environmental Engineering

University of California, Berkeley

Professor James Rector III, Chair

The study of attenuation, equivalently of the quality (Q) factor, in the near-surface has three main applications. Firstly, low Q values, which are fairly common in near-surface materials, aside from decreasing seismic energy, also distort the waveforms; treatment of this disturbance effect with inverse-Q filters requires reliable Q estimates. Secondly, attenuation is a seismic parameter which improves interpretation of seismograms, as it is correlated with lithological properties. Thirdly, establishing near-surface Q is important in assessing site effects on strong ground motion events in applications of earthquake modeling and seismic engineering design. In view of these applications, theoretical treatments of attenuation, as well as laboratory and field tests, aim at estimating Q as a function of frequency and strain level. To determine the applicability of using different types of Q measurements, laboratory vs. in-situ measurements, to predict Q behavior across the different frequency bands and strain-levels of interest, it is necessary to model and separate the attenuation mechanisms into scattering (heterogeneity of elastic properties causing energy to be redistributed in space) and intrinsic (energy absorption due to conversion to heat) components. The objective of the presented study was to separate scattering versus intrinsic attenuation in the near-surface from a shallow VSP experiment conducted in the Lawrence Livermore National Laboratory (LLNL) facility using permanent down-hole geophones and a vertical impact source. Given that the VSP array was above the watertable, the Q characterization lies within the vadose zone.

The first arrival of the vertically-incident transmitted P-wave was used to estimate the P-wave attenuation in the field data. Scattering attenuation estimates were established for a selected range of elastic models, which addressed both the effect of the variance of the elastic properties (density and velocity), as well as the effect of the structure of the variation, i.e. 1D versus 3D heterogeneity, on scattering. The elastic profiles were constructed from a superposition of interval values determined from log information (for the density profile) and first-break arrivals (for the velocity profile) and a high-frequency random component with variance range typical of sedimentary basins. The results for the scattering Q estimates related to one-way transmission and multiple

reflections are in the order of 20 to 100, as obtained from 1D analytical and elastic finite-difference models. Given the short propagation pathlengths in the experiment, the results show that attenuation due to lateral heterogeneity is non-significant. In addition, given the experimental geometry of shallow VSP studies, it is shown that the scattering estimates are affected from the presence of the near-field, local impedance, and interference effects, which are termed 'pseudo-Q' factors. The pseudo-Q factors result in a biased estimate for scattering Q derived from both time-domain and frequency-domain methods. Hence, to accurately model the scattering vs. intrinsic components of attenuation, the bias due to the pseudo-Q factors was accounted for.

The intrinsic attenuation was deduced from comparison of the field data Q estimates, which contain scattering attenuation, intrinsic attenuation and effects from pseudo-Q factors with the elastic synthetic Q estimates. Results yield very low intrinsic Q values, in the order of 4 to 15, for the low and high scattering attenuation estimates respectively. The intrinsic attenuation is attributed to the interaction of the free gas present in the vadose zone with the compressional wave, which is the only known mechanism that can lead to absorption at seismic frequencies (White, 1975; Dutta and Seriff, 1979). Visco-elastic modeling shows that aside from amplitude decay, an intrinsic attenuation mechanism is required to produce the pulse broadening observed in the field data. For a typical set of conditions in the vadose zone, analytical modeling shows that it is possible for the effect of the free gas to account for the intrinsic Q values estimated for the LLNL profile. It is anticipated that attenuation will be very high in vadose environments similar to the LLNL profile, with intrinsic attenuation being the primary loss mechanism. Further research is required to establish the Q filter characteristics due to the free gas effect in the vadose zone and verify if an approximation with standard visco-elastic models, such as the SLS, is appropriate.

Table of Contents

List of Figures

List of Tables

Acknowledgements

Firstly, I am deeply grateful to my academic advisor, Professor James Rector III, for his invaluable guidance and support throughout the course of my studies and research at the University of California, Berkeley. It has been a great privilege for me to work with him and learn from his deep knowledge and expertise in the field of applied geophysics. This work would not have been possible without him!

I am also most grateful to my thesis committee, Professor Glaser, Professor Neu, Professor Sitar and Professor Ruben, who helped me put this dissertation together and to the faculty and students of the geotechnical group in the Civil Engineering department at UC Berkeley to whom I owe a great deal of knowledge and support. I would like to thank Professor Neu of the Mathematical Department at UC Berkeley for spending a significant amount of time to help me understand the mathematics involved in my dissertation. Also I would like to thank Fred Herkenhoff of the Chevron Energy Technology Company for his guidance during the course of my two internships and throughout the course of my studies. Lastly, I would like to thank Professor Juan Fernandez-Martinez, Dr. Stefan Finsterle, and Professor Serge Shapiro, who through their fields' expertise added a new dimension to my work.

I would like to gratefully acknowledge the Jane Lewis Fellowship Committee for their scholarship provision in the academic years 2004-2005 and 2006-2007 and the Onassis Foundation Committee for their scholarship provision in the academic year 2008-2009. These three scholarships greatly facilitated the continuation of my studies. This research was partly supported through the Environmental Restoration Division of the Lawrence Livermore National Laboratory. From the Lawrence Livermore National Laboratory I would like to gratefully acknowledge the support and technical input provided by Robert Bainer and Lindee Berg and the field crew for their invaluable help in the completing experiment.

Last, but not least, I would like to thank my parents, Phaedon and Sissy, their companions Katerina and Nicholas, and my two sisters Dido and Phaidra for their presence in my life. Also I would like to thank my Berkeley and Brown family and friends from home for putting my pieces together. All these people have made me what I am. I hope to always be able to go back to Berkeley and share my memories with them

# Chapter 1

## Introduction

The study of attenuation has two main objectives. On the one hand, as attenuation results in seismic energy loss and distortion of the waveform, the objective is to remove its effect, in order to improve seismic imaging. On the other hand, given that attenuation depends on the soil and rock composition and structure of the subsurface, it can be used to infer lithological properties, including Q correlations with permeability and use of the ratio of the compressional (P-) to the shear (S-) Q ratio ($Q_P/Q_S$) as indicators of fluid saturation (Nur, 1972; O'Connell and Budiansky, 1974; O'Connell and Budiansky, 1979). Whether the objective is to remove the disturbing effect of attenuation, or to use attenuation as a seismic parameter to improve the interpretation of seismograms, the common goal is to accurately measure and predict attenuation.

Most studies in the near-surface suffer from low S/N, which implies that the Q factor is low as a result of i) the structural complexity characteristic of near-surface materials, which causes scattering, and ii) the presence of weak rocks and unconsolidated sediments, which may behave inelastically. The interest in near-surface Q merits special attention in oil and gas exploration, given that the near-surface Q degenerates the imaging of the deeper deposits of interest by absorbing energy and distorting the waveform, and interferes with the amplitude versus offset (AVO) behavior which is used in the inversion of elastic parameters. In addition, since the realization that the local geology (first couple of hundred meters) affects the ground response from strong earthquakes, the near-surface Q factor has been identified as one of the key parameters in site effect characterization.

In estimating attenuation, the Q values should reflect the frequency content and strain level of interest to the specific application. Moreover, it is important to establish the applicability of using different types of Q measurement, laboratory vs. field measurements, to predict Q behavior relevant to the application of interest and to check the validity of mathematical models with physical measurements. Therein lies the importance of separating the mechanisms of attenuation: in order to establish the frequency and strain-level dependence of attenuation, it is necessary to identify and quantify the contribution of each attenuation mechanism. The Q mechanisms are separated into scattering and intrinsic attenuation components, which are elastic and inelastic attenuation mechanisms respectively. Scattering attenuation is caused by heterogeneities in the elastic properties of the material; strictly speaking it does not entail any physical energy loss, but a redistribution of energy in space. On the other hand, intrinsic attenuation, otherwise termed as absorption, describes energy conversion to heat.

While many seismic studies have addressed the topic of attenuation, very few studies have dealt with quantifying the relative contribution of scattering and intrinsic attenuation (Chapter 2). Moreover, what seems to be a puzzle for attenuation measurement in the seismic frequency band is that though several in-situ studies suggest that the total attenuation is 2-10 times larger than the calculated scattering attenuation, most of the proposed absorption mechanisms, such as viscous flow, matrix anelasticity and intergranular friction, do not cause significant absorption attenuation at seismic frequencies (Peacock and Hudson, 1990; Gist, 1994a; Gist, 1994b). An absorption mechanism due to the presence of free gas has been proposed, which could cause a

dramatic decrease in $Q_P$ at seismic frequencies, but no change in $Q_S$ (White, 1975; Dutta and Seriff, 1979; Gist, 1994a). The effect of the free gas on P-wave attenuation was introduced to describe certain areas in a reservoir rock where the saturation may vary due heterogeneity of the reservoir rock (White, 1975).

The main objective of the dissertation study was to check whether intrinsic attenuation may exist in the seismic frequency band and to quantify the relative contribution of scattering vs. intrinsic attenuation of P-waves in the near-surface. To separate the two contributions, a shallow VSP experiment was conducted at the Lawrence Livermore National Laboratory (LLNL) facility using a vertical impact source at the surface and permanent 3-component down-hole receivers. Shot records included multiple offset and azimuth shot locations, however, this study focuses on the results from zero-offset which isolate the attenuation of the P-wave, itself theoretically free of converted waves. Limitations for angle-dependent attenuation estimation along with proposed future work are discussed in Chapter 8.

The results for vertical-incidence show evidence of intrinsic attenuation, which is attributed to the presence of the free gas in the vadose zone, defined as the zone above the watertable. Given that the attenuation measurements are in the seismic frequency band and for low strain-level associated with experimental sources, they cannot be used to predict strong motion response (which is lower frequency band and higher strain-level) nor can they be directly compared to high-frequency laboratory Q measurements. However, the results may be applied to future studies assessing different types of Q measurements and the methodologies may be applied directly to Q estimation studies and applications of inverse-Q filtering which are in the seismic experimental frequency band. In addition, they provide important information for the physics of attenuation in the vadose environment, which owing to similarities with the reservoir environment, may be applicable to oil and gas exploration. Lastly, the results of this study point to biases in Q estimation inherent to the geometry of Q estimation in the near-surface, which typically involve short source-receiver and receiver spacing distances. These biases are caused by the presence of the non-negligible near-field, differences in the local impedance, and interference phenomena from reflections originating beneath the medium of interest. Hence, a substantial part of this study was dedicated to addressing the biases due to these factors, which are termed ‘pseudo-Q’ effects.

Chapter 2 of this dissertation contains the mathematical definitions of Q, along with a brief description of the physical mechanisms of attenuation and selected methods of Q measurement in the time- and frequency-domains. This study started with an extensive literature review of previous analytical, experimental and numerical work related to seismic attenuation. Results of this literature review along with selected case histories of near-surface Q estimation are presented in Chapter 2 of this dissertation.

The description of the VSP experiment at LLNL can be found in Chapter 3 including the site geology, instrumentation, data acquisition and data processing. To model the scattering component of attenuation, firstly the profiles for the elastic properties (density and velocity) had to be constructed (Chapter 3). The profiles contained a deterministic component built from available log information and a random high-frequency component with variance range typical of sedimentary basins. Given the selected range of reflectivity profiles, upper and lower limit scattering attenuation estimates were developed using analytical models for scattering in 1D media based on the

ODA approach (O'Doherty and Anstey, 1971), and elastic finite-difference synthetics. Treatment of $Q_{scattering}$ in 1D heterogeneous media is presented in Chapter 4. In addition to scattering attenuation, Chapter 4 also addresses the bias in Q measurement caused by pseudo-Q factors, which include the effects from the near-field, local impedance and interference phenomena. Given the gap in the literature on near-field effects in shallow seismic studies, Chapter 5 includes a detailed presentation of several parameter estimation parameters that are affected by the near-field, along with the issues related to near-field removal. Chapter 6 closes the scattering attenuation topic, by considering the effects from random diffractions and refractions in 3D heterogeneous media. The results show that given the short propagation pathlengths in the experiment (~30m), attenuation due to lateral heterogeneity is non-significant.

Chapter 7 addresses the intrinsic component of attenuation deduced from comparison of the effective attenuation (without separation of mechanism) measured in the field data with the upper and lower scattering attenuation measured in the elastic synthetic data. The $Q_{intrinsic}$ values are in the order of 4-15, which shows that intrinsic attenuation is very high in the vadose zone. It is encouraging that similar values of $Q_{intrinsic}$ were estimated by White (1975) in his theoretical treatment of the free gas behavior in a reservoir environment. Moreover, through finite-difference elastic vs. visco-elastic modeling, it is shown that an intrinsic attenuation mechanism is required to cause the amount of pulse broadening present in the field data. Further research in modeling of the vadose zone conditions in terms of the free gas effect is required to determine the $Q_{intrinsic}$ behavior as a function of frequency, hence to solve the problem of scattering vs. intrinsic attenuation uniquely, or else with tighter range estimates than those presented in this study. Conclusions and further research questions are presented in Chapter 8.

## 1.1 References


Dutta, NC, and Seriff, AJ. “On White’s model of attenuation in rocks with partial gas saturation,” *Geophysics,* Vol. 44, 1806-1812, 1979.

Gist, GA. “Seismic attenuation from 3-D heterogeneities: A possible resolution of the VSP attenuation paradox,” *Society of Exploration Geophysicists Annual International Meeting, Expanded Abstracts,* 1042-1045,1994a.

Gist, GA. “Fluid effects on velocity and attenuation in sandstones,” *J. Acoust. Soc. Am*., Vol. 96, 115801173,1994b.

Nur, A. “Dilatancy, pore fluids and premonitory variations of $t_s/t_p$ travel times,” *Bull. Seismol. Soc. Amer.,* Vol. 62, 1217-1222, 1972.

O’Connell, RJ, and B. Budiansky, B. “Seismic velocities in dry and saturated cracked solids,” *J. Geophys. Res.,* Vol. 79, 5323-5426.

O’Doherty, RF, and Anstey, NA. “Reflections on amplitudes,” *Geoph. Prosp.,* Vol. 19, 430-458, 1971.

Peacock, S, and Hudson, JA. “Seismic properties of rocks with distributions of small cracks,” *Geoph. J. Int.,* Vol. 102, 471-484, 1990.

White JE. “Computed seismic speeds and attenuation in rocks with partial gas saturation,” *Geophysics.,* Vol. 40, 224-232, 1975.

# Chapter 2

## 2.1 Definitions and Terminology

### 2.1.1 Attenuation Coefficient

The most commonly used measure of attenuation is the attenuation coefficient, $\alpha$, which is the exponential decay constant of the amplitude of a plane wave traveling in a homogeneous medium. At two different distances $x_1$ and $x_2$ with respective amplitudes $A(x_1)$ and $A(x_2)$, the attenuation is given by (Toksöz and Johnston, 1981):

$$\alpha = \frac{1}{x_2 - x_1} \ln\left[\frac{A(x_1)}{A(x_2)}\right] \qquad (2.1.1.1)$$

with dimensions of inverse length.

### 2.1.2 Q

The dimensionless quality factor, Q, is an intrinsic property of rock, and it is a ratio of stored energy to dissipated energy. The relationship between the attenuation coefficient and quality factor is given by:

$$\frac{1}{Q} = \frac{\alpha c}{\pi f - \frac{\alpha^2 c^2}{4\pi f}} \qquad (2.1.2.1)$$

where c is the velocity, and *f* is the frequency (Futterman, 1962).

For large Q, the following approximation is valid (Futterman, 1962):

$$\frac{1}{Q} = \frac{\pi f}{c\alpha} \qquad (2.1.2.2)$$

For low-loss linear solids, an alternative definition can be formulated from the stress-strain relations. For a sinusoidally varying stress, the strain response is also sinusoidal. The stress and strain are related by the appropriate elastic modulus M, and the phase lag $\phi$ of strain behind stress. Allowing the modulus to be complex, it can be shown that (Toksöz and Johnston, 1981):

$$\frac{1}{Q} = \frac{M_I}{M_R} = \tan\phi \sim \phi \qquad (2.1.2.3)$$

Using equations (2.1.1.1) and (2.1.2.2) we define the value of *spatial* Q (Aki and Richards, 1980) given by the expression:

$$A(x) = A_0 \exp\left[-\frac{\pi f x}{cQ}\right] \qquad (2.1.2.4)$$

Expression 2.1.2.4 implies a propagating plane-wave. Therefore, for a spherical wave, geometrical spreading effects must be compensated.

### 2.1.3 Attenuation and Causality

In order to obey the principles of causality, attenuation is a necessary and sufficient condition for dispersion (Futterman, 1962). The frequency-dependent velocity $c(\omega)$ can be expressed as (Aki and Richards, 1980):

$$c(\omega) = c(\omega_0)\left[1 - \frac{1}{\pi Q(\omega)} \ln\left(\frac{\omega_0}{\omega}\right)\right] \qquad (2.1.3.1)$$

where $\omega_0$ is any fixed frequency.

## 2.2 Selected Methods for Q Measurement

This section presents the methods for Q measurement that were considered in the current study. For a more detailed description of different types of Q measurement, Tonn (1991) offers an excellent review of available methods, along with a comparison of the methods for his synthetic models. Given that several authors (e.g. Badri and Mooney, 1987; Tarif and Bourbie, 1987) have experienced a variation of extracted Q values from different types of measurements, this dissertation uses both selected time and frequency domain methods which are fairly common in the literature, to compare Q results, and establish which method is most appropriate given the geometry and inherent physics of the experiment. For reasons which will be discussed in detail in Chapter 4, the most stable method for Q measurement determined for this study was the peak amplitude decay method.

### 2.2.1 Time-domain

Amplitude decay method. The ratio of amplitudes for two different distances $x_1$ and $x_2$ (or times $t_1=x_1/c$ and $x_2/c$) yields (Tonn, 1991):

$$Q = \frac{\pi f \Delta x}{c}\left\{\ln\left[\frac{A(x_1)}{A(x_2)}\right]\right\}^{-1} \qquad (2.2.1.1)$$

or equivalently,

$$Q = \pi f \Delta t\left\{\ln\left[\frac{A(x_1)}{A(x_1)}\right]\right\}^{-1} \qquad (2.2.1.2)$$

where *f* is the dominant frequency, $\Delta x$ is the distance between the two receivers, and $.\Delta t$ time difference between the first-break arrivals at the two receivers. This method requires true amplitude recordings.

Rise time method. This method is based on the dispersion of the traveling wavelet consequent to attenuation. The method stems from the empirical relationship between the rise time, $\tau$, and attenuation (Gladwin and Stacey, 1974):

$$\tau = \tau_0 + c\int_0^t Q^{-1} dt \qquad (2.2.1.3)$$

For piecewise constant Q, we get:

$$\tau = \tau_0 + cQ\Delta t \qquad (2.2.1.4)$$

where $\tau_0$ is the risetime if the source, t is the traveltime and c is a constant.

Given that the constant c is source dependent, receiver dependent, and material dependent (Gladwin and Stacey, 1974; Kjartansson, 1979; Blair and Spathis, 1982; Muckelmann, 1985; Burkhardt et al., 1986), we do not use rise times to measure Q. However, we do use the rise times to separate the dispersion caused by scattering, as measured in the elastic synthetics, and the dispersion caused by the intrinsic and scattering attenuation mechanisms combined, as seen in the field data and visco-elastic synthetics.

### 2.2.2 Frequency-domain

Station spectral-ratio method. The station-ratio method can be used to determine Q between two stations at distances $x_1$ and $x_2$ using their ratios of amplitude spectra, $S_1/S_2$, in a selected frequency range (Jeng et al., 1999). The slope *m* of the linear equation:

$$\ln\left[\frac{S_1(x_1, f)}{S_2(x_2, f)}\right] = c + mf \qquad (2.2.2.1)$$

is equal to $\frac{\pi\Delta t}{Q}$. The constant c in this case takes into account the source function, receiver function, and geometric functions, hence, this method does not require true amplitude recordings (Jeng et al., 1999).

## 2.3 Literature Review

The study of attenuation is a broad subject involving several aspects of geophysical analysis. This dissertation started with an extensive literature review covering the theory and analytical derivations for attenuation, experimental field measurements, and laboratory measurements of Q, as well as numerical modeling.

### 2.3.1 Theoretical Framework

Intrinsic Attenuation. The concept of attenuation was introduced to describe the inelastic behavior of Earth materials. The most common measure of attenuation is the attenuation coefficient, introduced in Section 2.1.1. In the solution for a plane wave propagating in a homogeneous medium, the amplitude is given by:

$$A(x,t) = A_0 \exp\left(ikx - \omega t\right) \qquad (2.3.1.1)$$

where ω is the angular frequency and *k* is the wavenumber. Attenuation is introduced mathematically by allowing either the frequency or wavenumber to be complex. In the latter case,

$$k = k_R + i\alpha \qquad (2.3.1.2)$$

where α is the attenuation coefficient. The definition of Q follows as presented in Section 2.1.1.

For the solution of the seismic wave equation in a homogeneous medium, the main challenge was to describe mathematically dispersion in order to observe the principle of causality. For the linear wave equation, Futterman (1962) showed that absorption is a necessary and sufficient condition for dispersion, in other words dispersion must occur to observe causality. Moreover, Futterman (1962) derived the attenuation-dispersion pair, showing that they observe the Kramers-Krönig relations. In addition, his derivations required $Q^{-1}$ to be zero at zero frequency, and remarked that dispersion due to attenuation is not likely to be observed in the field because of the logarithmic dependence of phase velocity on frequency. Using a different approach, Kjartansson (1979) formulated a constant Q model that does not violate causality, which he accomplished by allowing the phase velocity to converge to zero in the long wavelength limit. Both the Futterman (1962) and Kjartansson (1979) models are constant Q models (the former above an arbitrary cutoff frequency $\omega_o$).

Several other investigators have derived the attenuation-dispersion relation by relaxing the constant Q assumption. Some of the most well-known models are the power

law model (Strick, 1967), Azimi's second and third model (Azimi et al., 1968), the Cole-Cole model (Cole and Cole, 1941), and the Standard Linear Solid model (Ben-Menahem and Singh, 1981). To judge which model is most appropriate to describe inelastic attenuation, it is necessary to define the physical mechanism that results in attenuation, and to quantify its frequency behavior, which could thereafter be approximated with one of the aforementioned models.

Scattering Attenuation. As noted by numerous authors, the effects of inelasticity on the propagating waveform of the medium itself can very well be indistinguishable from an entirely separate phenomenon, scattering. The earth, being composed of different rock materials, lends itself to distinct boundaries of changes in density and velocity, the product of which is equal to the impedance. As the propagating wave encounters a boundary with an impedance contrast, part of its energy is transmitted through the new medium, and part of it is reflected; this energy partitioning depends on the impedance contrast. At a fixed location, the seismogram records the primary wave, which is transmitted through each interface, plus the sum of multiple reflections that arrive later in the time record. Theoretically speaking, in a closed elastic medium, the volume integral of energy is constant in time, hence the energy recorded at each location over an infinite amount of time is also constant. However, from the perspective of measuring a spatial Q factor, as defined in expression 2.1.2.4 between two stations over a finite amount of time, the energy between the two stations would attenuate even if the medium were perfectly elastic. For practical purposes, when trying to isolate the Q factor corresponding to a specific wave type, such as the P-wave, it is common to observe the amplitude decay of the wave train corresponding to that particular type of wave. In the case of the P-wave, $Q_P$ is described by the amplitude decay in a time window containing the propagating P-wave, which is called the generalized primary. This time window contains the primary wave and short-period multiples, where the qualifier short-period denotes multiples arriving within the duration of the propagating wavelet. Multiples arriving later in the record are termed the coda. Hence, the mathematical problem that needs to be solved is to determine the amplitude decay caused by scattering, which includes the effect of transmission and multiple scattering.

Several authors have mathematically derived the amplitude and phase characteristics of the scattering filter, which for a 1D earth is termed the stratigraphic filter. The analytical results pertinent to the current experiment are discussed in detail in Chapter 4. However, for completeness, the main analytical advances are presented here. Backus (1962) analyzed scattering by averaging the elastic moduli in the wave equation, thus describing a 1D medium as an effectively anisotropic medium. However, his results are valid in the low-frequency wavefields. For the 1D problem, O'Doherty and Anstey (1971), as a result of mainly heuristic reasoning, provided a formula for the absolute value of the time-harmonic transmissivity (harmonic source) valid in the whole frequency domain. Their results were derived separately by Banik et al. (1985) using statistically-averaged wavefields, and by Resnick et al. (1986) and Ursin (1987) using the invariant embedding method. The ODA solution was also derived by Shapiro and Zien (1993) who used localization theory to compute the time-harmonic transmissivity caused by 1D velocity fluctuations; their result also allowed for non-vertical incidence. Shapiro et al. (1994) extended this result to include density fluctuations, for the time-harmonic transmissivity as well as for the transient transmissivity (impulse source). Scattering in

3D media was addressed by Müller and Shapiro (2004) who used a hybrid Q factor to quantify attenuation in an elastic anisotropic 3D random medium

In another series of interesting papers (Burridge et al., 1988; Burridge and Chang, 1989; de Hoop et al., 1991) an explicit expression for the transmissivity was obtained for vertical incidence. However, an integro-differential equation needs to be solved numerically, which makes these results harder to implement in geophysical applications.

### 2.3.2 Field Measurements

Most published field Q measurements do not deal with the problem of Q separation into scattering and intrinsic mechanisms. Hence their objective is to provide an effective Q value. In the near-surface, Q values are low (e.g. Badri and Mooney, 1987; Jeng et al., 1999), however, it is unclear what mechanism causes these low values, or, in light of the results of the current dissertation, whether these values involve pseudo-Q effects, such as the presence of the near-field (discussed in Chapter 5) which have not been included in the analysis.

The study of attenuation from a VSP dataset or check-shot surveys is nearly ideal and Q estimation has been done successfully in the past (Ganley and Kanasewich, 1980; Jahnsen et al., 1985; Staisby and Worthington, 1985). However, for VSP configurations with short receiver separation, interference phenomena and local impedance effects bias the attenuation estimates, and these have seldom been addressed. For example, Xu and Stewart (2006) when they encounter negative Q values in their VSP dataset assume 'poor coupling' which, however, may in fact be largely due to local impedance and interference factors.

Several researchers have conducted field experiments using either artificial sources or strong-motion data (e.g. Ambercrombie, 1997; Del Pezzo et al., 1995). The question of source type influence to Q measurement merits special interest, as it shows directly the relation of Q to frequency and strain. Gibbs et al. (1994) compared strong-motion to active source $Q_S$ measurements and observed constant frequency $Q_S$ and that non-linear effects were limited. However, to this day there has been no published study to compare $Q_P$ between strong-motion and artificial sources. Aside from comparison of strong-motion to artificial sources, it would be insightful to compare at the same site Q factors from different artificial sources, whether they are source monopoles or pressure sources, for different frequencies and strain levels. Badri and Mooney (1999) repeated Q measurements for explosive sources of different size and found a change in the Q values. However, they did not find a systematic trend of increasing strain (source size) with Q, which suggests that changes in Q may have been related to source directivity effects, and source frequency content.

An interesting study on scattering vs. intrinsic attenuation was presented by Del Pezzo et al. (1995), who compared coda-Q and direct S-wave Q from strong-motion data based on the approach of Wennerberg (1993). It would be interesting to test this approach in a near-surface environment using an artificial source. However, we expect several complications using this method in the near-surface, such as interference with the ground roll, and the fact that the P- and S- direct waves, as well as their coda, are not necessarily time-separated. In addition, there is the question of the S/N ratio in the coda, which may not be large enough for an artificial source.

Another promising possibility for measuring attenuation is from ambient noise

interferometry, as attempted recently by Prieto (2009). The main limitation for recovering the Green's functions from cross-correlation of noise sources is that the source distribution is uniformly distributed in the volume surrounding the receivers. However, the implications for attenuation measurement from cross-correlation in the case of non-uniform source distribution have not been assessed.

From the literature review, it appears that the experimental setting of the current dissertation and the main questions it answers are rather original. Firstly, the receiver array lies entirely in the vadose zone, hence the intrinsic attenuation values are expected to be higher than in other field experiments with similar profiles but with a shallower water tables. In addition, the configuration 'suffers' from pseudo-Q effects that have not been addressed in previous studies of Q in the near-surface. This study attempts to quantify the effects of scattering and intrinsic Q as well as the effects from pseudo-Q factors with a systematic approach that includes modeling of the scattering by both analytical and finite-difference solutions. By considering upper and lower limits for the scattering estimates, it establishes an intrinsic attenuation range, which is thereafter applied in visco-elastic modeling. Hence from a modeling standpoint, it is a rather extensive study of attenuation which has not been performed in past studies.

### 2.3.3 Laboratory Measurements

The current dissertation did not include any laboratory results, however, several laboratory studies are mentioned here to address the main conclusions and trends established from laboratory measurements.

Generally speaking, attenuation varies more than the seismic velocities as a result of changes in the physical state of materials. The attenuation of P- and S-waves depends on the physical state of the rock and the saturation conditions. Hence, the anelastic properties of the rocks supplement the elastic when inferring saturation conditions and pore fluids by seismic techniques. (Toksöz et al., 1979).

Given that laboratory measurements are generally made at ultrasonic frequencies, in order to extrapolate the results to seismic frequencies, it is necessary to define the mechanism involved in intrinsic attenuation along with the pressure and frequency dependence.

Some of the mechanisms that have been proposed include: matrix inelasticity, including frictional dissipation due to relative motion along the grain boundaries and crack boundaries (Walsh, 1966), attenuation due to fluid flow, including relaxation due to shear motions at pore-fluid boundaries (Walsh, 1968; 1969; Solomon, 1973), dissipation in a fully saturated rock due to the relative motion of the frame with respect to fluid inclusions (Biot, 1956; Stoll and Bryan, 1970), squirting phenomena (Mavko and Nur, 1975; O'Conell and Budiansky, 1977), energy absorbed in systems undergoing phase changes (Spetzler and Anderson, 1968), and partial saturation effects such as gas pocket squeezing (White, 1975). The latter mechanism is especially important in considering the deduced intrinsic Q values from the current study (discussed in Chapter 7), given that the medium sampled in the VSP well lies in the vadose zone. In addition, this mechanism is potentially the only mechanism that when extrapolated to the seismic frequency band can produce non-negligible attenuation (Gist, 1990).

Johnston et al. (1979) provide an excellent review of the main results from laboratory experiments. These include:

Frequency Dependence. Q may be frequency independent over a wide frequency range ($10^{-2} – 10^{-7}$ Hz), especially for some dry rocks. However, $Q^{-1}$ is proportional to frequency in liquids, so that in highly porous and permeable rocks $Q^{-1}$ may have a frequency dependent component.
Strain Amplitude. Attenuation appears to be independent of strain amplitude for low strains such as those associated with seismic waves.
Fluid Saturation. Attneuation for fluid-saturated rocks is higher than for dry rocks and depends on the degree of saturation, fluid type, and frequency in a complicated way. For rocks fully saturated $Q_P$ is greater than $Q_S$.
Pressure and Stress Dependence. Attenuation decreases with increasing confining pressure. This is usually attributed to the closing of cracks in the rock matrix.
Temperature Dependence. Q is generally independent on temperature.

## 2.4 References


Aki, K, and Richards, PG., "Quantitative seismology," *W.H. Freeman and Co.*, 1980.

Ambercrombie,RE. "Near-surface attenuation and site effects fromcomparison of surface and deep borehole recornings," BSSA, Vol.87, 731-744, 1997.

Azimi, SA, Kalinin, AV, and Pivovarov, BL. "Impulse and transient characteristics of media with linear and quadratic absorption laws: Izv", Earth Physics, Vol. 2, 42-54, 1968.

Badri, M, and Mooney, HM. "Q measurements from compressional seismic waves in unconsolidated sediments," Geophysics, Vol. 52, 772-784, 1987.

Backus, GE. "Long-wave elastic anisotropy produced by horizontal layering," Journal of Geophysical Research, Vol. 67, 4427-4440, 1962.

Banik, NC, Lerche, I, and Shuey, RT.1985, "Stratigraphic filtering, Part I : Derivation of the O'Doherty-Anstey formula," Geophysics, Vol. 50, 2768; "Part II: Model spectra," Geophysics, Vol. 50, 2775, 1985.

Ben-Mehanem, A, and Singh, JI. "Seismic waves and sources", Springer-Verlag, 1981.

Biot, MA. "Theory of propagation of elastic waves in a fluid-saturated porous solid. I. Low frequency range", Journal of Acoustical Society of America, Vol. 28, 168-178, 1956.

Biot, MA. "Theory of propagation of elastic waves in a fluid-saturated porous solid. I. High frequency range", Journal of Acoustical Society of America, Vol. 28, 179-191, 1956.

Blair, DP, and Spathis, AT. "Attenuation of explosion-generated pulse in rock masses", Journal of Geophysical Research, Vol. 87, 3385-3892, 1982.

Burckhardt, H, Pfaffenholz, J, and Schütt, R. "Measurement of Q on natural rock samples in different frequency ranges", DGMK Report 254, 83-119, 1986.

Burridge, R, and Chang, HW. "Multimode, one-dimensional wave propagation in a highly discontinuous medium," Wave Motion, Vol. 11, 231-249, 1989.

Burridge, R, Papanicolaou, G, and White, BS. "One-dimensional wave propagation in a highly discontinuous medium," Wave Motion, Vol. 10, 19-44, 1988.

Cole, KS, and Cole, RH. "Dispersion and absorption in dielectrics, I – Alternating current characteristics", Journal of Chemical Physics, Vol. 9, 342-351, 1941.

de Hoop, MV, Chang, H-W, and Burridge, R. "The pseudo-primary field due to a point source in a finely layered medium," Geophysical Journal International, Vol. 104, 489-506, 1991.

Del Pezzo, E, Ibanez, J, Morales, J, Akinci, A, and Maresca, R. "Measurements of intrinsic and scattering seismic attenuation in the crust," BSSA, Vol. 85, 1373-1380, 1995.

Futterman, WI. "Dispersive body waves," Journal of Geophysical Research, Vol. 67, 13, 5279-5291, 1962.

Ganley, DC, and Kanasewich, ER. "Measurements of absorption and dispersion from checkshot surveys," Journal of Geophysical Research, Vol. 85, 5219-5226, 1980.

Gibbs, JF, Boore, DM, Joyner, WB, and Fumal, TE. "The attenuation of seismic shear waves in Quaternary alluvium in Santa Clara Valley, California," BSSA, Vol. 84, 76-

90, 1994.

Gist, GA. “Seismic attenuation from 3-D heterogeneities: A possible resolution of the VSP attenuation paradox,” *Society of Exploration Geophysicists Annual International Meeting, Expanded Abstracts*, 1042-1045, 1994.

Gladwin, MT, and Stacey, FD. “Anelastic degradation of acoustic pulses in rock”, Physics of the Earth and Planetary Interiors, Vol. 8, 332-336, 1974.

Jannsen, D, Voss, J, and Theilen, F. “Comparison of methods to determine Q in shallow marine sediments from vertical reflection seismograms,” Geophysical Prospecting, Vol. 23, 479-497, 1985.

Jeng, Y, Tsai, J-Y and Song-Hong, C. “An improved method of determining near-surface Q”, Geophysics, Vol. 64, 668-680, 1987.

Johnston, DH, and Toksöz, MN. “Definitions and Terminology”, in Toksöz, MN., and. Johnston, DH. “Seismic Wave Attenuation,” Society of Exploration Geophysicists: Geophysics reprint series, chapter I, 1-5, 1981.

Johnston, DH, Toksöz, MN, and Timur, A. “Attenuation of seismic waves in dry and saturated rocks: II Mechanisms,” Geophysics, Vol.44, 691-711, 1979.

Kjartansson, E. “Constant Q wave propagation and attenuation”, Journal of Geophysical Research, Vol. 84, 4737-4748, 1979.

Mavko, G, and Nur, A. “Melt squirt in the asthenosphere”, J. Geophys. Res., Vol. 80, 1444-1448, 1975.

Muckelmann, R. “Theoretische und experimentelle untersuchungen von P- und S-wellen in sanden unter besonderer berücksichtingung ihter dämpfungseigenschaften”, PhD Thesis , University of Kiel, 1985.

Müller, TM, and Shapiro, SA, “Scattering attenuation in randomly layered structures with finite lateral extent: A hybrid Q model,” Geophysics, Vol. 69, 1530-1534, 2004.

O’Conell, RJ, and Budiansky, B. “Viscoelastic properties of fluid saturated cracked solids”, Journal of Geophysical Research, Vol. 82, 5719-5736, 1977.

O’Doherty, RF, and Anstey, NA. “Reflections on amplitudes,” *Geoph. Prosp.*, Vol. 19, 430-458, 1971.

Prieto, G, Lawrence, JF, and Berosa, GC. “Anelastic earth structure from the coherency of the ambient seismic field,” Journal of Geophysical Research, submitted 2009.

Resnick, JR, Lerche, I, and Shuey, RT. “Reflection, transmission, and the generalized primary wave,”Geophysical J. Roy. Astr. Soc., Vol. 87, 349-377, 1986.

Shapiro, SA, Zien, H, and Hubral, P. “A generalized O’Doherty-Anstey formula for waves in finely layered media,”Geophysics, Vol. 59, 11, 1760-1762, 1994.

Shapiro, SA, and Zien, H. “The O’Doherty-Anstey formula and localization of seismic waves,” Geophysics, Vol. 58, 5, 736-740, 1993.

Solomon ,SC. “Shear wave attenuation and melting beneath the mid-Atlantic ridge,” J. Geophys. Res., Vol.79, 6044-6059, 1973.

Spetzler, H, and Anderson, DL. “The effect of temperature and partial melting on velocity and attenuation in a simple binary system”, J. Geophys. Res., Vol. 73, 6051-6060, 1968.

Stainsby, SD, and Worthington, MH. “Q estimation from vertical profile seismic data and

anomalous variations in the North Sea," Geophysics, Vol. 50, 615-626, 1985.

Stoll, RD, and Bryan, GM. "Wave attenuation in saturated sediments", Journal of Acoustical Society of America, Vol.47, 1440-1447, 1970.

Strick, E. "The determination of Q, dynamic viscosity and transient creep curves from wave propagation measurements", Geophysical Journal of the Royal Astronomical Society, Vol. 13, 197-218, 1967.

Tarif, P, and Bourbie, T. "Experimental comparison between spectral ratio and rise time techniques for attenuation measurement", Geophysical Prospecting, Vol. 25, 668-680, 1987.

Toksöz, MN, Johnston, DH, and Timur, A. "Attenuation of seismic waves in dry and saturated rocks I. Laboratory Measurements", Geophysics, Vol. 44, 681-690,1979.

Tonn, R. "The determination of the seismic quality factor Q from VSP data: A comparison of different computational methods," Geophysical Prospecting, Vol. 39, 1-27, 1991.

Ursin, B. "The plane-wave reflection and transmission response of a vertically inhomogeneous acoustic medium", in Bernabini, M, Carrion, P, Jacovitti, G, Rocca, F, Treitel, S, and Worthington, M., Eds., Deconvolution and inversion, Oxford, Blackwell Scientific Publications, 189-207, 1987.

Walsh, JB. "Seismic wave attenuation in rock due to friction," J. Geophys. Res., Vol. 71, 2591-2599, 1966.

Walsh, JB. "Attenuation in partially melted material," J. Geophys. Res., Vol.73, 2209-2216, 1968.

Walsh, JB. "New analysis of attenuation in partially melted rock," J. Geophys. Res., Vol.74, 4333-4337, 1969.

Wennerberg, I. "Multiple scattering interpretation of coda-Q measurmenets," BSSA, Vol. 83, 279-190, 1993.

White JE. "Computed seismic speeds and attenuation in rocks with partial gas saturation," Geophysics., Vol. 40, 224-232, 1975.

Xu, CR, and Stewart, R. "Estimating seismic attenuation (Q) from VSP data," CSEG Convention, CSEG Recorder, September Issue, 57-61, 2006.

# Chapter 3
# Experimental Method

## 3.1 Site Geology

The Lawrence Livermore National Lab facility, located in Livermore, CA, is underlain by over 100 m of unconsolidated, heterogeneous alluvial sediments, consisting of clays, silts, sands and gravels, which form complex fluvial structures of inter-bedded paleostream channels. Depth to the water table is greater than 33m in the southeast corner of LLNL and about 10 m in its northwestern corner. The complex stratigraphy of the site results in a complex pattern of hydraulic conductivity, which has been modeled into a set of distinct hydrostratigraphic units (Noyes et al, 1999). The hydrostratigraphic units also show small-scale heterogeneities with a distinct P-wave velocity signature, as in the case of a perched aquifer, which has an anomalously high P-wave velocity due to the relationship between saturation and P-wave velocity (Crews et al., 2006). Figure 3.1.1 shows a hydrostratigraphic cross-section, which includes the well used in the current VSP study. The well description log (Figure 3.1.2) for this study indicates a geologic profile of interbedded thin layers of loosely deposited clayey and silty sands, silts, clays and gravels, which is typical of the alluvial sediments in the area.

## 3.2 Instrumentation and Data Acquisition

The VSP was conducted in well W-19, which is located in the SE corner of the Lawrence Livermore National Lab facility. Figure 3.2.1 shows the location of the well, along with the location of two other VSP studies by Milligan et al. (1999) and Crews et al. (2006) and a seismic surface study that was conducted by the author in 2005. The VSP consists of a down-hole 3-component 28 Hz geophone array with 12 levels at 3.03 m (10 ft) spacing, with the bottom level at 42.4 m (140 ft) depth. The well was originally used as a pump-and-treat well and contains a PVC casing of 15 cm (5'') diameter. The geophones were grouted with a cement-bentonite mix, in an effort to suppress tube waves, and improve coupling. Two multi-azimuth VSP data sets were recorded in July 2006 and February 2007, with shot locations shown in Figure 3.2.1. The zero-offset data were collected with a hammer shot, whereas for the multi-azimuth offset data an EWG-2 Bison elastic wave generator was used, which is shown in Figure 3.2.2. The shot locations started from an offset of 3.03 m (10 ft) to 84.8 m (280 ft) with 3.03 m (10 ft) spacing. The data was recorded on a 48 channel Strataview with sample interval 0.1 milliseconds and total recording length 1 second in SEG-Y format. To improve signal-to-noise ratio, 3-5 stacks were used per shot location, which were recorded as separate *files. No digital and analog filters were used in the recording.

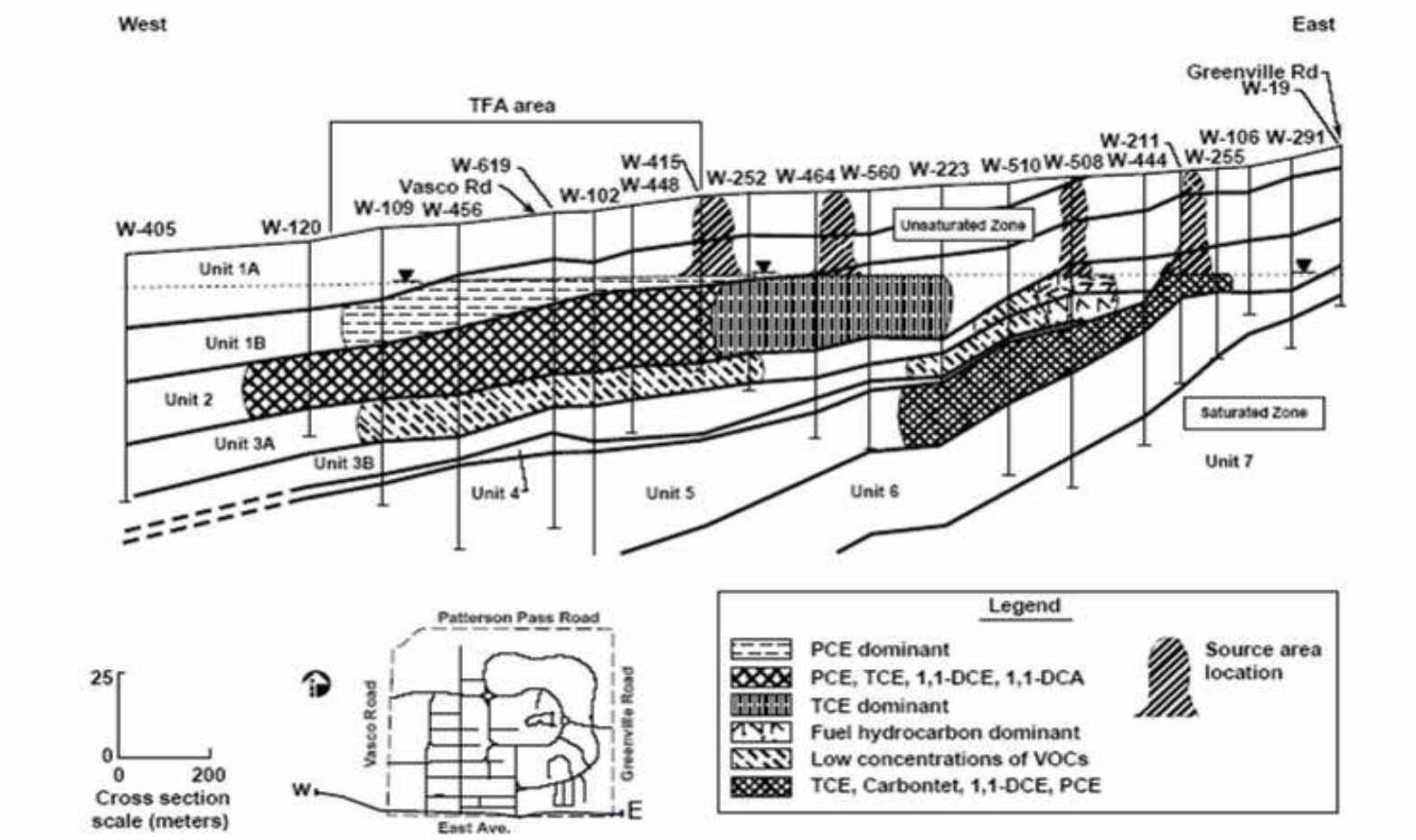


Figure 3.1 1 Hydrogeologic cross-section at the LLNL. VSP well is located in the eastern section (W-19).

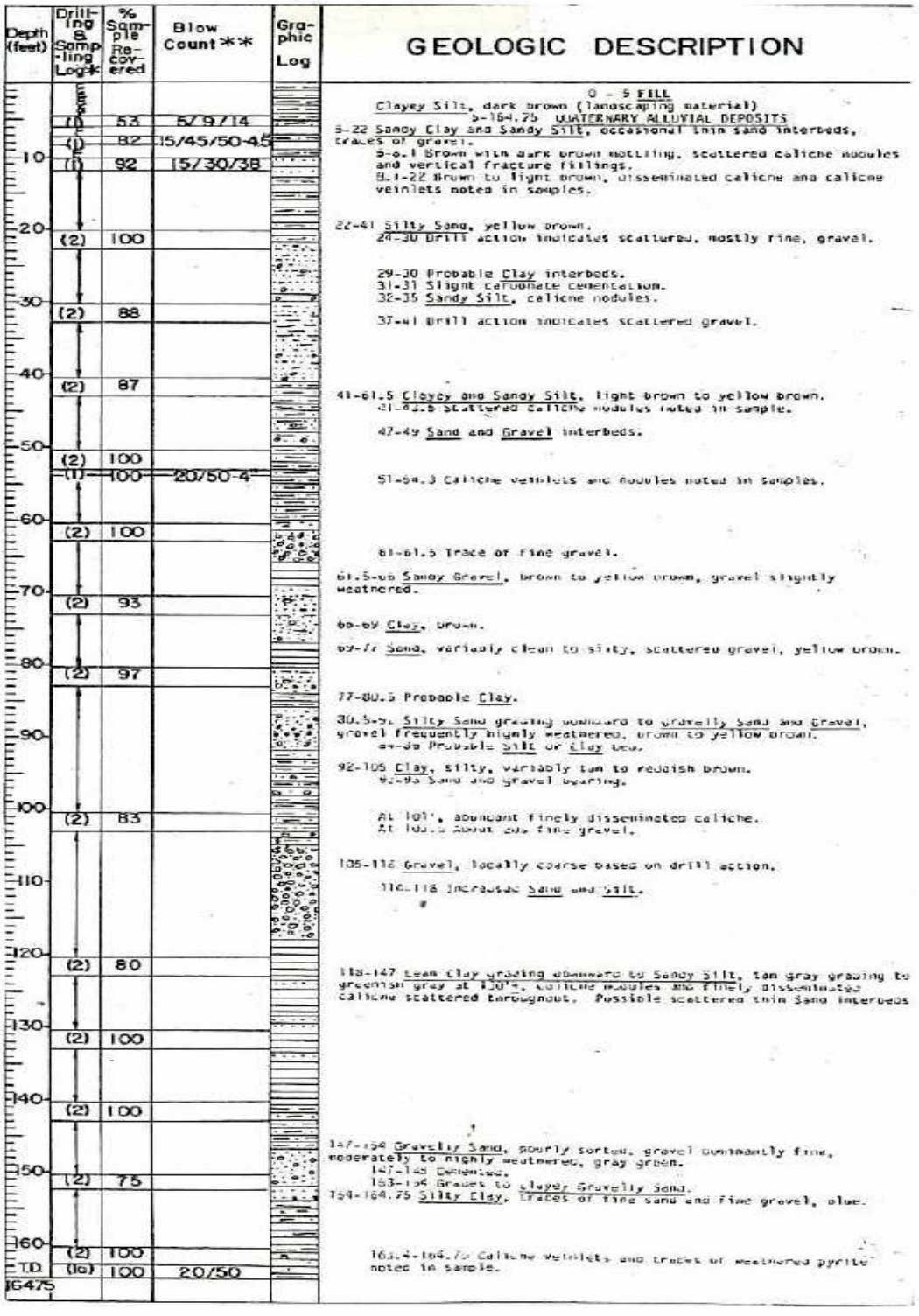


Figure 3.1 2 Geologic log description for well 19.

## 3.3 Data Processing

### 3.3.1 Channel Mapping

The seismic data was loaded onto Landmarks ProMax 2.0.0.3 software for processing. After loading the seismic geometry, the first breaks were picked to determine the correspondence of channel number to receiver levels, and their orientation into a common axis frame. Thus, from the zero-offset data, the channels were mapped onto their levels based on their first break times being constant at each level and increasing with increasing depth. Next the vertical component of each level was determined, as the one have the maximum energy in the zero-offset dataset, given the source radiation pattern was maximum in the z-direction. Polarity shifts were corrected so that, by convention, a positive arrival past the first-break corresponded to a compression.

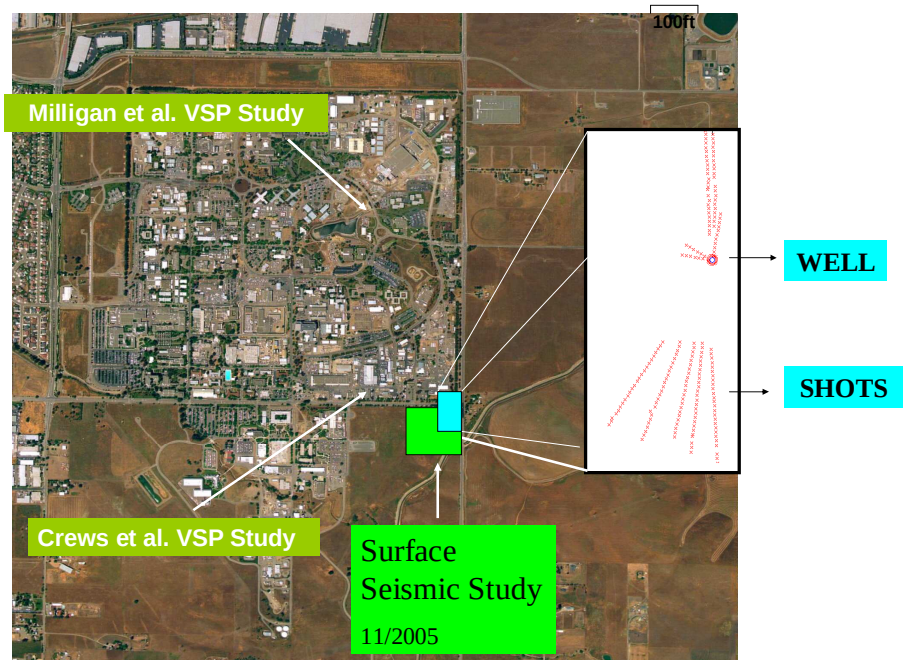


Figure 3.3.1 1The LLNL facility with locations of the present VSP study (shown in blue), and former seismic studies (shown in green).

### 3.3.2 Horizontal Rotations

The horizontal angle relative to a common axis frame for the two horizontal components of each level was calculated by using a shot location of intermediate offset (~ 13 m), which would contain adequate signal of the P-wave in the horizontal components. The direction parallel to azimuth was termed the global x-axis and the rotation perpendicular to the azimuth the global y-axis. The angles of the horizontal receivers with the x- and y- axes were determined based on a linear regression forced to pass through the origin of the velocity time history of the two horizontal components in

an 11millisecond window past the first-break time. The rotation into a global x- and y-axis frame of the horizontal components yielded the ‘x-horizontal component’ and ‘y-horizontal component’. The data rotation was completed by doing a deterministic rotation of the x- and y- horizontal components to a direction parallel to each source-well azimuth (termed as the ‘horizontal strong component’, given the fact that it contains most of the P-wave energy of the direct wave) and the direction perpendicular to the source-well azimuth (termed the ‘horizontal weak component’). An example of such a pair is shown in Figure 3.3.2.1.

Figure 3.3.1 2EWG-2 Bison elastic wave generator.

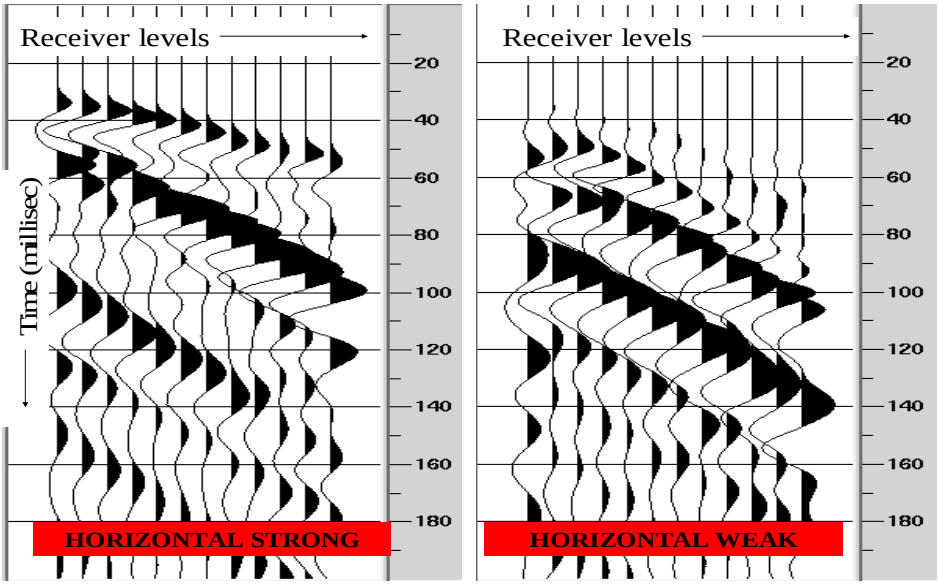

Figure 3.3.2 1 Example of deterministic horizontal rotation yielding a horizontal 'strong' and horizontal 'weak' component, respectively in the direction parallel and perpendicular to the azimuth.

### 3.3.3 Selection of down-going waves

To measure the attenuation in a profile, whether for vertical-incidence, or non-vertical incidence, one needs to measure the attenuation of the down-going waveform that is transmitted through each interface and reinforced by similarly transmitted down-going multiples. Given the fact that the velocity tends to increase with depth, it is possible that the first arrival is not this down-going waveform, but may instead be a head wave, or a reflection from an interface beneath the recording level. Thus, if we want to isolate the down-going waveform recorded at each receiver, it is sufficient to select the records with a positive vertical component past the first-break arrival – positive as a result of the convention used in the current study whereby in the zero-offset data, the vertical component had a positive first-arrival corresponding to a compression - and disregard all other records. Moreover, it makes sense that for a given receiver level, the first arrival in the vertical component will be positive for the short offsets, thus a down-going waveform, and may become negative for the longer offsets, thus an upcoming waveform, which was the case observed in the data. The result from this selection was that in lieu of 2532 source-receiver level pairs recorded (211 source locations * 12 receiver level locations), only 711 source-receiver level pairs qualified. Nevertheless, there was sufficient data to come up with the scattering Q and intrinsic Q profiles and also to draw conclusions on the angle dependence of attenuation.

### 3.3.4 Vertical Rotations

The last step of rotations was to rotate the data to the direction of the down-going P-arrival, by using the horizontal 'strong' component and the vertical component at each receiver level and rotating the two components in the direction of maximum velocity

arrival in an 11 millisecond time window past the first-break arrival. The angle of vertical rotation is given by a linear regression passing through the origin of the particle velocity amplitude time history on the horizontal and vertical axes (Figure 3.3.4.1).

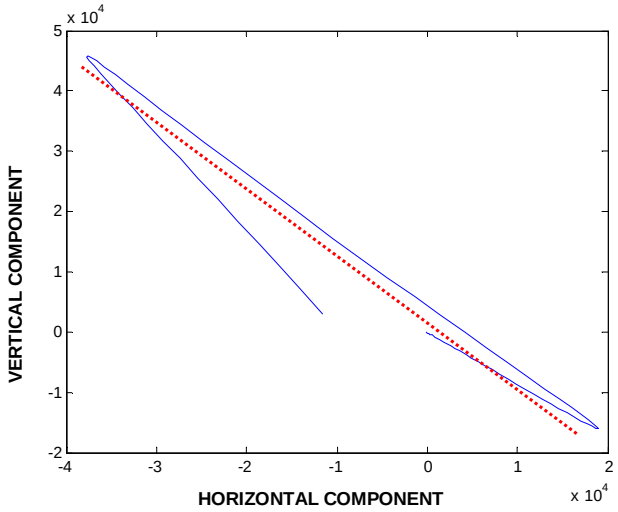


Figure 3.3.4 1Linear regression in 11 millisecond window of vertical and horizontal components for a source-receiver pair, to determine the vertical angle of rotation.

## 3.4 Zero-offset Shot Gather

The vertical component for the zero-offset shot gather is shown in Figure 3.4.1. Due to attenuation, the pulse of the first arrival shows broadens with increasing depth. On average, 3 shot repetitions were recorded per shot location, where each 'zero-offset' source location corresponded to an offset of 1m at $30^{o}$ intervals in azimuth. Figure 3.4.2 shows how the amplitude and frequency content increases progressively as a result of compaction of the material in the vicinity of the source.

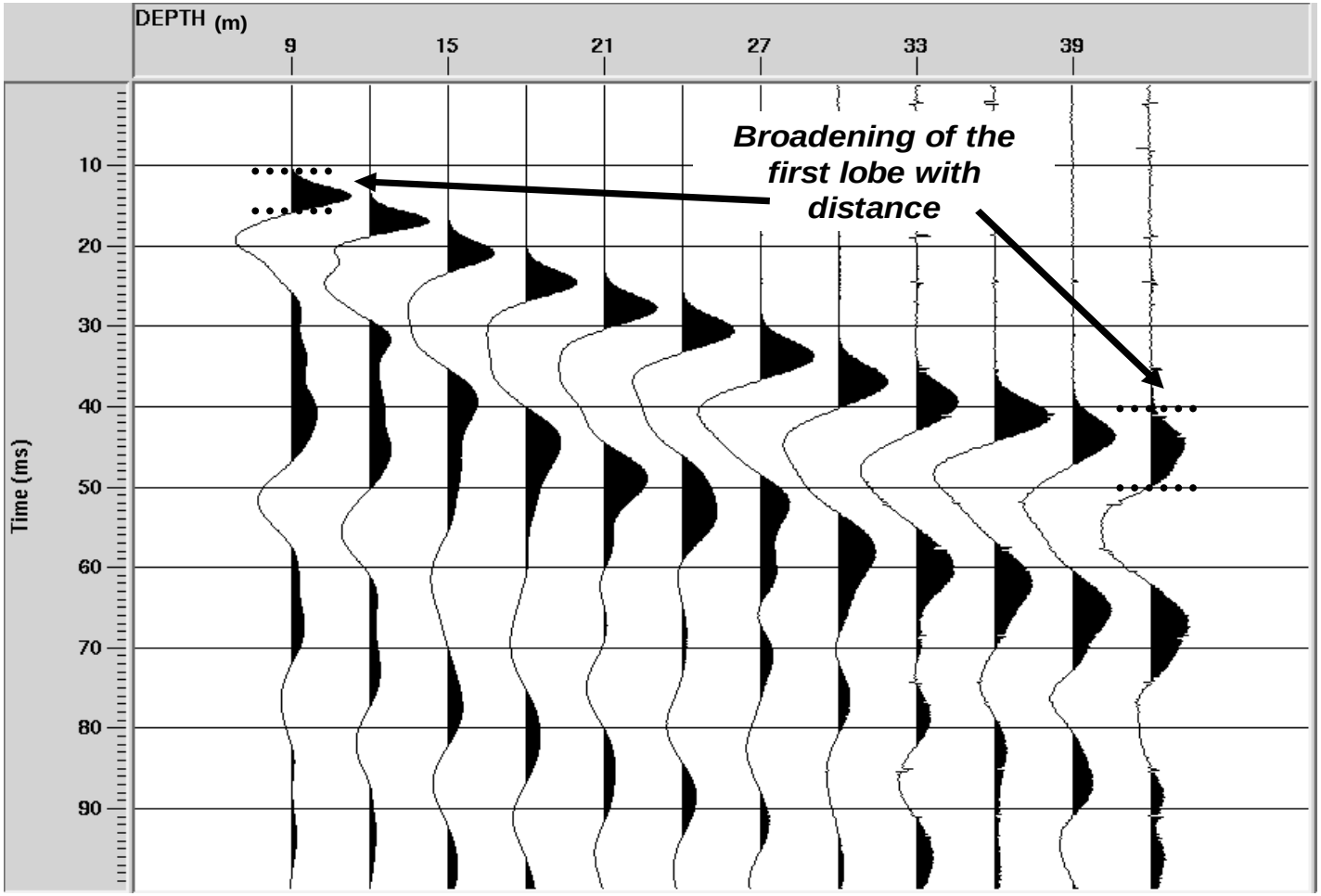

Figure 3.4 1Zero-offset shot gather. Notice the broadening of the P-arrival with distance as a result of attenuation. The displayed traces are scaled to their individual maximum value.

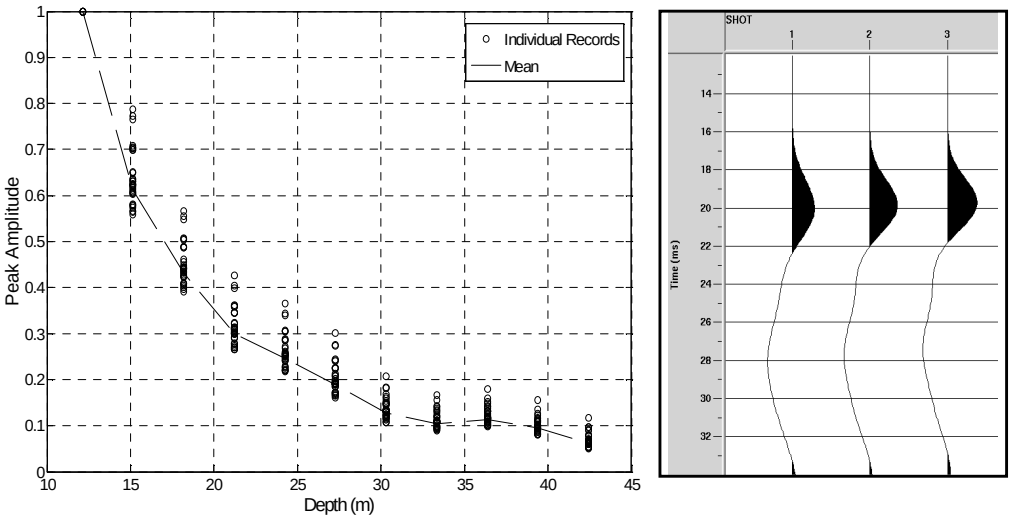


Figure 3.4 2Variation of peak amplitude of first arrival versus depth (left). Receiver-gather showing an increase in amplitude and frequency as a result of compaction with no scaling between the traces. The dashed line shows the mean value of the peaks.

## 3.5 Generation of Synthetic Velocity and Density Logs

- Velocity Log

  The first-breaks of the zero-offset data (Figure 3.4.1) were picked to determine a coarse interval P-wave velocity profile. The interval velocities were relatively low, ranging from 680 m/sec (2250 ft/sec) in the first 9.09 m (30 ft) up to 1212 m/sec (4000 ft/sec) at 42.4 m (140 ft) depth. The P-wave velocity at the surface is 242 m/sec (800 ft/sec). The low velocities are due to the unconsolidated and unsaturated conditions of the profile. Superimposed on the low frequency interval values, were two high-frequency components: a deterministic component obtained from quadratic fitting of the interval values with the gamma ray and resistivity logs (shown in Figure 3.5.1), and a high-frequency random component. The S-wave model was created by taking one half to one third of the P-wave velocity profile, for either a sandy or clayey layer.

- Density Log

  To create the density profile, we used the log description (Figure 3.1.2) to assign background densities to the different layers. We then added two high frequency components: one obtained from quadratic fitting of the interval values with the gamma ray log, which indicated a correlation of gamma ray with clay content, and a second high-frequency random component.

Figure 3.5.2 shows the VSP geometry and the starting model of the density and velocity profiles for impedance variance, $C_{\rho c}(0)$, equal to 0.0031. As discussed in Chapter 4, this initial model was perturbed for difference values of $C_{\rho c}(0)$ in order to estimate a range of possible $Q_{scattering}$ values.

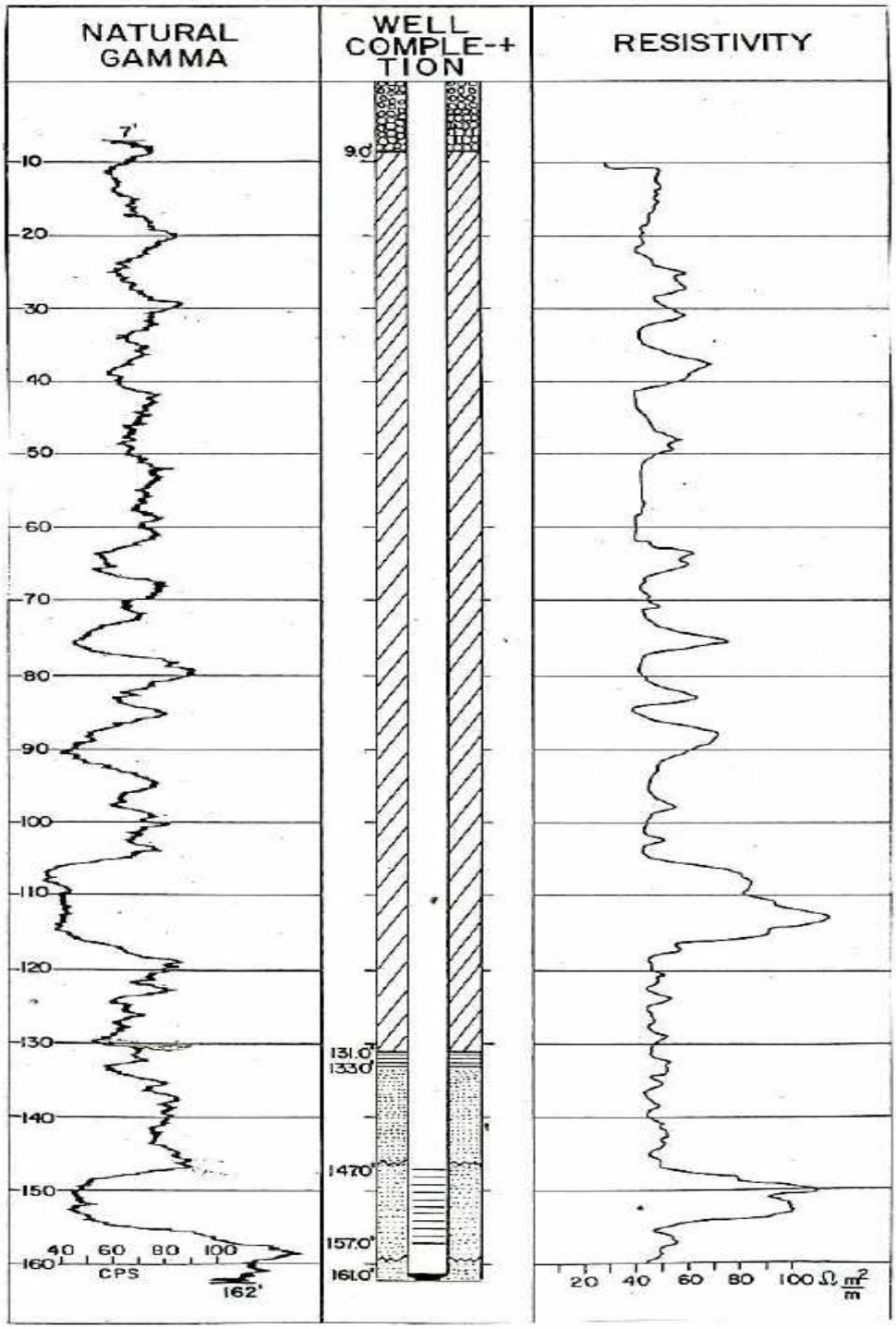


Figure 3.5 1 Natural gamma and resistivity logs for well 19.

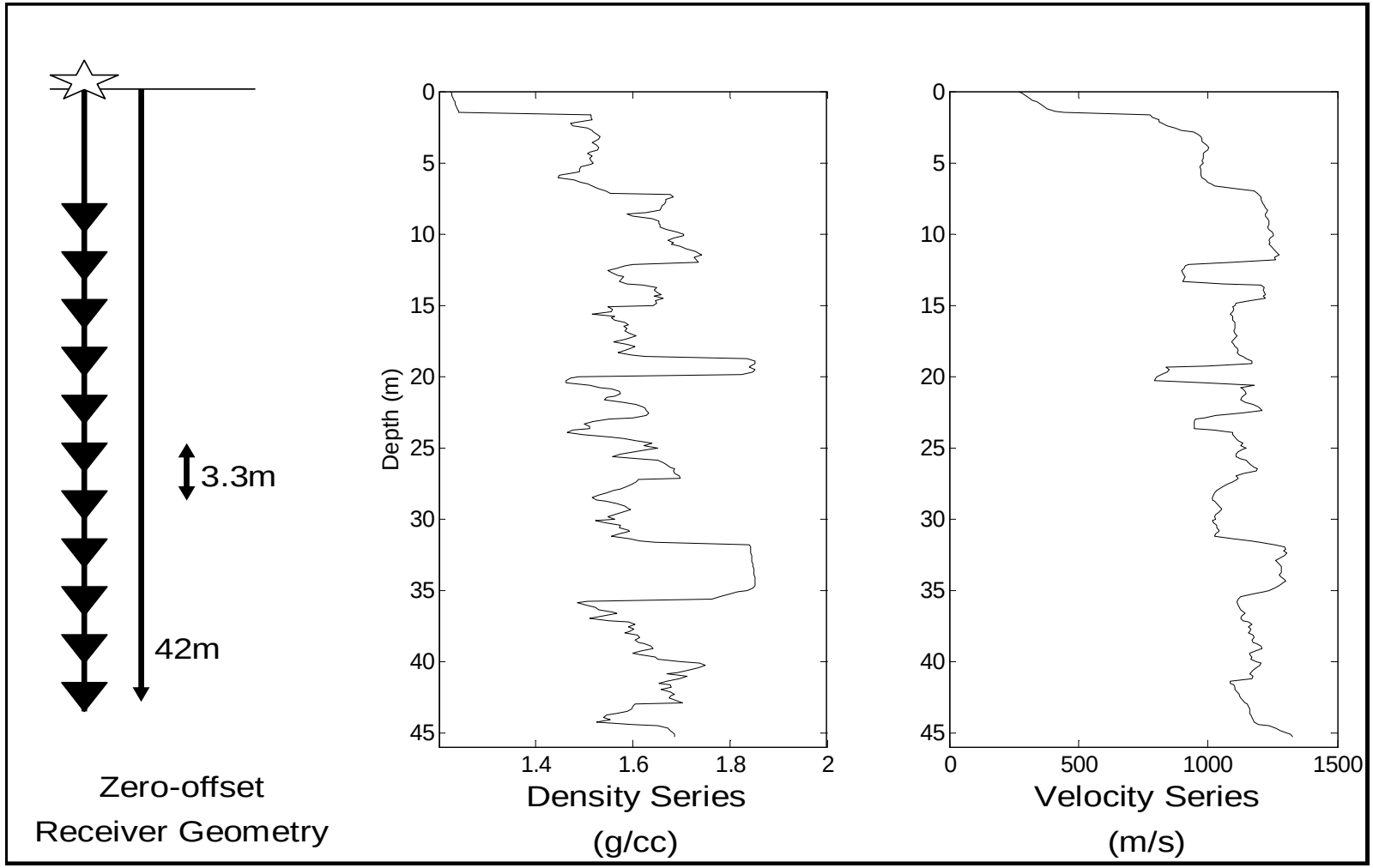


Figure 3.5 2VSP geometry (left) and density (center) and P-wave (right) synthetic profiles with $C_{\rho c}(0)$,=0.0031.

## 3.6 Conditioning the Amplitudes Prior to Q Measurement

Aside from the attenuation mechanisms of intrinsic and scattering Q which are to be measured in this study, there are several additional factors that influence amplitude and need to be accounted for so that they do not bias the Q measurements. These factors are:

- Radiation Effects

The radiation effects come in two flavors: the receiver radiation and the source radiation. By the previous discussion on the receiver rotations, both horizontal and vertical, of the three-component receivers, the effect of the radiation pattern of the receiver has been accounted for. The remainder radiation effect is for the source. Should the source have been a pressure source, which would imply that energy was directed equally to all directions from the source, thereby rendering the correction for the source radiation redundant. However, both for the case of the hammer shot, as well as for the case of the elastic wave generator source that were employed in this experiment, the source is a source monopole in the z-direction, which implies to the limit that the radiation is maximum in the z-direction and zero in the horizontal directions (for further discussion on source types refer to Aki and Richards, 1980). The source radiation effect can be corrected using Snell's law by a multiplication of the velocity in the r-direction (the direction of the primary wave) by the cosine of the take-off angle $\theta_{source}$, which is equal to:

$$\theta_{source} = \arcsin\left(\left(\frac{V_{source}}{V_{receiver}}\right)\sin(\theta_{receiver})\right) \qquad (3.4.1)$$

where $\theta_{receiver}$ is the angle of incidence at the receiver.

- Geometrical Spreading

Geometrical spreading refers to the phenomenon of energy spreading over a larger area as a wave propagates from a point source, which requires that the flux be constant with increasing propagation distance to honor the energy conservation law. The geometrical spreading term for seismic propagation in a homogeneous medium in three dimensions is 1/r, whereas for two dimensions it is $1/\sqrt{r}$. For a 1D medium an Ursin geometrical spreading correction (Ursin, 1990) is applied for either 2D propagation (which is equivalent to 3D with a line source) or 3D propagation.

- Instrument Response

Ideally, based on the amplitude and phase characteristics of the receiver specifications, the receiver response can be corrected for its amplitude and phase filtering effects. In the present study, only the amplitude of the attenuation is considered, and for higher frequencies than 28 Hz, so the instrument response correction is not further discussed.

- Local Impedance

To compensate for differences in the local impedance between the source and receiver, the receiver response may be multiplied by the transmission coefficient ($T_{rs}$) between the medium of the receiver and the shot (Prof. Dr. Serge Shapiro, personal communication):

$$T_{rs} = \frac{2\rho_{receiver}C_{receiver}}{\left(\rho_{receiver}C_{receiver} + \rho_{source}C_{source}\right)} \qquad (3.4.2)$$

Application of expression (3.4.2) requires some consideration for what values should

be used for the densities and velocities, which depend on the source frequency content, and hence are not necessarily the values at the [x,y,z] location of the source and receiver points. The local impedance correction is revisited in Chapter 4 as a 'pseudo-Q' factor.

- Interference Effects

Interference effects refer to the interference with the first arrival of multiple reflections originating beneath the depth of the receiver of interest. As discussed by Spencer et al. (1982), interference phenomena dominate the amplitude responses in cases of short receiver spacing, which applies to the geometry of the current study. The effect of interference on attenuation measurements is described in detail in Chapter 4, where interference is classified as a 'pseudo-Q' factor.

- Near-field Effect

Due to the short source-receiver distances involved in the current experiment, it is shown that the near-field is non-negligible. Moreover, the presence of the near-field biases the Q estimates, by causing the Q values to be underestimated. The near-field effects on Q measurement, as well as other examples of parameter estimation bias due to the near-field are dealt with in Chapter 5. Chapter 5 also addresses the issues with near-field removal and modeling requirements to account for its effect.

## 3.6 References


Aki, K, and Richards, PG., "Quantitative Seismology," *W.H. Freeman and Co.*, 1980.

Crews J, Rector III, JW, and Bainer RW. "Velocity imaging of the shallow subsurface using 3D inversion of VSP data to visualize a saturated portion of the vadose zone at Lawrence Livermore National Laboratory," *The Leading Edge*, Vol. 25, 362-365, 2006.

Milligan, P, Rector III, JW, and Bainer, R. "3-D Velocity Imaging in the Shallow Subsurface Using Multi-well, Multi-offset VSP Data: a Case Study from the Lawrence Livermore National Laboratory Site," *Journal of Environmental and Engineering*, Vol. 5, 27-37, 2000.

Noyes M, Maley MP, and Blake, RG. "Defining hydrostratigraphic units within the Heterogeneous Alluvial Sediments at Lawrence Livermore National Laboratory," *University of California, Livermore, CA: LLNL Report*, UCRL-JC-139779, 2000.

Spencer, TW, Sonnad, JR, and Butler, TM. "Seismic Q-Stratigraphy or dissipation," *Geophysics*, Vol. 47, 16-24, 1982.

Ursin, B. "Short Note: Offset-dependent geometrical spreading in a layered medium," *Geophysics*, Vol. 55, 492-496, 1990.

# Chapter 4
# Scattering in 1D Media

## 4.1 Theoretical Treatment

We present the estimates for the scattering component of attenuation by firstly considering the effects from 1D heterogeneity, which is a common approximation used for a sedimentary basin. In their famous paper, O'Doherty and Anstey (1970) provided an excellent presentation of the physical mechanism of scattering attenuation caused by thin layering, which includes the effects from transmission and multiple reflections. Given the impedance series in a 1D profile (forward problem), the computation of the transmission loss is rather straightforward, and is captured by the transmission coefficient. The boundary conditions in the solution of the elastic seismic wave propagation equation in a homogeneous medium require that displacement and particle velocity are continuous across the boundary, otherwise the boundary becomes un-welded. Assuming the original velocity amplitude of the wave is 1 and that the wave is split into a reflected wave of velocity amplitude $r_v$ and transmitted wave of amplitude $t_v$, continuity across the boundary requires that:

$$1 + r_v = t_v \tag{4.1.1}$$

Energy is equal to the square of the amplitude of the particle velocity times a factor, which is equal to the impedance (Y) and is taken as the product of ρV. Thus we have:

$$\rho_1 V_1 \, 1^2 = \rho_1 V_1 \, r_v^{\,2} + \rho_2 V_2 \, t_v^{\,2} \tag{4.1.2}$$

Substitution of $1 + r_v = t_v$ into and solving the energy relation for $r_v$ gives:

$$r_v = \frac{Y_1 - Y_2}{Y_1 + Y_2} \tag{4.1.3}$$

where $Y_i$ is the impedance of the ith layer. Siimilarly for $t_v$:

$$t_v = \frac{2Y_1}{Y_1 + Y_2} \tag{4.1.4}$$

The ratio of reflected energy to transmitted energy gives the energy reflection coefficient:

$$r_{ven} = \frac{\left(Y_1 - Y_2\right)^2}{\left(Y_1 + Y_2\right)^2} \tag{4.1.5}$$

And similarly for the energy transmission coefficient:

$$t_{ven} = \frac{4Y_1 Y_2}{\left(Y_1 + Y_2\right)^2} \tag{4.1.6}$$

For n + 1 layers, the particle velocity transmission coefficient after n interfaces is:

$$T_n = \prod_1^n t_i = \prod_1^n \frac{2Y_i}{Y_i + Y_{i+1}} = \prod_1^n \left(1 + r_i\right) \tag{4.1.7}$$

The reverse journey being:

$$T_1 = \prod_1^n \frac{2Y_{i+1}}{Y_{i+1} + Y_i} = \prod_1^n \left(1 - r_i\right) \tag{4.1.8}$$

It is easy to verify that:

$$T_n = \frac{\prod_i 2Y_i}{\prod_i Y_i + Y_{i+1}} = \frac{\frac{Y_1}{Y_{n+1}} \prod_i 2Y_{i+1}}{\prod_i Y_i + Y_{i+1}} = T_1 \frac{Y_1}{Y_{n+1}} \tag{4.1.9}$$

Hence,

$$T_n = T_1 \frac{Y_{n+1}}{Y_1} \tag{4.1.10}$$

Expression (4.1.10) shows that the transmission is identical in either direction apart from a scale factor which depends upon the properties of layers 1 and n+1.

To include the effects of multiple reflections, several numerical algorithms have been proposed as, for instance the reflectivity method (Fuchs and Müller, 1971) for a point source, or e.g. the Thomson-Haskell method for a plane wave. However, as the number of layers increases, these algorithms become very time consuming, hence the problem of wavefield propagation in a 1D medium is more efficiently solved by different averaging procedures. A seminal theory for the whole frequency domain was developed by O'Doherty and Anstey (1971) to describe scattering attenuation caused by thin layering, which includes the effects from transmission and multiple reflections. The primary wave and short-period multiples, where the qualifier short-period denotes multiples arriving within the duration of the propagating wavelet, form the generalized primary. Multiples arriving later in the record are termed the coda. Through mostly heuristic reasoning, O'Doherty and Anstey (1970) provided a formula for the time-harmonic transmissivity in the whole frequency domain. Their result was later derived by Banik et al. (1985) who used stochastic averaging of the reflection coefficient series to obtain the amplitude and phase of transmissivity.

Instead of using statistical averaging, which assumes an ensemble of realizations (hence dissimilar to the geophysical reality which is a single realization), Shapiro and Zien (1993) used localization theory to derive the time-harmonic transmissivity for vertical and non-vertical incidence caused by 1D velocity fluctuations; Shapiro et al. (1994) extended this theory to include 1D density fluctuations. The squared slowness and density functions are assumed to be stationary and ergodic. Ergodic means that ensemble averaging can be replaced by spatial averaging in a single realization. The transmissivity is derived for a medium of length L, with depth dependent squared slowness ($1/c^2_{true}$) and density ($\rho_{true}$), imbedded between two homogeneous half-spaces of equal density and velocity. The squared slowness and density are separated into constant parts, $1/c_0^2$ and $1/\rho_0$, and fluctuating parts, $\mu$ and $\rho$, which are small fluctuations with standard deviations $O(\varepsilon)$ (Shapiro et al., 1994):

$$\frac{1}{c^2_{true}} = \frac{1}{c_0^2}\left(1+\mu(z)\right) \tag{4.1.11}$$

$$\rho_{true} = \rho_0\left(1+\rho(z)\right) \tag{4.1.12}$$

For a plane time-harmonic wave, with circular frequency $\omega$, incident on the stack of layers at angle $\theta$, the time-harmonic transmissivity can be expressed as:

$$T(\omega) \propto \exp(-\alpha(\omega)L + i\phi(\omega)L + ikx\sin\theta) \tag{4.1.13}$$

where $\alpha(\omega)$ is the attenuation, and $\phi(\omega)$ is the phase caused by scattering. The attenuation

is given by (Shapiro et al., 1994):

$$\alpha(\omega,\theta) = C(0)\frac{k^2 a \cos^2 \vartheta}{4(1+4k_0^2 a^2 \cos^2 \vartheta)} \qquad (4.1.14)$$

where $a$ is the correlation length, $k=|\omega/c|$, $k_0=|\omega/c_0|$ and C(0) determined from the quantity C defined as:

$$C = 4C_{\rho\rho} - \frac{4C_{\rho\mu}}{\cos^2 \vartheta} + \frac{C_{\mu\mu}}{\cos^4 \vartheta} \qquad (4.1.15)$$

Expression (4.1.15) contains the cross-correlation functions $C_{\rho\rho} = <\rho(z)\rho(z+\xi)>$, $C_{\rho\mu} = <\rho(z)\mu(z+\xi)>$ and $C_{\mu\mu} = <\mu(z)\mu(z+\xi)>$.

Defining the quality factor Q as $Q^{-1} = \frac{2\alpha}{k}$ (Johnson and Toksöz, 1981), expression (4.1.14) can be written as (Shapiro et al., 1994):

$$Q^{-1} = C(0)\frac{ka \cos^2 \vartheta}{2(1+4k_0 a^2 \cos^2 \vartheta)} \qquad (4.1.16)$$

As seen from the variograms of the density, velocity and impedance fluctuation series for the LLNL profile (Figure 3.5.2) the series are not stationary (Figure 4.1.1). However, Shapiro et al. (1994) showed for the case of noticeable non-stationarity that their theory was robust in modeling attenuation in real series. The estimated correlation lengths, $a$, were approximately 2, 0.5, and 1m from the density, velocity and impedance series respectively (Figure 4.1.1). These values are comparable to correlation lengths established from well-log statistics by White (1990), who found $a$ in the order of 1.5 to 3 m. Figure 4.1.2 shows $Q^{-1}$ as a function of frequency at vertical incidence; $Q^{-1}$ reaches its maximum value for normalized frequency, $ka$, equal to 0.5.

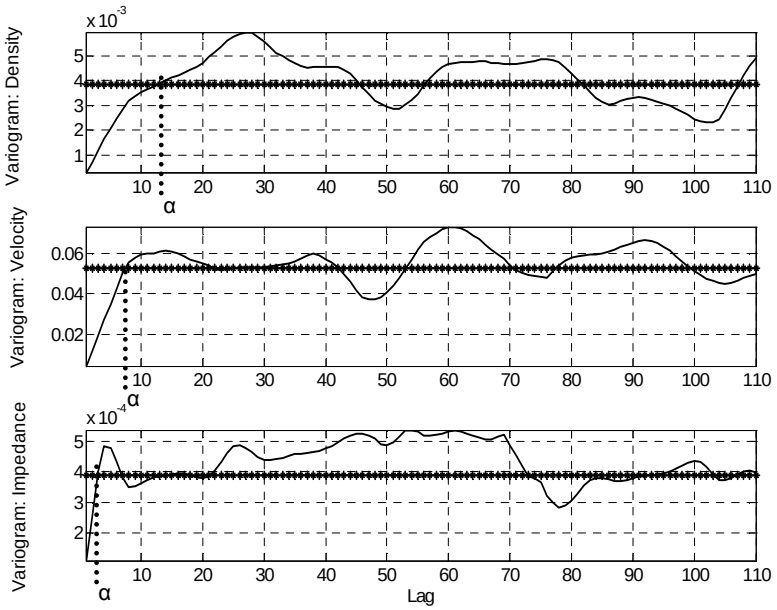


Figure 4.1 1Variograms for the density, velocity and impedance series of the modeled series at LLNL suggesting non-stationarity. Dotted lines show the approximate correlation lengths α equal to 2, 1 and 0.5 m as computed from the density, velocity and impedance variograms respectively.

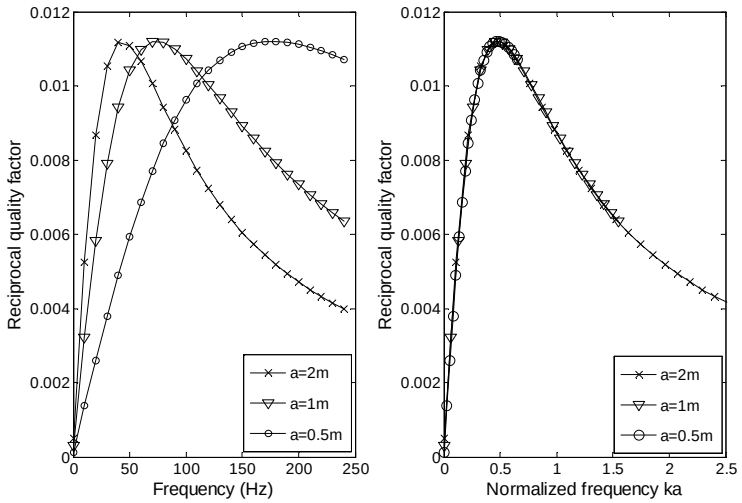


Figure 4.1 2Reciprocal quality factor as a function of frequency for the different correlation lengths computed from the series at LLNL using the Shapiro et al.(1994) ODA derivations (left). The reciprocal quality factor is also plotted as a function of normalized frequency, which attains its maximum value at kα = 0.5 (right).

## 4.2 Verification of 1D Scattering Theory and Effects from Pseudo-Q Factors

The attenuation predicted from the analytical solution in expression (4.1.14) is compared to the attenuation measured in elastic finite-difference synthetics computed with the code E3D (Larsen et al., 2001). The results computed are for a 1D medium is described by the elastic series shown in Figure 3.5.2. To make the comparison valid, the synthetics should honor the following conditions, which are assumed in the Shapiro et al. (1994) derivations:

I. the incident wave should be a plane wave.
II. the local impedance in the vicinity of the source and receiver should be equal.
III. the material beneath each receiver should be constant. This ensures that no multiple reflections originating beneath the receiver interfere with the generalized primary.

Condition I implies that for a point source, the source-receiver distance approaches infinity. Should this distance be finite, but relatively large, a spherical divergence correction is sufficient to correct the amplitudes for spreading, hence provide reliable estimates for Q, which themselves assume a plane propagating wave. However, as discussed in detail in Chapter 5, for small source-receiver distances, the near-field may be non-negligible and consequently bias the attenuation estimates.

Figure 4.2.1 shows the effect of the near-field in the peak amplitude of the first arrival for the finite-difference elastic synthetics computed for the LLNL profile shown in Figure 1. To quantify the effect of the near-field, we considered two scenarios: a) one with the dimensions of the LLNL experiment, and b) one with a remote source, which was modeled by adding a 1 km homogeneous layer over the reflectivity series. The input source function was a 120Hz Gaussian monopole force. To approximate finite-difference synthetics for a plane wave, we used the geometry for the remote source which has a negligible near-field term, and applied a spherical divergence correction factor to account for spreading of the far-field term.

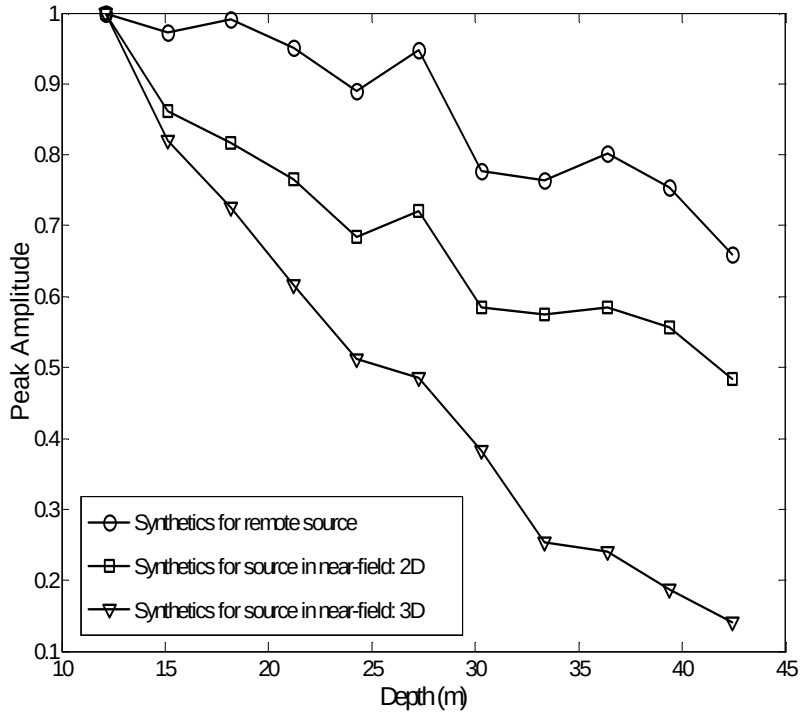


Figure 4.2 1Near-field effects: Peak amplitude decay of the first arrival versus depth for the elastic synthetics computed for a remote source and for a source in the near-field using 2D and 3D finite-differences.

To compensate for differences in the local impedance between the source and receiver, the receiver response may be multiplied by the transmission coefficient ($T_{rs}$) between the medium of the receiver and the shot (Prof. Dr. Serge Shapiro, personal communication):

$$T_{rs} = \frac{2\rho_{receiver} C_{receiver}}{\left(\rho_{receiver} C_{receiver} + \rho_{source} C_{source}\right)} \tag{4.2.1}$$

Application of expression (4.2.1) requires some consideration for what values should be used for the densities and velocities. If the source and receiver are embedded in thin layers and the seismic signal is bounded in frequency, then the density and velocity values may not correspond to the exact properties of the thin layers. For example, embedding a receiver in an infinitely thin layer of very high impedance would have a minimal effect in the receiver response for a source function containing low and intermediate frequencies, and a large effect for a high-frequency source function. A heuristic approach is to use Backus-averaged impedances (Backus, 1962) at the source and receiver locations in expression (4.2.1), with the length of the Backus-averaging window increasing as a function of the source center frequency. To satisfy condition II in our synthetics, we embedded the source and receiver in layers of thickness greater than 3 wavelengths computed for a center frequency of 120Hz.

Condition III was implemented by considering for each receiver level a separate model with constant properties beneath its depth (Figure 4.2.2: Model with no interference). The synthetics for the continuous series were also computed, which include the effect of multiple reflections originating beneath the receivers (Figure 4.2.2: Model with interference). The synthetics for the 'no interference' and 'with interference' models are shown in Figure 4.2.3. For predominantly cyclic sequences, the multiples constituting the downgoing wave are opposite in sign to those present in the upcoming wave. Consequently, the interference effect due to multiples originating beneath the receiver is primarily destructive.

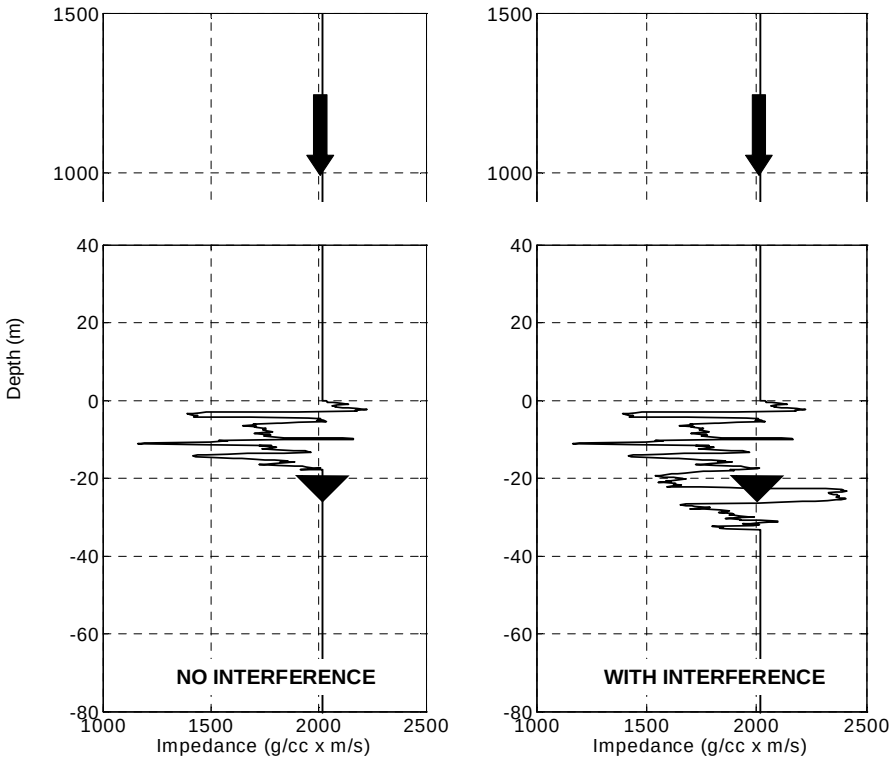


Figure 4.2 2 Impedance series used to model the receiver response with no interference effects (left) and with interference effects (right). In both cases, the near-field effect is suppressed by considering a remote source overlying a 1km homogeneous overburden. The shot location is shown by arrow and the receiver location by an inverted triangle.

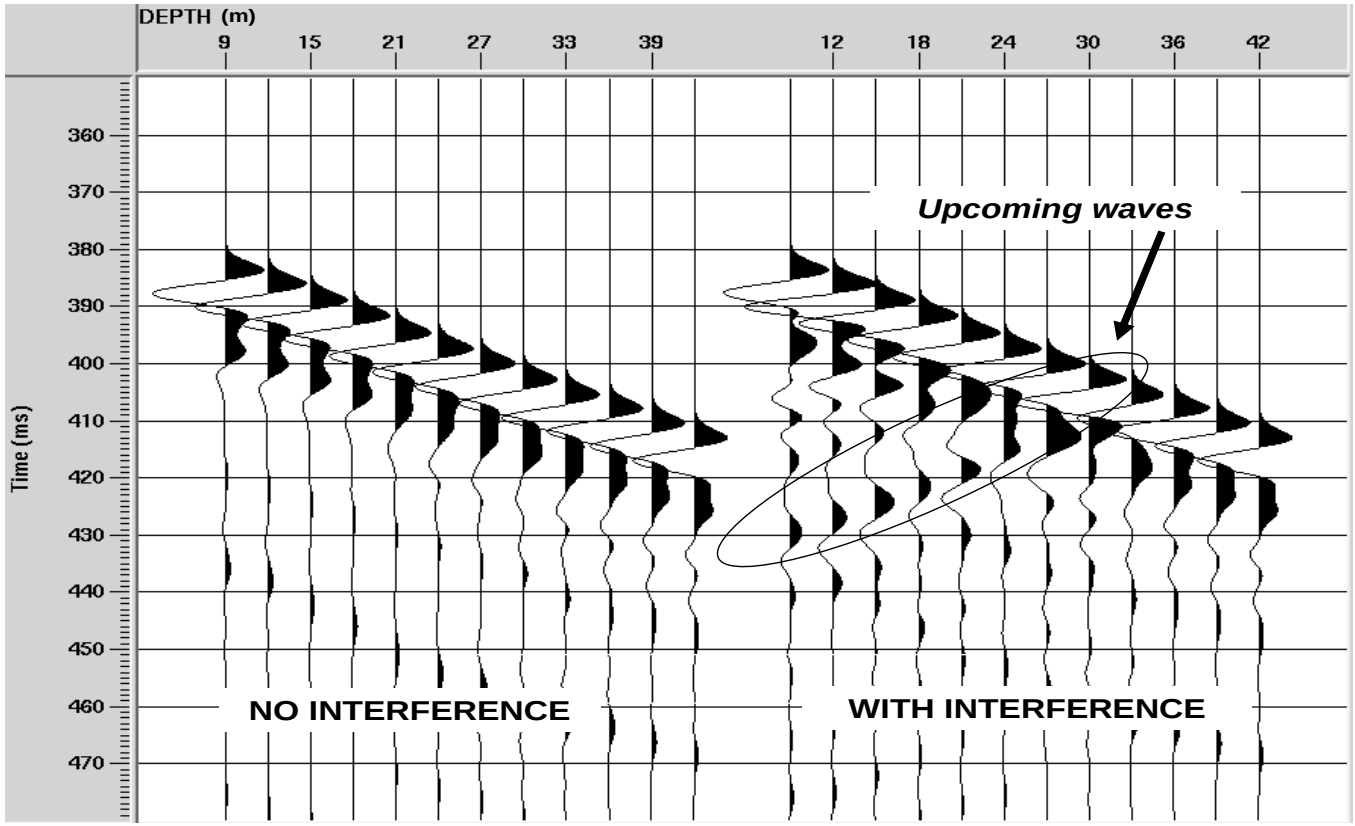


Figure 4.2 3Shot-gather for the elastic finite-difference synthetics computed for the model with no interference (left) and with interference (right) for the series at LLNL. The source function was a 120Hz Gaussian. The interference phenomena are seen through the upcoming waves interfering with the first-arrival (right). In the display each trace is scaled to its maximum value.

Figure 4.2.4 shows the peak amplitude decay of the first arrival for the two models, and verifies that for the 'with interference' model the amplitude decay is more pronounced. The peak amplitudes for Q predicted by expression (4.1.16) and using expression (2.2.1.2) for $f$ = 120 Hz, $a = 1$ m, and a peak amplitude of 1 at 12 m depth, are plotted for comparison. Figure 4.2.5 shows that the spectra from the 'with interference' model fluctuate across the frequency band as a result of the predominantly destructive, but also constructive, interference. Space-domain filtering suppresses the interference effect, however, as shown in Figure 4.2.6, applying the spectral ratio method (Chapter 2) even for the space-domain filtered data, yields very unreliable Q estimates.

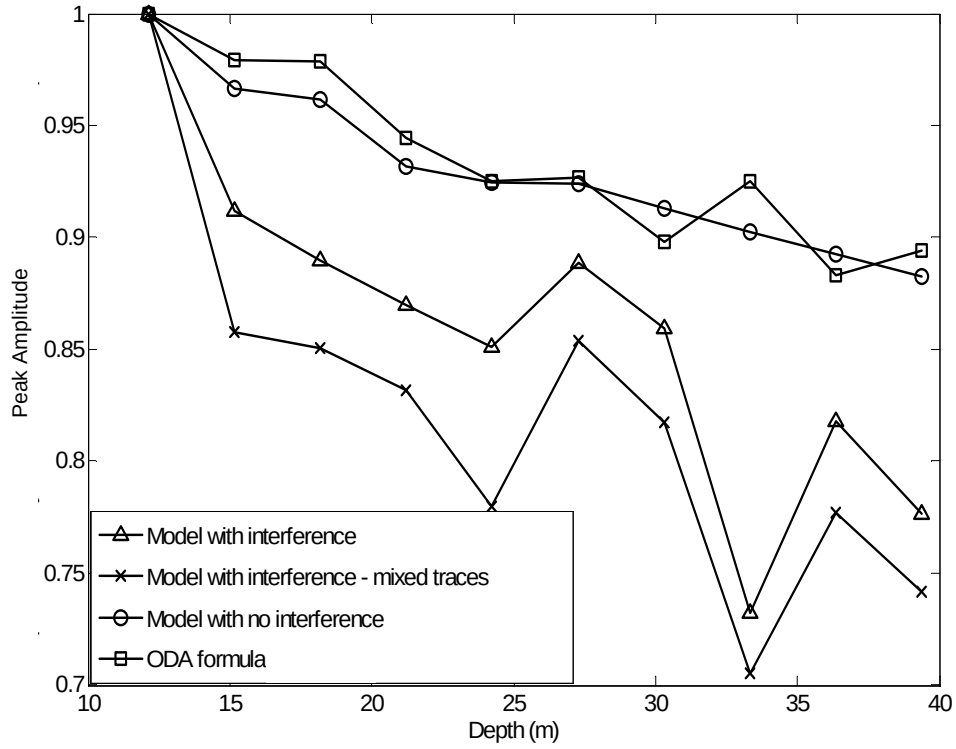


Figure 4.2 4 Peak amplitude decay versus depth for the elastic finite-difference models with interference and no interference. For comparison, the peak amplitudes computed from the Shapiro et al. (1994) ODA derivations are plotted, which agree with the model with no interference synthetics.

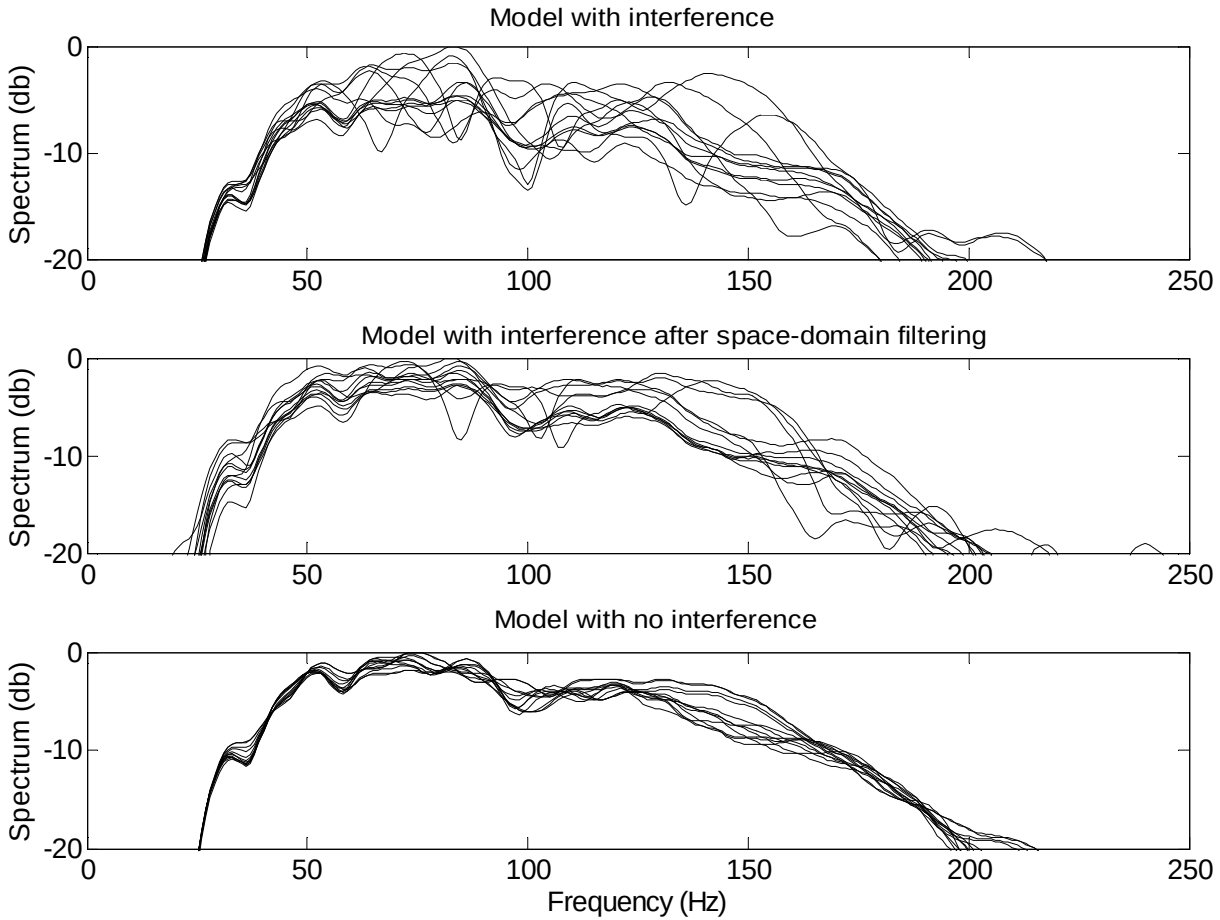


Figure 4.2 5 Effect of interference in the amplitude spectra: model with interference (top), model with interference after space-domain filtering (middle) and model with no interference (bottom). The interference phenomena result in fluctuations in the spectra (top).

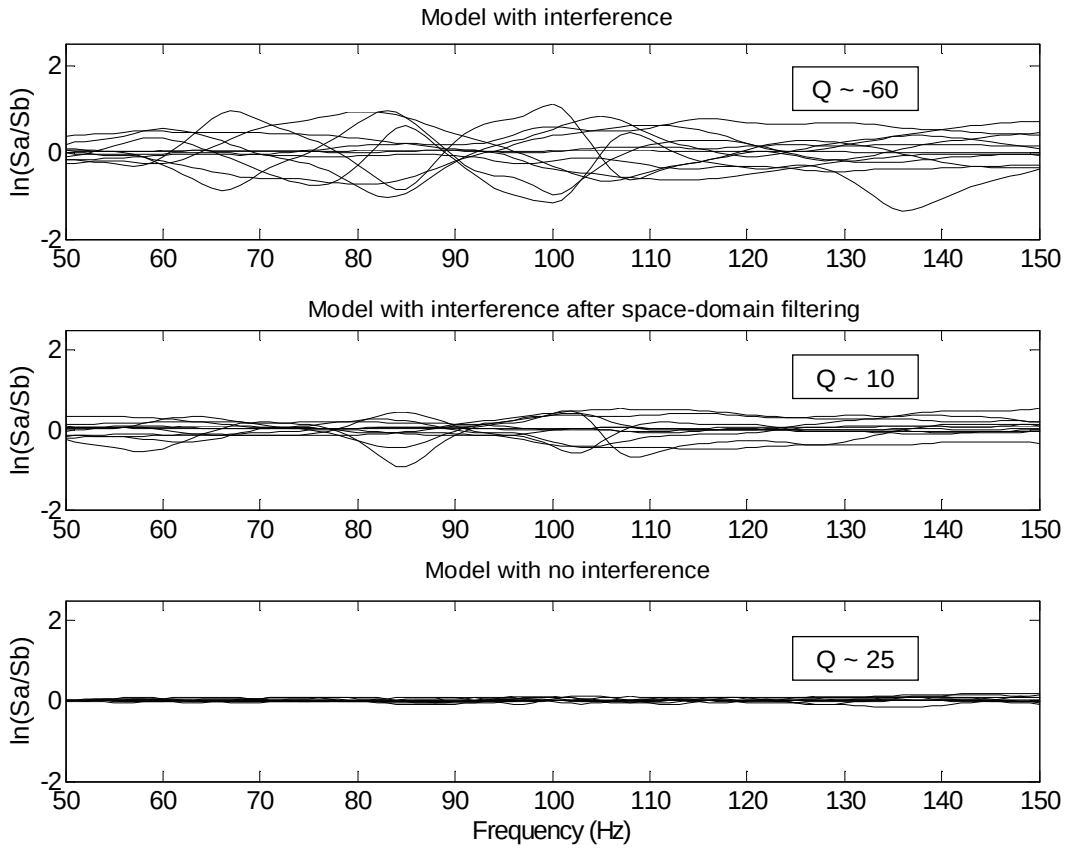


Figure 4.2 6 To compute the Q factor using the spectral-ratio method, the slope m of the line is used, which corresponds to $\frac{\pi \Delta t}{Q}$ . The effect of interference is shown, which results in very unstable Q estimates.

This result is consistent with the findings of Spencer et al. (1982) who observed that for small receiver separations, the variability in the spectra caused by the impedance series local to the receiver is too large to extract meaningful attenuation values characteristic of the medium between the receivers. Consequently, Spencer et al. (1982) recommended using a minimum receiver separation which ensures the attenuation approaches its mean value; they also showed that in the case of thin layering and large attenuation this minimum separation increases. For Q = 50 and a layer thickness of 1.5 m, they suggested that a 60 m separation should yield reasonable Q estimates. The implication for the LLNL experiment, where the receiver separation is small (~3 m), is that interval Q values on the receiver separation scale may not be meaningful. However, given the presence of thin layering suggested from log information (in the order of 0.2m) and the presence of large attenuation observed in the field data (Figure 3.4.2), the interval Q values may be meaningful for separations in the order of 10 m.

As shown from above, the near-field, local impedance, and interference phenomena affect the attenuation estimates derived from both time-domain and frequency-domain methods. Given that these factors are not related to the transmissivity of the medium between the receivers, they are treated as pseudo-Q factors. It is also important to note that none of the conditions I-III are met in the experimental geometry at LLNL, therefore, in our study we made a distinction between $Q_{scattering}$ corresponding to the transmissivity of the medium between the receivers, and $Q_{apparent\text{-}scattering}$ corresponding to the combined effect of $Q_{scattering}$ and the pseudo-Q factors. Aside from small fluctuations, the synthetics for the 'no interference' model agree well with the analytical model, yielding $Q_{scattering}$, computed from (2.2.1.2), on the order of 100. Hence, it was verified that the theoretical formulation of Shapiro et al. (1994) captures the attenuation in the elastic synthetic data, if the synthetics honor conditions I-III. On the other hand, in the presence of local impedance and interference effects (Figure 4.2.4), the Q values are underestimated, and the measured $Q_{apparent\text{-}scattering}$ is on the order of 40. The presence of the near-field causes further apparent attenuation and results in $Q_{apparent\text{-}scattering}$ on the order of 10 (Figure 4.2.1).

## 4.3 Effect of Variance on 1D Scattering

As discussed previously, the reflectivity series for the LLNL profile was not known. Although the low-frequency profile could be inferred from the log description and seismic data, an assumption for the level of the high-frequency fluctuations was introduced. The approach followed was to construct the high-frequency variations based on a reasonable variance range determined for the geological setting at LLNL, thereby predicting minimum and maximum scattering attenuation estimates. Typical variances range from 0.004 to 0.009, however, for near-surface materials perhaps higher variances may be expected. Hence, in the models a $C_{\rho c}(0)$ range from 0.0031 to 0.0186 was considered. Figure 4.3.1 shows the impedance series and peak amplitude decay computed from the elastic finite-difference synthetics for a plane wave. The measured $Q_{apparent\text{-}scattering}$ range was in the order of 10 to 5, for the lower and upper variances respectively. As predicted from equation (4.1.16), as the variance increases, the Q factor decreases, hence the peak amplitude decay is more pronounced. In addition, the observed fluctuations of peak amplitude with depth increase with increasing variance, as the interference and local impedance effects become more prominent. This suggests that

there is an additional benefit of using the peak amplitude decay method to separate scattering vs. intrinsic attenuation: in the absence of an intrinsic attenuation mechanism, for short receiver separations, fluctuations should be large, however, if intrinsic attenuation is present, the peak amplitude decay curve should be smooth. This point is revisited in Chapter 7 which addresses intrinsic attenuation. Lastly, it is concluded that the amplitude decay method is more stable for Q estimation with prominent interference effects than frequency-domain methods such as spectral ratio, given that time-domain methods of Q measurement smooth out the effect of different frequencies, therefore, they are less affected by zeros in the spectrum resulting from destructive interference at discrete frequencies.

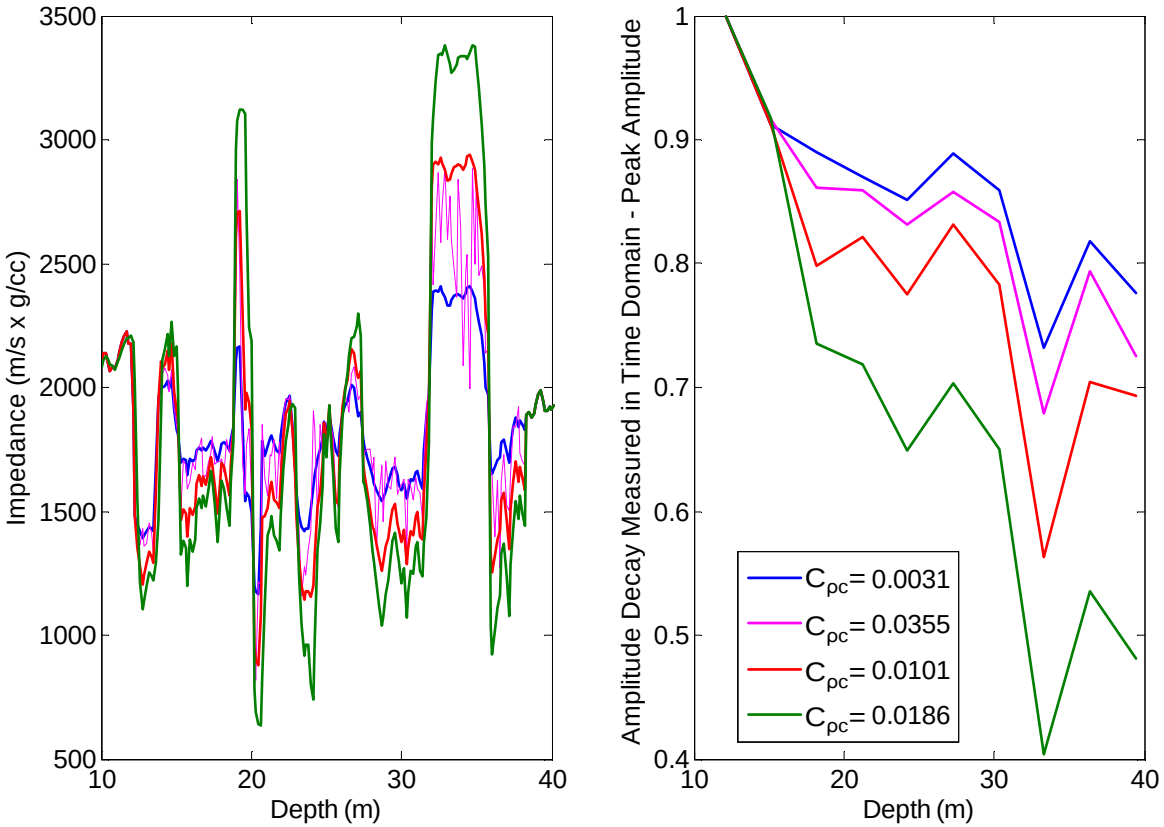


Figure 4.3 1Impedance series (left) and peak amplitude decay of the first arrival versus depth (right) computed from elastic finite-differences using the LLNL profiles with a variance, $C_{\rho c}(0)$, range of 0.0031 to 0.0186. Higher variance results in higher amplitude attenuation and more pronounced fluctuations in amplitude due to interference phenomena.

## 4.4 References


Backus, GE. “Long-wave elastic anisotropy produced by horizontal layering,” Journal of Geophysical Research, Vol. 67, 4427-4440, 1962.

Banik, NC, Lerche, I, and Shuey, RT.1985, “Stratigraphic filtering, Part I : Derivation of the O’Doherty-Anstey formula,” Geophysics, Vol. 50, 2768; “Part II: Model spectra,” Geophysics, Vol. 50, 2775, 1985.

Fuchs, K, and Müller, G. “Computation f synthetic seismograms with the reflectivity method and comparison with observation,” Geophys. J. Roy. Astr. Soc., Vol. 23, 417-433, 1971.

Johnston, DH, and Toksöz, “Definitions and Terminology”, in Toksöz, MN., and. Johnston, DH. “Seismic Wave Attenuation,” Society of Exploration Geophysicists: Geophysics reprint series, chapter I, 1-5, 1981.

Larsen, S, Wiley, R, Roberts, P, and House, L. “Next-generation numerical modeling: incorporating elasticity, anisotropy and attenuation,” Society of Exploration Geophysicists Annual International Meeting, Expanded Abstracts, 1218-1221, 2001.

O’Doherty, RF, and Anstey, NA. “Reflections on amplitudes,” *Geoph. Prosp.*, Vol. 19, 430-458, 1971.

Shapiro, SA, Zien, H, and Hubral, P. “A generalized O’Doherty-Anstey formula for waves in finely layered media,”Geophysics, Vol. 59, 11, 1760-1762, 1994.

Shapiro, SA, and Kneib, G. “Seismic attenuation by scattering: Theory and numerical results,” Geophysical Journal International, Vol. 114, 373-391, 1993.

Shapiro, SA, and Zien, H. “The O’Doherty-Anstey formula and localization of seismic waves,” Geophysics, Vol. 58, 5, 736-740, 1993.

Spencer, TW, Sonnad, JR, and Butler, TM. “Seismic Q-Stratigraphy or dissipation,” Geophysics, Vol. 47, 1, 16-24, 1982.

White, B, Sheng, P, and Nair, B. “Localization and backscattering spectrum of seismic waves in stratified lithology,” Geophysics, Vol. 55, 9, 1158-1165, 1990.

# Chapter 5

## The Effect of the Near-field on Shallow Seismic Studies

Seismic studies in the near-surface typically involve path lengths that are on the order of a wavelength. For such short path lengths, it is shown that the near-field is strongly present in the recorded waveforms, thereby affecting parameter estimation. Several authors have analyzed the effects of the near-field in specific problems, attempting to either mitigate these effects, as in the case of cylindrical beamformers in seismic surface wave velocity estimation (Zywicki and Rix, 2005), or revise the description of the problem to include the effects of the near-field, as in the case of shear wave splitting (Favier et al. 2004), the signature of an air gun array (Ziolkowski et al., 1982), and virtual refractions due to the violation of the far-field approximation (Mikesell et al., 2008). Starting with the traditional definition of the near-field as "all positions within a small fraction of a wavelength from the source" (Aki and Richards, 1980), this chapter firstly shows that the near-field is indeed an issue in shallow seismic studies. Using the solution of the elastic wave equation in a homogeneous medium for a source monopole, which is the appropriate description for an elastic impact source, the contribution of the near-field to the total solution is estimated.

Motivated by the many geophysical techniques that rely on the far-field approximation, such as Kirchhoff migration and Q measurement, the issues involved in near-field suppression and removal are analyzed. It is shown that methods such as time-domain or polarization filtering are inadequate for near-field removal in realistic media. Given this, the task at hand becomes that of incorporating the near-field effects in parameter estimation in the near surface. It is established that accurate representation of the near-field requires 3D elastic modeling.

The effects of the near-field in shallow seismic studies which are analyzed in this chapter are Q measurement, rotation of 3-component sensors, and migration.

Contrary to reflection studies, which involve 2-way propagation, the VSP geometry involves 1-way propagation and, thus, parameter estimation is more likely to be impacted by the presence of the near-field. This experimental study is an example of biased Q estimates when one does properly account for the near-field.

In relation to the effect of the near-field in rotation of 3-component sensors, it is shown that the direction of maximum energy of the first arrival does not coincide with the direction of the P-wave given by Snell's law, which itself assumes plane waves. This suggests that in order to accurately rotate the 3-component sensors the near-field effect must be taken into account.

With respect to migration, a number of investigators have reported on the issues regarding shallow seismic data. These include structural complexities with strong lateral velocity variations, steep dips, wide apertures, and coherent noise such as ground roll or air waves (Bradford et al., 2002; Bradford et al., 2006; Pasasa et al., 1998). In the face of these issues, these studies establish the advantage of Prestack Depth Migration over Poststack Migration. Nevertheless, to the best of my knowledge, the effect of the near-field in migration has not yet been assessed. To this end, migration results of synthetic data for a shallow scatterer are presented, which compare migration of the total field to migration of the far-field using Kirchhoff Migration. For short source-target-receiver distances, it is shown that Kirchhoff Migration is affected by the near-field, a result that is consistent with the fact that Kirchhoff Migration uses a far-field approximation

(Yilmaz, 1987). Hence, migration in the near-field may be more efficient with elastic Reverse-Time schemes, should they incorporate source descriptions for a monopole source. This assertion merits further study.

## 5.1 The Near-Field for a Monopole Source

One of the common sources used in shallow seismic studies is an elastic impact source, such as a hammer or weight-drop, described mathematically by a monopole in the z-direction. Such a point source F(t) = G g(t), for G constant and g the time-dependent source function, acting in the z-direction in an unbounded homogeneous elastic solid, results in a displacement (White, 1965):

$$U_r = \frac{G\cos\theta}{4\pi r\rho}\left\{\frac{2}{r^2}\int_{\frac{r}{V_P}}^{\frac{r}{V_S}} t'\,g(t-t')dt' + \frac{1}{V_P^2}\,g\left(t-\frac{r}{V_P}\right)\right\} \tag{5.1.1}$$

$$U_\theta = 0 \tag{5.1.2}$$

$$U_\phi = \frac{G\sin\theta}{4\pi r\rho}\left\{\frac{1}{r^2}\int_{\frac{r}{V_P}}^{\frac{r}{V_S}} t'\,g(t-t')dt' + \frac{1}{V_S^2}\,g\left(t-\frac{r}{V_S}\right)\right\} \tag{5.1.3}$$

Here, $U_r$, $U_\theta$, and $U_\varphi$ are the displacement components in spherical coordinates (Figure 5.1.1) while $V_p$ and $V_s$ are the primary and shear wave velocities, and $\rho$ is the density. The integral terms, which die off as $1/r^3$ , are referred to as the "near-field" terms to indicate that they are important only at close distances. The terms proportional to 1/r, on the other hand, are called the "far-field" terms as they dominate the solution at far distances from the source. If we let

$$g^I(t) = \int_{-\infty}^{t} g(t')dt \tag{5.1.4}$$

$$g^{II}(t) = \int_{-\infty}^{t} g^I(t')dt \tag{5.1.5}$$

the first integral in expression (1) becomes

$$\int_{r/V_p}^{r/V_s} t'\,g(t-t')dt = \frac{r}{V_p}g^I\left(t-\frac{r}{V_P}\right) - \frac{r}{V_s}g^I\left(t-\frac{r}{V_S}\right) + g^{II}\left(t-\frac{r}{V_P}\right) - g^{II}\left(t-\frac{r}{V_S}\right) \tag{5.1.6}$$

As shown in White (1965), substitution of (6) into expressions (1) and (3) gives

$$U_r = \frac{G\cos\theta}{4\pi r\rho}\left\{\frac{1}{V_p^{\,2}}\,g\left(t-\frac{r}{V_p}\right) + \frac{2}{rV_p}\,g^I\left(t-\frac{r}{V_p}\right) + \frac{2}{r^2}\,g^{II}\left(t-\frac{r}{V_p}\right) - \frac{2}{rV_s}\,g^I\left(t-\frac{r}{V_s}\right) - \frac{2}{r^2}\,g^{II}\left(t-\frac{r}{V_s}\right)\right\} \tag{5.1.7}$$

$$U_\phi = \frac{G\sin\theta}{4\pi r\rho}\left\{\frac{1}{rV_p}g^I\left(t-\frac{r}{V_p}\right)+\frac{1}{r^2}g^{II}\left(t-\frac{r}{V_p}\right)\right.$$
$$\left.-\frac{1}{rV_s}g^I\left(t-\frac{r}{V_s}\right)-\frac{1}{r^2}g^{II}\left(t-\frac{r}{V_s}\right)-\frac{1}{V_s^2}g\left(t-\frac{r}{V_s}\right)\right\} \qquad (5.1.8)$$

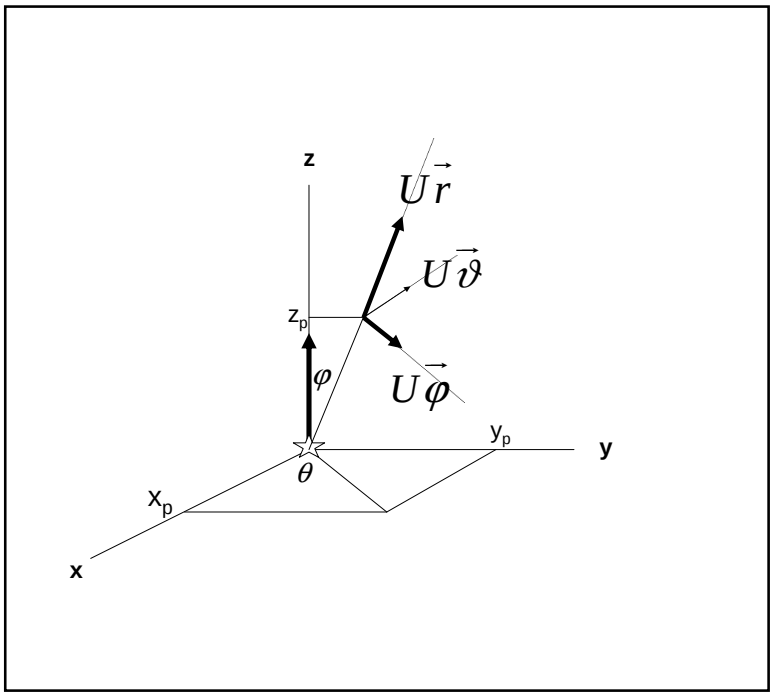


Figure 5.1 1Displacement components at point P: ($x_p$,$y_p$,$z_p$) shown in spherical coordinates for a point source at the origin, which is a monopole in the positive z-direction.

As seen in expressions (5.1.7) and (5.1.8), the far-field in the r- and φ-components arrives, respectively, at the primary and shear wave velocity. It has, moreover, the same waveform as the force. The near-field, on the other hand, arrives in both components with the P-wave velocity and has duration $r/V_s - r/V_p + T$, where T is the duration of the source function. The near-field waveform has two components, both being integrals of the force function and, consequently, of lower frequency than the far-field.

To calculate the relative contribution of the near-field to the total solution as a function of distance, using (5.1.7) and (5.1.8), we generate the synthetic velocity seismograms for a homogeneous medium with properties $V_p$=3000 m/s, $V_s$=1500 m/s, and $\rho$=2.1g/cc, and a 100-Hz Gaussian source monopole for the force function in the z-direction (Figure 5.1.2). Figure 5.1.3 shows the r- and φ-components of the total and near-field responses as a function of distance. As expected, the near-field dies off faster with distance than the far-field, resulting in an arrival frequency spectrum that transitions from lower to higher frequency as distance increases (Figure 5.1.4).

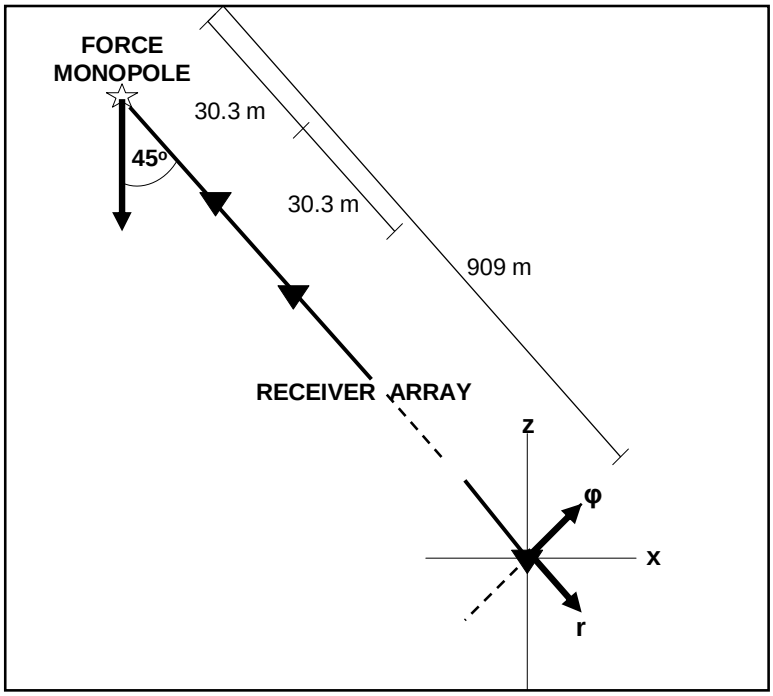


Figure 5.1 2Acquisition geometry which shows the direction of the monopole source z- and the r- and φ- components of the receiver that correspond, respectively, to the P-wave and S-wave displacement directions.

The effect of the near-field on an arrival spectrum is the opposite of what would be expected by attenuation. Attenuation describes the loss of seismic energy of a propagating seismic plane wave in a medium. It is commonly measured by the attenuation coefficient α, defined as the exponential decay constant of the amplitude *A* of a plane wave traveling a distance *x* in a homogeneous medium (Toksöz and Johnston, 1981):

$$A(x) = A_o e^{-\alpha x} \tag{5.1.9}$$

The Q (quality) factor is defined as:

$$\frac{1}{Q} = \frac{aV}{\pi f} \tag{5.1.10}$$

where *V* is the phase velocity and *f* is the frequency. Since the attenuation is associated with a particular mode of wave propagation, setting *V* equal to $V_p$ and measuring the amplitude decay of the P-wave arrival with distance, yields the spatial Q factor for a P-wave.

To correct for the curvature of the wavefront resulting from a point source, it is common to apply a spherical divergence factor prior to measuring attenuation. If the source is a monopole, however, the spherical divergence correction recovers the amplitude loss of only the far-field term. Therefore, the attenuation values obtained from propagation distances in the near field using the far field corrections are severely underestimated. To demonstrate this, we consider a homogeneous elastic medium, where the attenuation is zero by definition, and measure the amplitude in the time-domain of the seismograms after spherical divergence correction. The result is an apparent loss of

amplitude (Figure 5.1.5). In particular, for the model parameters given above, the near-field constitutes approximately more than 30% and 10%, respectively, of the total amplitude at distances of 50m and 150m. Clearly, when total propagation distances are short, it is necessary to account for or remove the effect of the near-field prior to measuring attenuation.

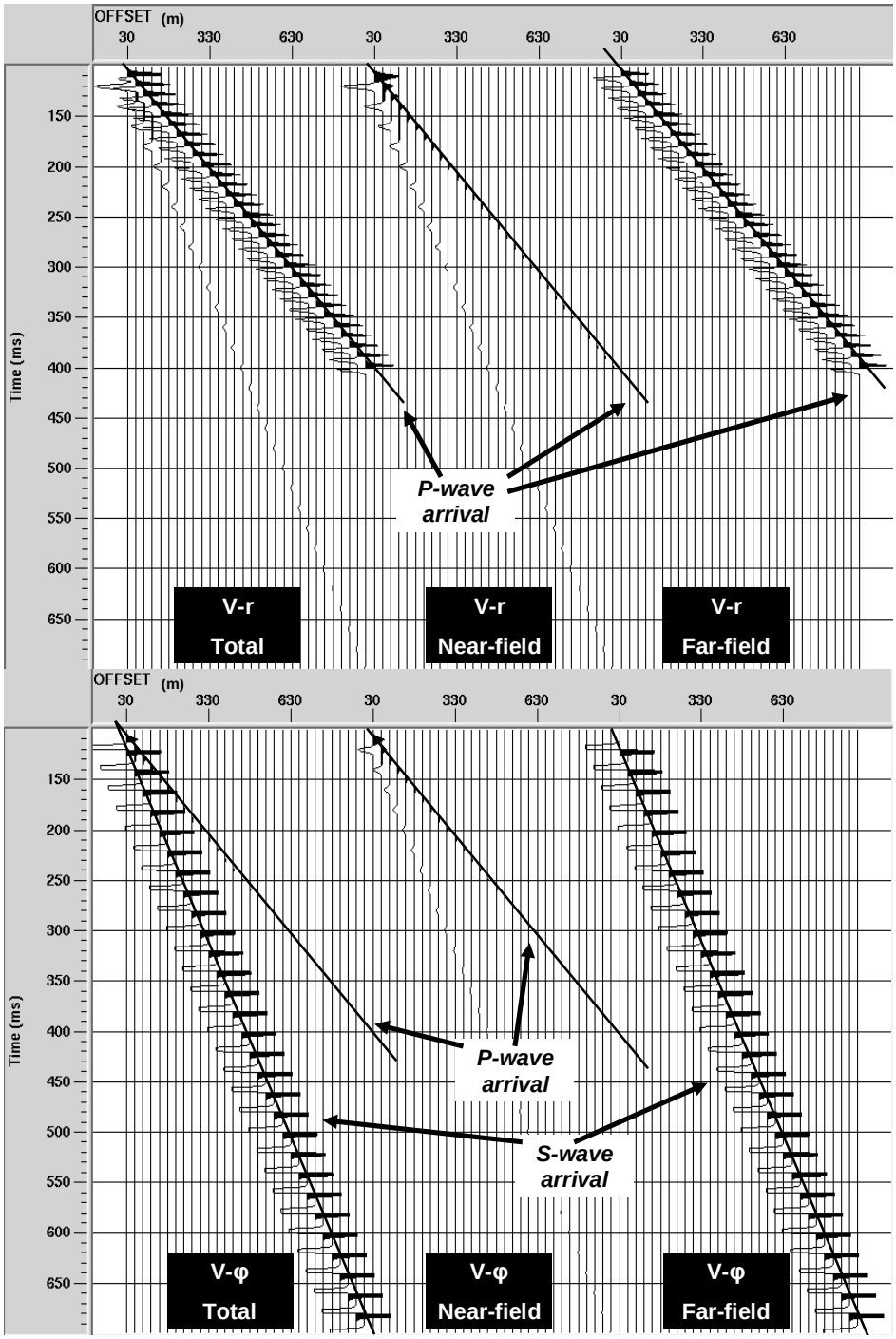


Figure 5.1 3 Synthetic velocity seismograms computed for the geometry shown in Figure 5.1.2 for a 100Hz Gaussian source monopole. The medium properties are $V_p$=3000m/s, $V_s$=1500m/s, ρ=2.1g/cc. The display shows the total, near-, and far-field terms of the r-component (top) and the φ-component (bottom) with no scaling between the traces.

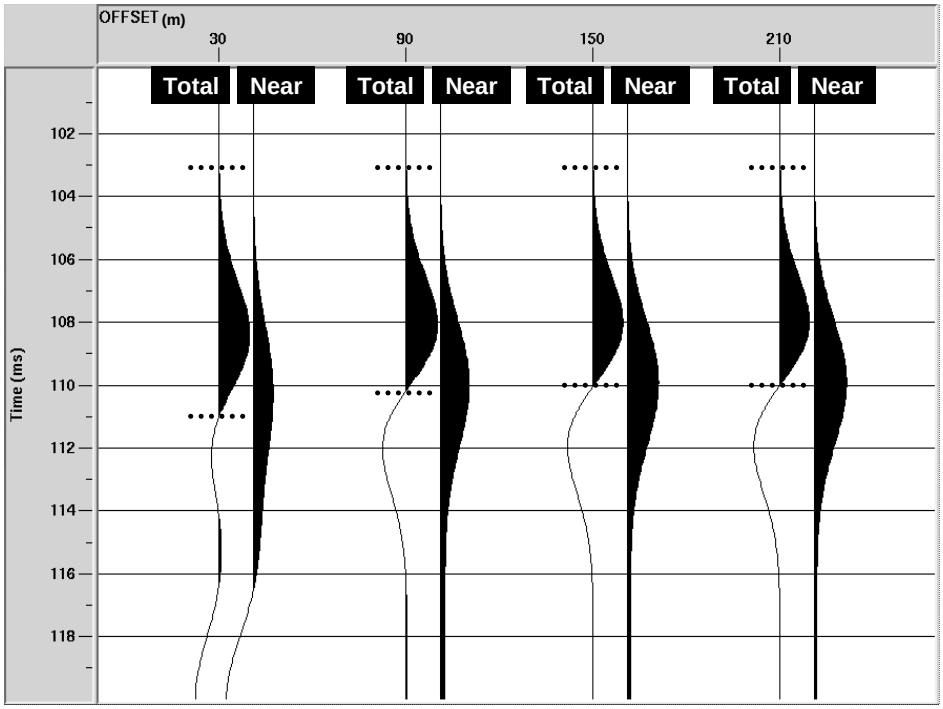

Figure 5.1 4 Selected offsets of the synthetic velocity seismograms of the total and near-field r-component, as computed in Figure 5.1.2, with traces aligned to the first-break time and scaled to their individual maximum values. The dashed lines show the change in frequency of the total field with distance resulting from the near-field attenuation with distance, which is lower frequency than the far-field.

Given that the near-field spectrum has lower frequency than the far-field spectrum, it seems reasonable to assume that the near-field could be removed through time-domain filtering. Indeed, differentiation and application of a zero-phase 75-80-190-200 Butterworth filter results in suppression of the near-field, which improves the attenuation measurements computed from the average velocity amplitudes in a homogeneous medium (Figure 5.1.5).

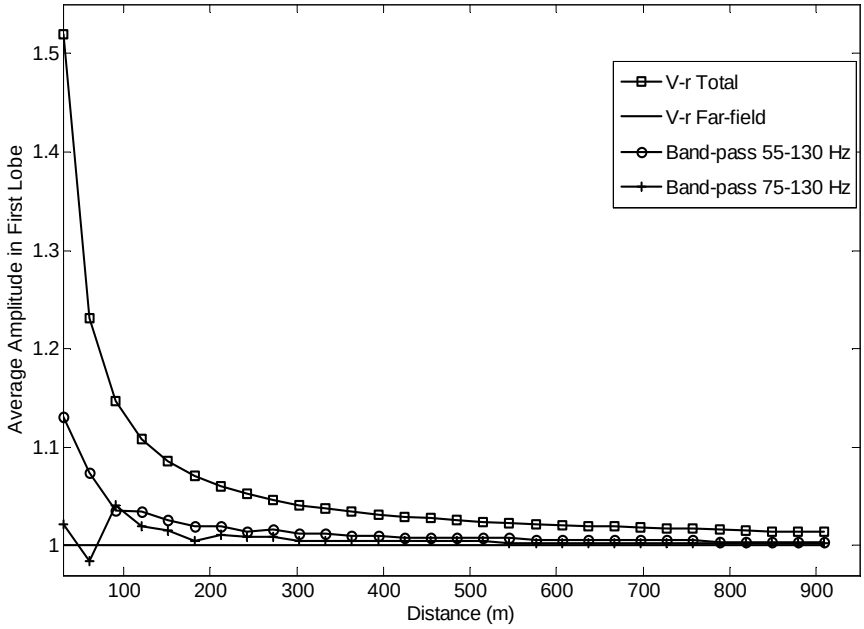


Figure 5.1 5Average amplitude in the time domain of the total solution, and far-field solutions as a function of distance, computed for 100Hz Gaussian source monopole in a homogeneous medium with properties $V_p$=3000m/s, $V_s$=1500m/s, $\rho$=2.1g/cc measured after spherical divergence.

A second potential for near-field removal is polarization filtering. As shown in equations (5.1.7) and (5.1.8), the near-field is proportional in the r- and φ-components. To remove the near-field, we define:

$$U_{hybrid} \equiv U_r - 2\cot(\vartheta)U_\phi = \frac{G\cos\theta}{4\pi r\rho}\left\{\frac{1}{V_p^{\,2}}g\left(t-\frac{r}{V_p}\right)-\frac{2}{V_s^{\,2}}g\left(t-\frac{r}{V_s}\right)\right\} \qquad (5.1.11)$$

Here, the subscript hybrid indicates the very fact that the new displacement time series contains both the r- and φ- components of displacement. If the distance is large enough for the P- and S-wave arrivals to be time-separated, so that the far-field S-wave does not interfere with the far-field P-wave, then $U_{hybrid}$ contains only (i) the far-field P-wave as the P-arrival, and (ii) a scaled S-wave, which arrives later in the record and thus does not interfere with the first lobe (Figure 5.1.6).

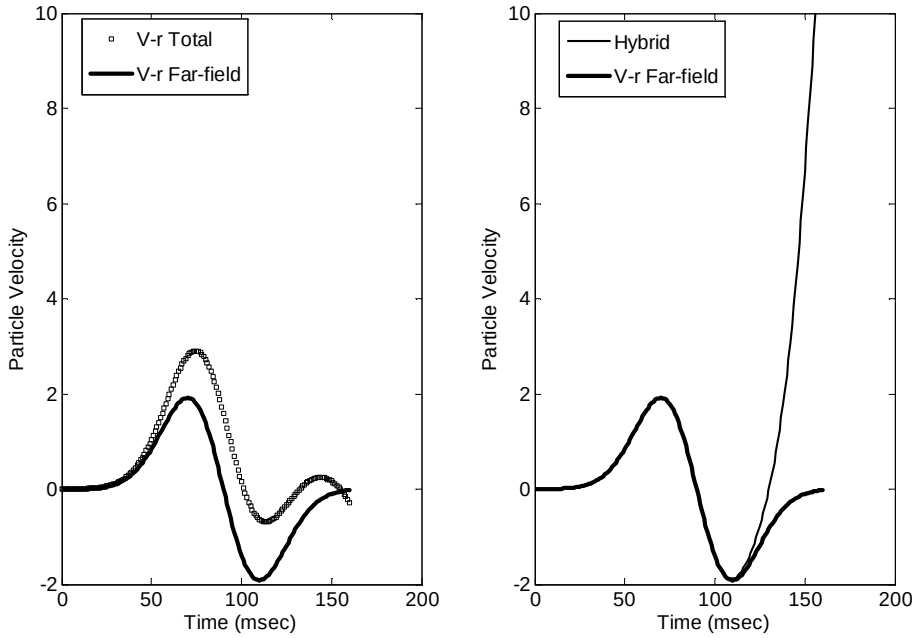


Figure 5.1 6 Comparison between the velocity r-component of the total and far-fields vs. the 'hybrid' component.

We evaluated whether the construction of the hybrid component can be applied to 3-component sensors for a 1D medium. We modeled a three-layer medium (Figure 5.1.7) and computed the synthetic solution for two geometries: (i) a source embedded in the near-field and (ii) a source in the far-field but with identical angles of incidence to the first plane boundary. The source used was a 100-Hz Gaussian monopole force in the z-direction. The synthetics were computed using the 3D finite-difference code E3D (Larsen et al., 2001) both for the acoustic as well as for the elastic model.

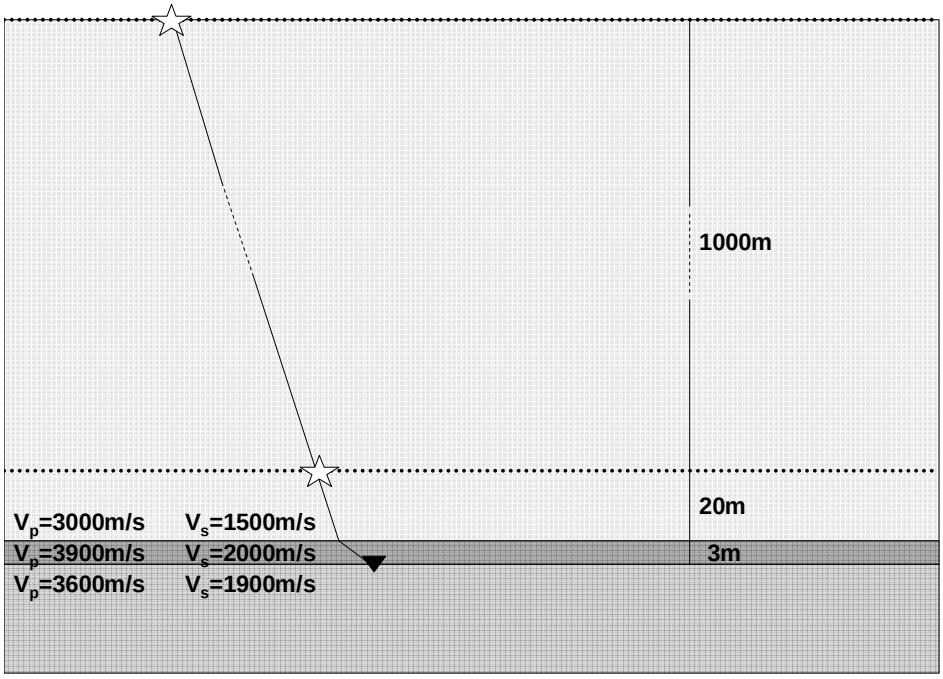

Figure 5.1 7 Model parameters for the synthetics computed for a close and remote source (asterisks).

For the acoustic medium, the hybrid component constructed for the source in the near-field has the same waveform as the r-component for the source in the far-field (Figure 5.1.8). In the acoustic case, therefore, it is possible to remove the near-field using 3-component data. In general, the near-field signature is identical for an acoustic and an elastic homogeneous medium in the time interval $r/V_p$ to $r/V_s$. The difference, however, is that, in the acoustic medium, the near-field displacement will monotonically increase with time after the point $r/V_s + T$; this corresponds to the limit $V_s \rightarrow 0$ in expression (5.1.1). In this sense, the solution for a force monopole in an acoustic medium is a-physical; yet, it may be used for the purposes of modeling the near-field.

For a 1D elastic medium, the hybrid component does not remove the near-field correctly (Figure 5.1.9). A plausible explanation is that the initial P-wave is subsequently converted to S-wave reflections and refractions which contain both converted near- as well as far-field terms, causing interference with the P-wave that is measured in the first lobe of the r-component. Even though our explanation is not mathematically founded in this paper, our results demonstrate that in realistic media a polarization filter may not be effective in removing the near-field.

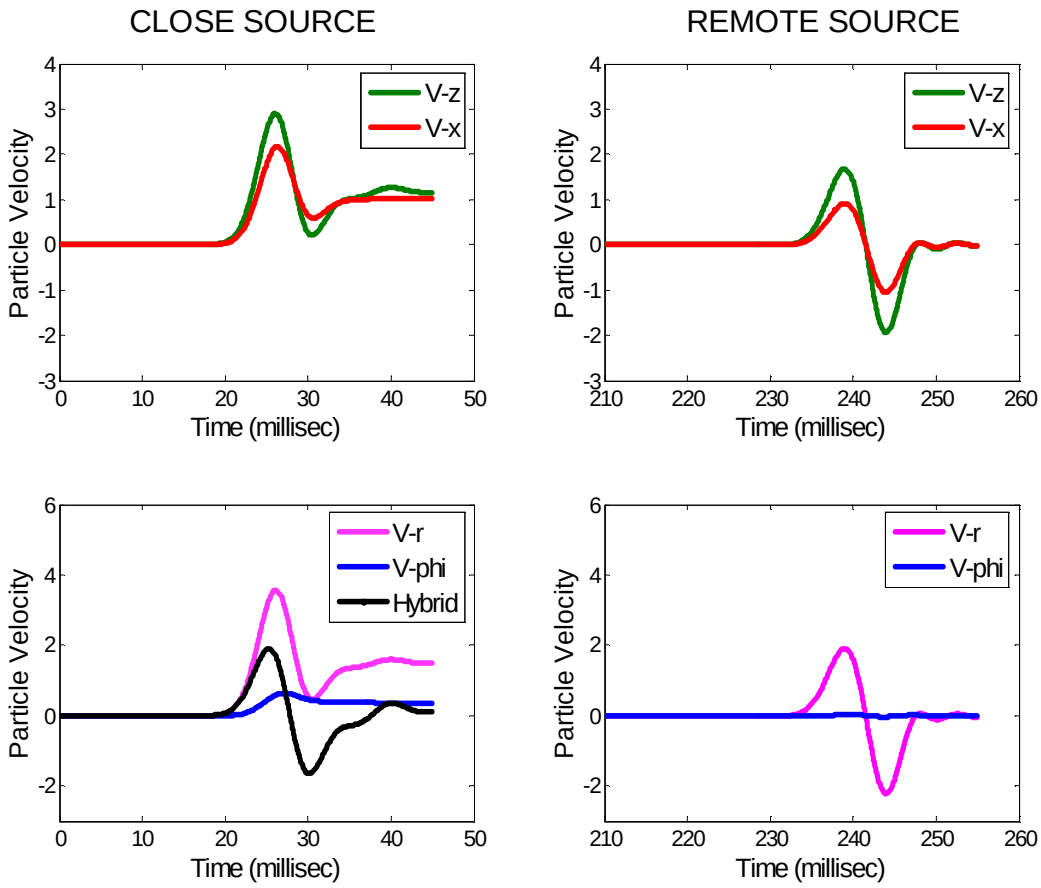


Figure 5.1 8 Synthetic acoustic velocity seismograms for the shot location close to the receiver (left) and the remote source (right). After rotation of the V-z and V-x components to the r- and φ-component, the 'hybrid' component is computed for the source in the near-field (bottom left) which has the same waveform over its first lobe as the r-component of the source in the far field (bottom right).

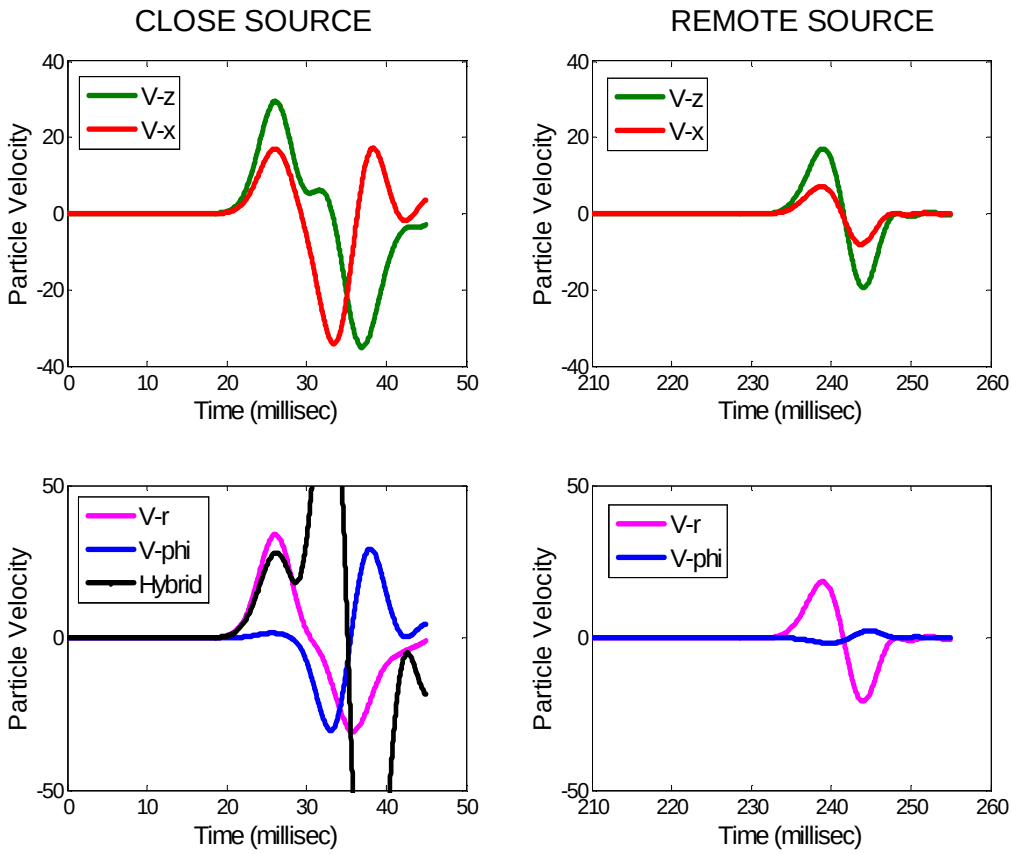


Figure 5.1 9 Synthetic elastic velocity seismograms for the shot location close to the receiver (left) and the remote source (right). After rotation of the V-z and V-x components to the r- and φ-component, the 'hybrid' component computed for the source in the near-field (bottom left) does not match the r-component of the source in the far field (bottom right).

## 5.2 The Near-field in Realistic Media: Implications to Q Measurement

As already discussed, the presence of the near-field causes the attenuation values to be underestimated. It also masks the Q behavior as a function of frequency via an apparent loss of amplitude of the lower frequencies with distance. Given the short offsets involved in this study, along with the fact that prop agation is 1-way for a VSP geometry, we expect the effect of the near-field to be non-negligible.

The results show that the near-field by itself causes an apparent amplitude loss of comparable order to the effects of scattering and intrinsic attenuation (Figure 4.2.1). If not accounted for, the near-field bias would result in Q values as low as 3, in lieu of them being in the order of 50 and 10, respectively, for the scattering and intrinsic Q values. To attenuate the near-field, we attempted time-domain filtering which, though, had no significant impact on amplitude measurements of either the recorded waveforms or the elastic synthetics. The question is what this time-domain filtering does to the Q values and whether or not it can suppress the near-field in realistic media.

The effect of differentiating and low-cut filtering has three consequences: i) increasing the center frequency of the data, ii) removing the Q effect of the low frequencies, and iii) possibly removing the near-field. Increasing the center frequency results in a decrease of amplitude as a function of distance for a constant Q. If Q is frequency dependent, then the Q values derived from low-cut filtered data may be smaller or larger compared to the Q values for the unfiltered data, depending on the behavior of Q as a function of frequency, and consequently the result is, respectively, a decrease or increase of amplitude with distance. To check whether time-domain filtering indeed suppresses the near-field, we compared the amplitudes of the elastic synthetic data for the remote source and the source in the near-field after application of the same filter. We found that the Q values for the synthetics of the remote source were overall much larger than the Q values for the synthetics of the source in the near-field. This implies that the near-field occupies a similar frequency band as the far-field, when scattering occurs, and that its suppression through time-domain filtering is not possible. Though we have not yet established the description of a physical mechanism, our data processing results suggest that the combination of scattering, and intrinsic attenuation possibly distorts the near-field spectrum such that it may not occupy solely the low frequencies as it propagates through a heterogeneous medium.

With respect to the dimension of propagation, 2D modeling fails to capture the full effect of the near-field, even with application of the appropriate 2D spreading correction term (Figure 4.2.1). Bleistein (1986) gives 2D to 2.5D correction factors which would be adequate to equate the 2D and 3D synthetic solutions in a 1D heterogeneous medium. His method, however, is based on a far-field approximation which cannot be applied to modeling in the near-field.

Our conclusion is that attenuation measurements in the near-surface require compensation for the near-field while the numerical modeling of the near-field should be in 3D. Moreover, in order to capture the effects of intrinsic attenuation on the total field, it is worthwhile to do 3D viscoelastic modeling, and to assess the effect of different intrinsic attenuation models (e.g. Voigt Q model, Standard Linear Solid) in the attenuation of the near-field. The implication of viscoelasticity on the near-field requires further study.

## 5.3 Rotation in the Near-field

Rotation of 3-component down-hole geophones to the direct P-wave is commonly achieved by searching the direction of maximum energy past the first-break time using a linear regression of the vertical and horizontal components (Figure 5.3.1). Based on this rotation, the φ-component, being perpendicular to the direction of maximum energy (r-component), contains minimum (theoretically zero) energy past the first-break time. This is correct, however, only if the data does not contain any near-field. If, on the other hand, the near-field is non-negligible, the energy past the first-break time is not minimum (i.e., non-zero even theoretically) in the φ-component, as follows from equation (5.1.3).

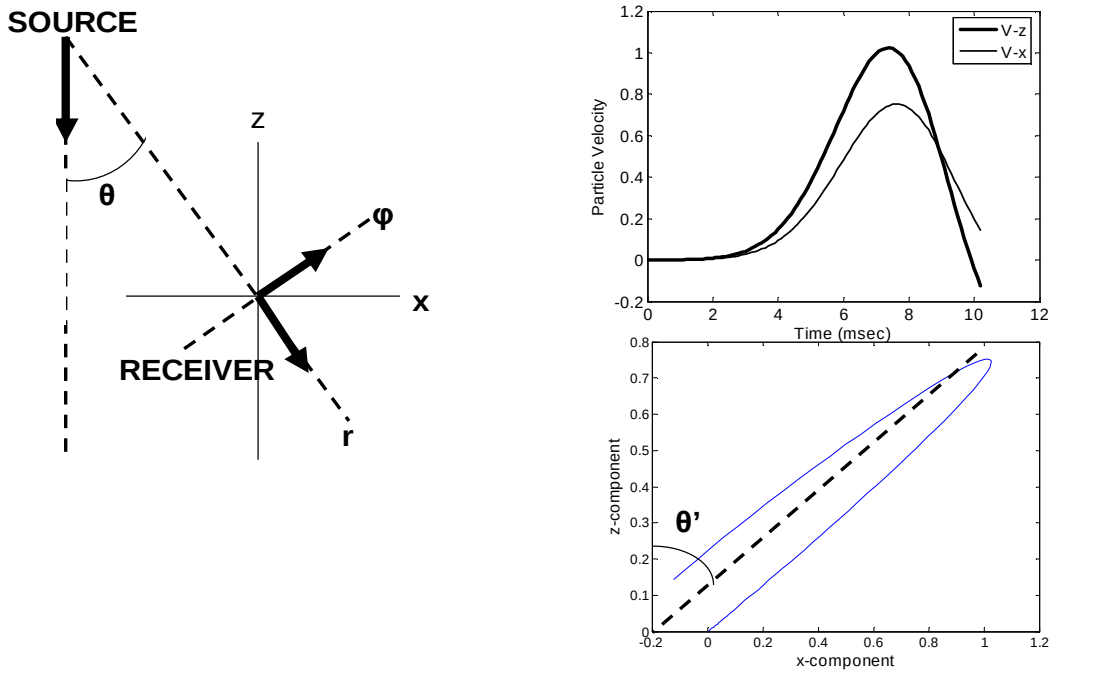


**i) θ** 'deterministic' angle of incidence

**ii) θ'** angle given by linear regression

Figure 5.3 1The concept of the deterministic angle of incidence (left) vs. the angle computed through linear regression through the origin from the V-z and V-x components (right)

The presence of the near-field leads, therefore, to a discrepancy between the deterministic rotation angles derived from raytracing, which obeys Snell's law, and the angles calculated from linear regression of the horizontal and vertical components. Figure 5.3.2 shows the deviation of the deterministic rotation angles from the angles computed by a linear regression between the vertical and horizontal components of the source-receiver plane in a homogeneous medium. The error is higher the shorter the distance to the source, where the near-field is greater, and the larger the angle of incidence, which implies a lower amplitude in the r-component relative to the φ-component.

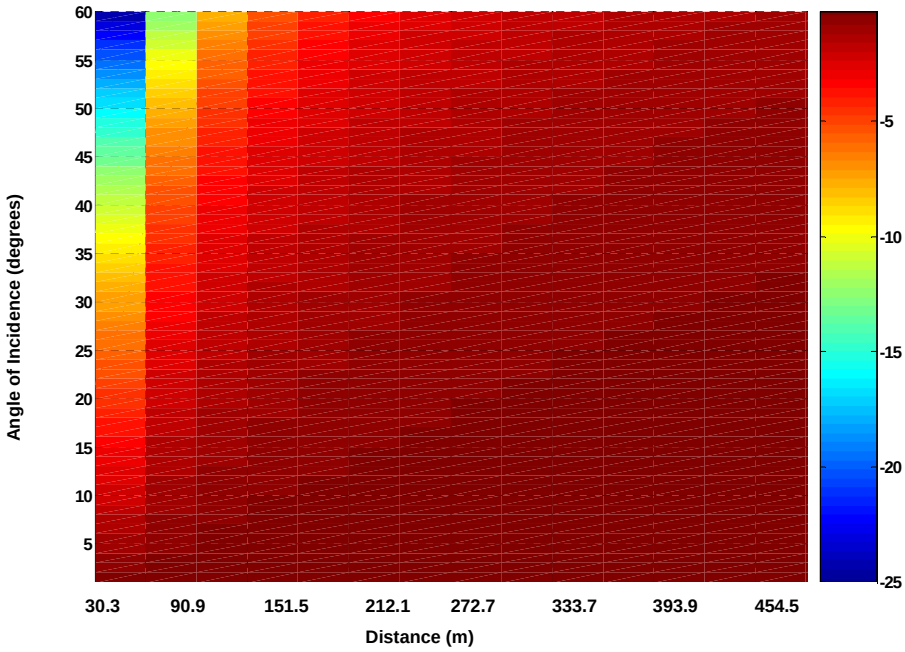


Figure 5.3 2 Deviation of the deterministic angle from the angle computed through linear regression as a function of angle of incidence and distance. The minimum distance computed was 30.3m.

Figure 5.3.3 shows the same result but for the seismograms differentiated and low-cut, which, as previously discussed, suppresses the near-field, minimizing, consequently, the error between the deterministic rotation and a rotation based on linear regression between the source-receiver plane components. Such a discrepancy was noted also in the field data from our VSP experiment; especially, from the receivers closest to the surface, thus, containing more near-field.

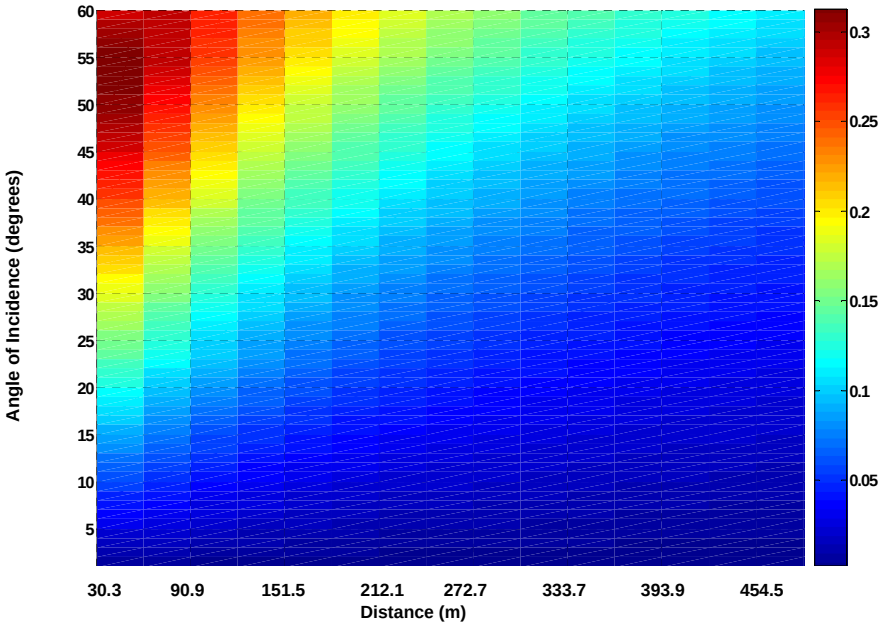


Figure 5.3 3 Deviation of the deterministic angle from the angle computed through linear regression as a function of angle of incidence and distance, after differentiation and low-cut filtering. The minimum distance computed was 30.3m. The error is less than 0.35 degrees.

## 5.4 Effect of the Near-field on Migration

Some of the known issues of migration in the near-surface include lateral velocity variations, wide apertures, steep dips, and coherent noise (such as the air wave and surface waves). We study also the effect of the near-field by comparing the migration results for a point scatterer using the total field and far-field solutions given by expressions (5.3.1)-(5.3.3). Through the concept of an exploding reflector, we constructed the z-component that would be recorded at the surface for a 100-Hz Gaussian force monopole from a point scatterer in a homogeneous medium with $V_p$=3000m/s, $V_s$=1500m/s, and $\rho$=2.1g/cc. We migrated the solution for the total field and the far-field only, for two scatterer depths: 7.5m and 15m. Prestack Kirchhoff time migration of the total field for the 7.5m scatterer results in an approximately 2ms delay relative to that of the far-field (Figure 5.4.1). This result is consistent with the fact that Kirchhoff migration uses a far-field approximation (Yilmaz, 1987), and is thus expected to produce better imaging results where the near-field is negligible. Figure 16 shows the same results for the deeper scatterer at 15m; however, the improvement in the migration results is more subtle between migration of the total and far-fields, given that the near-field has been further attenuated.

Finally, we computed the synthetic solution using 3D elastic finite-differences, by modeling the scatterer as a 9m edge box with twice the impedance of the homogeneous medium. The ground-roll and direct waves were removed through subtraction of the traces computed for the equivalent homogeneous model. Figure 5.4.2 shows the

migration results for the 7.5m and 15m scatterer depths. In addition to the presence of the near-field, the poor imaging results using Kirchhoff migration are further affected by the interference of the P-to-S converted wave with the P-wave reflection. Elastic Reverse-Time migration schemes may handle such interference, and possibly solve issues of migration in the near-field, should they include a description for the source radiation of a monopole, which requires further study. Lastly, to account for intrinsic attenuation effects, migration should include intrinsic attenuation, which is another topic meriting further study.

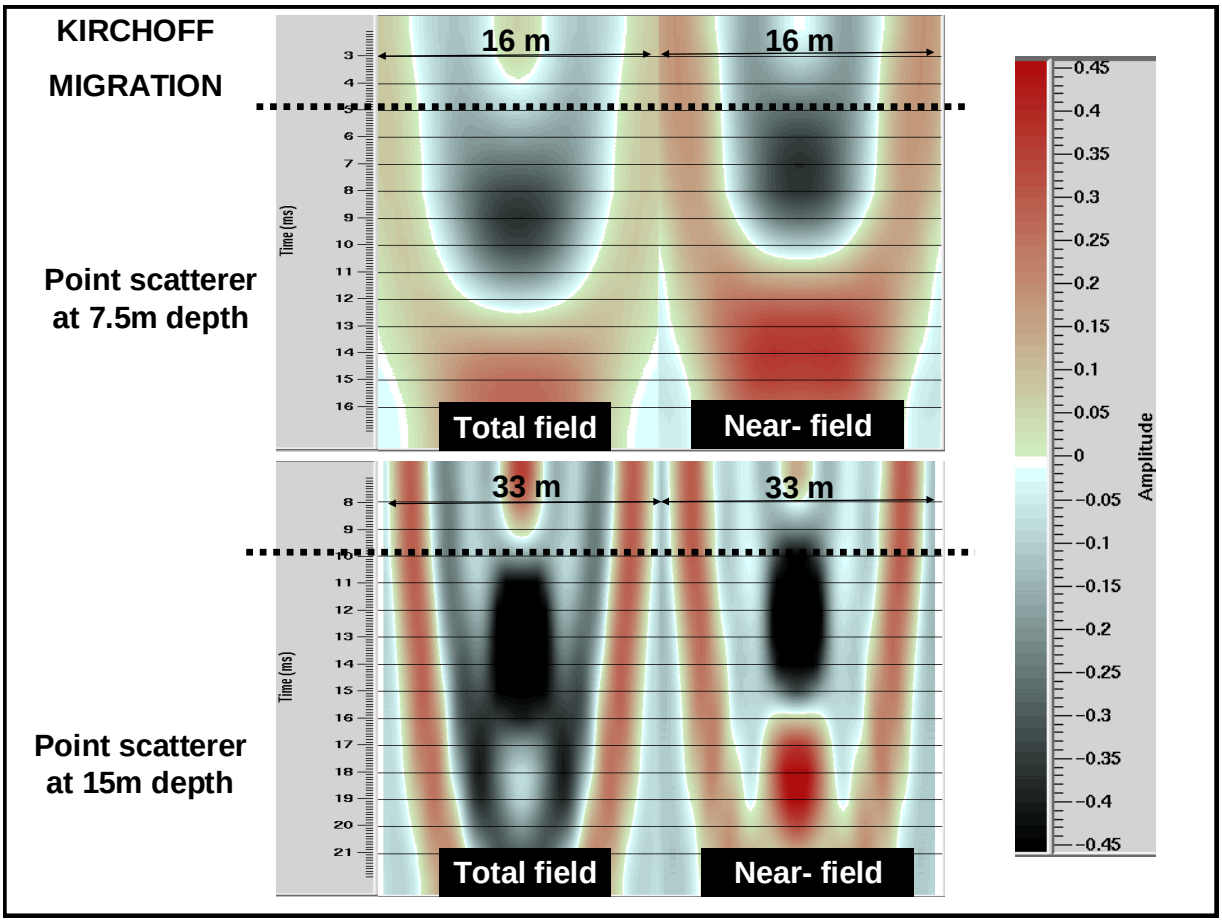


Figure 5.4 1 Migration results for the point scatterer at 7.5m (top) and 15m (bottom) in a homogeneous medium with $V_p$=3000m/s, $V_s$=1500m/s, $\rho$=2.1g/cc and a 100Hz Gaussian source monopole. Kirchhoff migration of the total field results (left) results in a time delay relative to migration of the far-field (right). The delay is more pronounced for the shallow scatterer (~2ms). Dashed line indicates the zero-offset reflection arrival time.

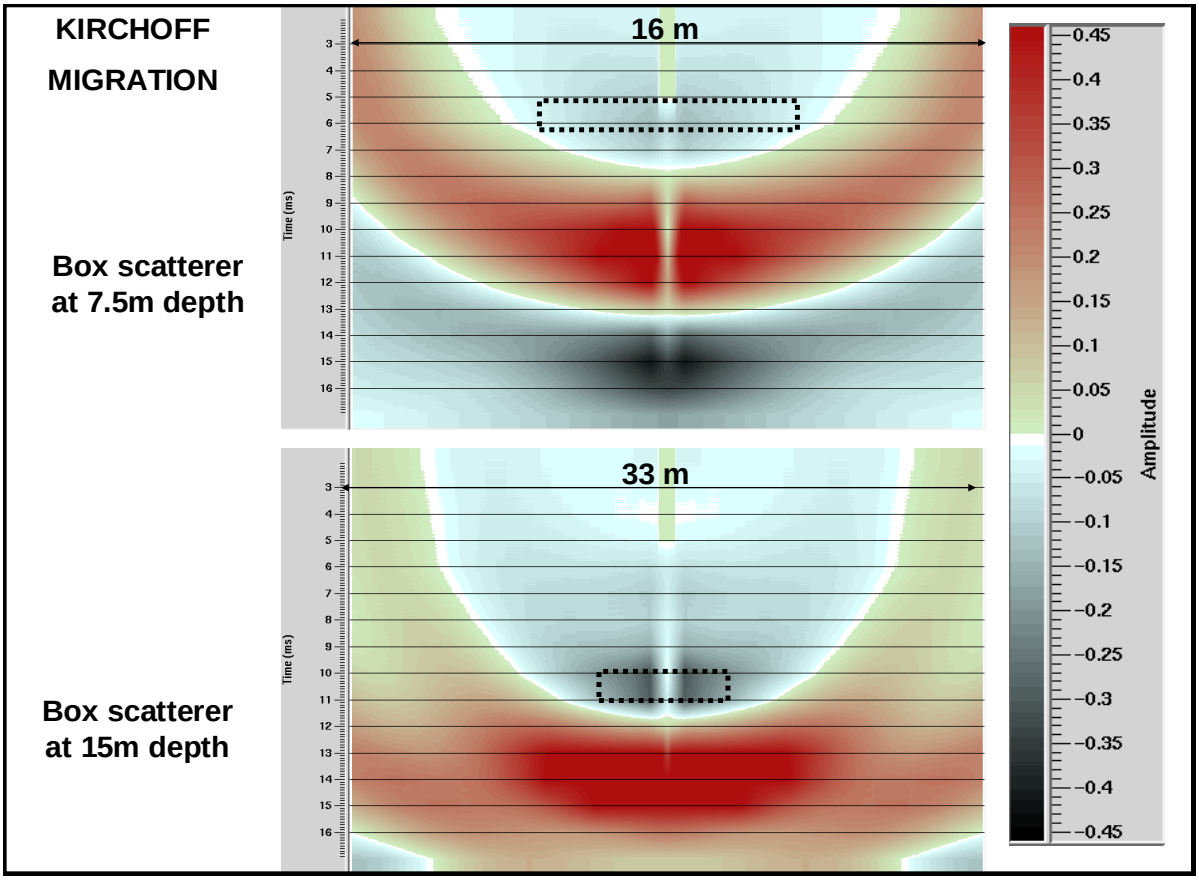


Figure 5.4 2 Migration results for elastic finite-difference synthetics computed for the box scatterer at 7.5m depth (top) and 15 m depth (bottom) in a homogeneous medium with $V_p$=3000m/s, $V_s$=1500m/s, $\rho$=2.1g/cc and a 100Hz Gaussian source monopole. Dashed line shows the expected time and lateral extent of the migrated scatterer.

## 5.5 Summary

Motivated by the fact that most seismic studies in the near-surface involve travel paths comparable to a seismic wavelength, we demonstrate that the presence of the near-field in shallow seismic studies is non-negligible. This is important as most investigators have extrapolated seismic reflection processing for deeper targets to the near surface, without, though, incorporating the near-field in their processing approaches. We show that time-domain filtering and polarization filtering methods fail to remove the near-field in realistic media. Hence, we conclude that parameter estimation in shallow seismic studies has to account for the presence of the near-field. To this regard, we show that modeling of the near-field should be in 3D, and that, in addition, to include the effects of intrinsic attenuation, the modeling should be viscoelastic.

In terms of attenuation measurements in the near-surface, we show that, if not accounted for, the near-field underestimates the Q measurements and distorts the Q behavior as a function of frequency. Moreover, Q estimation with VSP geometry is more affected by the near-field, than it is in reflection studies, as it involves 1-way propagation.

To demonstrate the near-field bias in attenuation, we present results from a VSP experiment conducted at LLNL, where the near-field causes an apparent attenuation of an order comparable to the combined effects of scattering and intrinsic Q. In addition, we show that the presence of the near-field measured in 3-component data produces an error in the rotation angles, which may be minimized through differentiation and low-cut filtering of the seismic data prior to rotation. Finally, we present migration results for a shallow scatterer using Kirchhoff migration and show that the presence of the near-field causes a delay in the migrated sections. In light of this result, we suggest further study of migration in the near-surface with viscoelastic Reverse-Time migration methods.

## 5.6 References


Aki, K, and Richards, PG. “Quantitative Seismology,” W.H. Freeman and Co., 1980.

Baker, GS, Steeples, DW, and Schmeissner, C. “In-situ, high-frequency P-wave velocity measurements within 1 m of the earth's surface,” Geophysics, Vol. 64, 323-325l, 1999.

Bleistein, N, “Two-and-one-half dimensional in-plane wave propagation,” Geophysical Prospecting, Vol. 34, 686-703, 1986.

Bradford, JH, and Sawyer, DS. “Depth characterization of shallow aquifers with seismic reflection PartII: Prestack depth migration and field examples,” Geophysics, Vol. 67, 98-109, 2002.

Bradford, JH, Liberty, LM, Lyle, MW, Clement, WP, and Hess, S. “Case History: Imaging complex structure in shallow seismic-reflection data using prestack depth migration,” Geophysics, Vol. 71, 175-181, 2006.

Favier, N, Chevrot, S, and Komatitsch, D. “Near-field influence on shear wave splitting and traveltime sensitivity kernels,” Geophys. J. Int., Vol. 156, 467-482, 2004.

Johnston, DH, and Toksöz, “Definitions and Terminology”, in Toksöz, MN., and. Johnston, DH. “Seismic Wave Attenuation,” Society of Exploration Geophysicists: Geophysics reprint series, chapter I, 1-5, 1981.

Larsen, S, Wiley, R, Roberts, P, and House, L. “Next-generation numerical modeling: incorporating elasticity, anisotropy and attenuation,” Society of Exploration Geophysicists Annual International Meeting, Expanded Abstracts, 1218-1221, 2001.

Mikesell D, Van Wijk, K, Calvert, A, and Haney, M. “The virtual refraction: useful spurious energy in seismic interferometry,” Geophysics, Vol. 74, 13-17, 2009.

Pasasa, L, Wenzel F, and Zhao, P. “Prestack Kirchhoff depth migration of shallow seismic data,” Geophysics, Vol. 63, 1241-1247, 1998.

Yilmaz, O.“Seismic data processing,” SEG, 1987.

White, JE, “Seismic waves: radiation, transmission and attenuation,” International Series in the Earth Science, McGraw Hill, 1965.

Ziolkowski, A, Parkes, G, Hatton, L, and Haugland, T. “The signature of an air gun array,” Geophysics, Vol. 47, 1413-1421, 1982.

Zywicki, D, and Rix, GJ, “Mitigation of near-field effects for seismic surface wave velocity estimation with cylindrical beamformers,” Journal of Geotechnical and Geoenvironmental Engineering, August Issue, 970-977, 2005.

# Chapter 6
# Scattering in 3D Media

## 6.1 Theoretical Treatment

From forward modeling, it is well known that lateral heterogeneity affects amplitude versus offset (AVO) behavior, hence preprocessing of lateral heterogeneity effects on amplitudes is often necessary prior to AVO inversion used in lithological analysis and direct detection of hydrocarbons (Sen et al., 2007). In addition to AVO behavior, as suggested by Gist (1994) and Müller and Shapiro (2004), lateral heterogeneity also affects amplitudes at vertical incidence. Therefore, in establishing accurate scattering versus intrinsic attenuation estimates, in this study we also considered the effects of 3D heterogeneities.

Müller and Shapiro (2004) used a hybrid Q factor to quantify attenuation in an elastic anisotropic 3D random medium. The hybrid Q factor contains one component caused by 1D scattering ($Q_{1D}$) and a second component caused by random diffractions and refractions ($Q_{diff}$). The derivation of $Q_{1D}$ is described in detail in Shapiro and Hubral (1999) and is similar to the theory presented by Shapiro et al. (1994). The derivation of $Q_{diff}$ is based on the Rytov approximation (Rytov et al., 1989), which takes into account random diffraction and refraction, but neglects backscattering caused by 1D scattering. Diffraction and refraction of randomly distributed heterogeneities result in a random focusing and defocusing of wave energy, and, consequently result in amplitude fluctuations with increasing propagation distances (Müller and Shapiro, 2004). Shapiro and Kneib (1993) showed that the relationship between the variance of log-amplitude variations, $\sigma_\chi^2$, and the coefficient of scattering attenuation, $\alpha$, of a plane wave is :

$$\alpha = \frac{\sigma_\chi^2}{L} \tag{6.1.1}$$

where L is the propagation distance.

For the case of a Gaussian correlation function, $B_n(r) = \sigma_n^2 \exp\left(-\frac{x^2}{a_x^2} - \frac{y^2}{a_y^2} - \frac{z^2}{a_z^2}\right)$, where $a$ stands for the correlation lengths, with $a_x = a_y = a_\perp$ and $a_z = a_\parallel$, and $\sigma_n^2$ is the variance of the squared slowness fluctuations, the log-amplitude variations are in 3D:

$$\sigma_\chi^2 \approx \sigma_n^2 \frac{\sqrt{\pi}}{4} \frac{a_\parallel}{a_\perp} k^3 a_\perp^3 D \left(1 - \frac{\arctan(2D)}{2D}\right) \tag{6.1.2}$$

and in 2D:

$$\sigma_\chi^2 \approx \sigma_n^2 \frac{\sqrt{\pi}}{4} \frac{a_\parallel}{a_\perp} k^3 a_\perp^3 D \left(1 - \frac{1}{\sqrt{2}D} \sqrt{\sqrt{1+4D^2} - 1}\right) \tag{6.1.3}$$

where $D = \frac{L}{(ka_\perp^2)}$ (Müller and Shapiro, 2004).

To account for the scattering and random diffraction and refraction effects, Müller and Shapiro (2004) suggested that $Q_{hybrid}^{-1}$ is a linear combination of the two $Q^{-1}$ factors, such that $Q_{hybrid}^{-1} = Q_{1D}^{-1} + Q_{diff}^{-1}$, which they verified numerically. Equations (6.1.2) and (6.1.3) imply that the importance of random diffractions depends on the

parameter $\gamma = a_{\|} / a_{\perp}$.

6.2 Verification of 3D Scattering Theory

For the LLNL experiment, the computed vertical correlation length, $a_{\|}$, was in the order of 1 m, which implies that the effect of random diffractions is small. Figure 6.2.1 shows the 2D and 3D $Q_{diff}^{-1}$ factors computed for the LLNL series with variance, $C_{\rho v}(0)$, equal to 0.0186 for a range of $\gamma$ values. The maximum $Q_{diff}^{-1}$ factor considered, computed for the maximum variance, assuming 3D heterogeneity and for $\gamma$ equal to 0.2, yields $Q_{diff}^{-1} < 0.005$, whereas $Q_{1D}^{-1}$ is greater than 0.07. In the absence of geostatistical data, we cannot formally justify a $\gamma$ range, yet we found it unlikely that $\gamma$ should be less than 0.2.

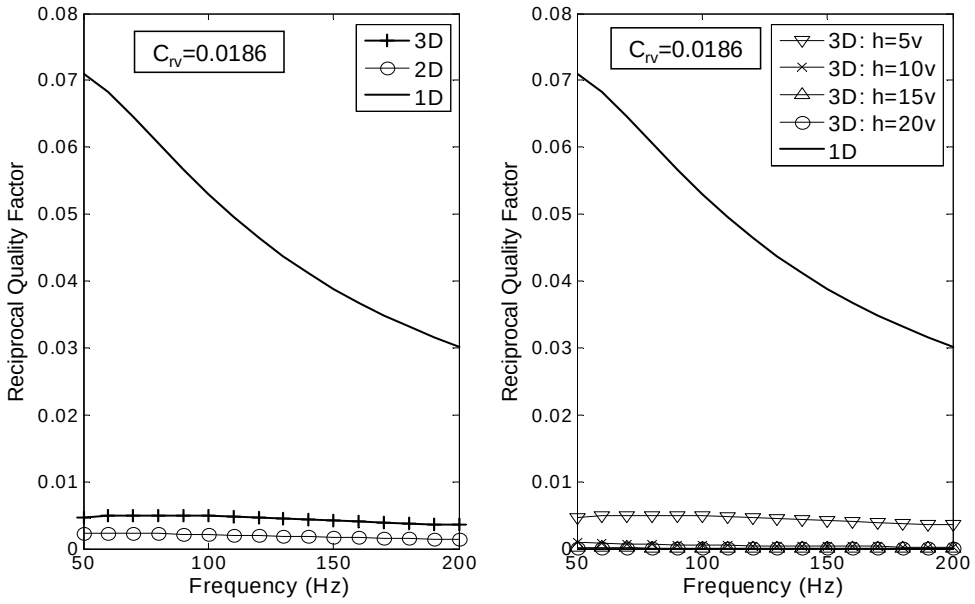


Figure 6.2 1Reciprocal quality factors versus frequency caused by 2D and 3D heterogeneities ($Q_{diff}^{-1}$) (left). Reciprocal quality factors versus frequency caused by 3D heterogeneities as a function of horizontal to vertical correlation length ratio (right). For comparison, the reciprocal quality factor due to scattering in 1D ($Q_{1D}^{-1}$) is also plotted. The results are shown for the LLNL profile with variance, $C_{\rho c}(0)$, equal to 0.0186.

Müller and Shapiro (2004) also suggested that even in the case of small $a_{\|}$, there may be an additional vertical correlation length that corresponds to larger inhomogeneities, hence the attenuation from random diffractions may be larger if the

larger $a_{\|}$ value is the correlation length contributing to attenuation. To verify that indeed the effects from random diffractions were not larger than the $Q_{diff}^{-1}$ factors predicted for $a_{\|}$ = 1 m, we also ran elastic finite-difference synthetics with 2D heterogeneity. To construct the 2D model, we used the 1D model, and applied a random component laterally, which after smoothing with a 5 m Gaussian in the horizontal direction, yielded vertical and horizontal variance approximately 0.019, and $\gamma$ equal to 0.2. We found that the vertical incidence Q estimates were similar for the 1D and 2D models. Therefore, we concluded that given the small vertical and horizontal correlation lengths, and short propagation pathlengths, lateral heterogeneity has a negligible effect in the measured attenuation at LLNL.

6.3 References

Gist, GA. “Seismic attenuation from 3-D heterogeneities: A possible resolution of the VSP attenuation paradox,” *Society of Exploration Geophysicists Annual International Meeting, Expanded Abstracts*, 1042-1045, 1994.

Müller, TM, and Shapiro, SA, “Scattering attenuation in randomly layered structures with finite lateral extent: A hybrid Q model,” Geophysics, Vol. 69, 1530-1534, 2004.

Sen, MK, Lane, FD, and Foster, DJ. “Anomalous reflection amplitudes from fractured reservoirs – Failure of AVOA?,” The Leading Edge, September Issue, 2007.

Shapiro, SA, and Kneib, G. “Seismic attenuation by scattering: Theory and numerical results,” Geophysical Journal International, Vol. 114, 373-391, 1993.

Shapiro, SA, Zien, H, and Hubral, P. “A generalized O’Doherty-Anstey formula for waves in finely layered media,”Geophysics, Vol. 59, 11, 1760-1762, 1994.

Shapiro, SA, and Hubral, P. “Elastic waves in random media,” Springer, 1999.

Rytov, SM, Kravtsov, YA, and Tatarskii, VI, “Wave propagation through random media,” Springer Verlag, 1989.

# Chapter 7
# Intrinsic Attenuation

## 7.1 Deducing Intrinsic Attenuation

From the estimates of $Q_{apparent\text{-}scattering}$, which combine the $Q_{scattering}$ and pseudo-Q effects, we approximated $Q_{intrinsic}$ using the expression:

$$\frac{1}{Q_{\text{int}rinsic}} = \frac{1}{Q_{field}} - \frac{1}{Q_{apparent-scattering}} \tag{7.1.1}$$

Should an inverse filter for the pseudo-Q effects be applied to the field data and elastic finite-difference synthetics, this would result in the familiar expression (Spencer et al., 1982):

$$\frac{1}{Q_{\text{int}rinsic}} = \frac{1}{Q_{total}} - \frac{1}{Q_{scattering}} \tag{7.1.2}$$

There is an inherent difficulty in obtaining an inverse filter for the pseudo-Q effects. Firstly, in realistic media, neither a time-domain filter nor a polarization filter can adequately remove or suppress the near-field (Chapter 5). Secondly, the local impedance correction (equation 4.2.1) requires some heuristic manipulation to establish the effective local impedance value which is a function of the center frequency of the source. Lastly, the interference effects require either comparison of synthetics 'with interference' and 'no interference' models, which in the case of a large receiver array would require numerous forward models, or an analytical treatment of interference effects by combining transmissivity and reflectivity estimates. The latter can be accomplished by approximating the recorded wavefield as the sum of two components: (a) the transmitted generalized primary in the medium overlying the receiver (medium A) plus (b) the reflected generalized primary in the medium beneath the receiver up to a maximum depth for which the two-way traveltime equals the duration of the generalized primary (medium B), which would then be convolved by (a) (Prof. Dr. Serge Shapiro, personal communication). Hence, to remove interference effects, one would have to subtract (b) from the total recorded wavefield (Figure 7.1.1).

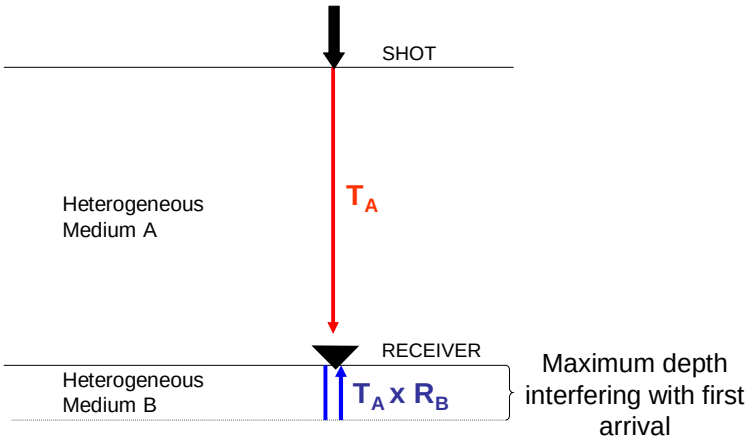


Figure 7.1 1Sketch showing the recorded wavefield contributions: wavefield transmitted through overburden (1-way) corresponding to transmissivity of medium A ($T_A$) plus wavefield transmitted through overburden and later reflected from the interfaces in medium B (2-way) corresponding to reflectivity of medium B ($R_B$) Hence to remove interference effects, one must subtract $T_A$ * $R_B$ from the recorded wavefield., where * stands for convolution in the time-domain.

In view of the challenges involved in computing an inverse filter for the pseudo-Q effects, the most practical solution was to use the 3D elastic synthetics, which contain both the scattering as well as pseudo-Q factors due to near-field, local impedance, and interference effects, and use equation (7.1.1) to estimate $Q_{intrinsic}$. Table 1 summarizes the Q estimates using the peak amplitude decay method (expression 2.2.1.2) for a center frequency of 120 Hz. For the low and high variance range of impedance profiles considered, we found interval $Q_{intrinsic}$ values between 4 and 15. We then computed visco-elastic finite-difference synthetics for the low and high variance profiles, with input $Q_{intrinsic}$ values as shown in Table 7.1.1. For the low and high variance models, we approximated the $Q_{intrinsic}$ profile with two interval values which increased with depth. We also considered a model with mixed variance, namely with $C_{\rho c}(0)=0.0186$ at depths < 25 m and $C_{\rho c}(0)=0.0031$ at depths > 25 m, which allowed for $Q_{intrinsic}$ to be continuous in the profile. Visco-elastic synthetics were generated with the E3D code (Larsen et al., 2001) which uses a standard linear solid (SLS) with a single relaxation mechanism for which the center frequency is specified (in our case $f_{center}$ = 120 Hz). A description of the SLS visco-elasticity used in E3D can be found in Robertsson et al. (1994).

Figure 7.1.2 shows the peak amplitudes of the first arrival in the field data, elastic and visco-elastic synthetics. The first observation is the non-uniqueness of the visco-elastic models that match the field peak amplitude curve. The second observation is that in the presence of intrinsic attenuation, the fluctuations in peak amplitude become less pronounced in the synthetics. Given that the field peak amplitude decay curve has a smooth appearance, this implies that an intrinsic attenuation mechanism is at work,

whereas a larger attenuation due to scattering (for a variance larger than the variance range we considered) would result in a jigsaw appearance of the curve caused by interference phenomena. This suggests the advantage of having small receiver separations in modeling scattering versus intrinsic attenuation effects.

Table 7.1 1Summary of Q estimates.

| Variance | Depth Interval | $Q_{scattering}$ | $Q_{apparent\text{-}scattering}$ | $Q_{intrinsic}$ | $Q_{field}$ |
|---|---|---|---|---|---|
| $C_{\rho c}(0)=0.0031$ | z<25 m | 100 | 11 | 4 | 3 |
| $C_{\rho c}(0)=0.0031$ | 25m<z<42m | 100 | 7 | 7 | 3.5 |
| | | | | | |
| $C_{\rho c}(0)=0.0186$ | z<25m | 20 | 6 | 6 | 3 |
| $C_{\rho c}(0)=0.0186$ | 25m<z<42m | 20 | 5 | 15 | 3.5 |
| | | | | | |
| $C_{\rho c}(0)=0.0186$ | z<25m | 20 | 6 | 6.5 | 3 |
| $C_{\rho c}(0)=0.0031$ | 25m<z<42m | 100 | 7 | 7 | 3.5 |

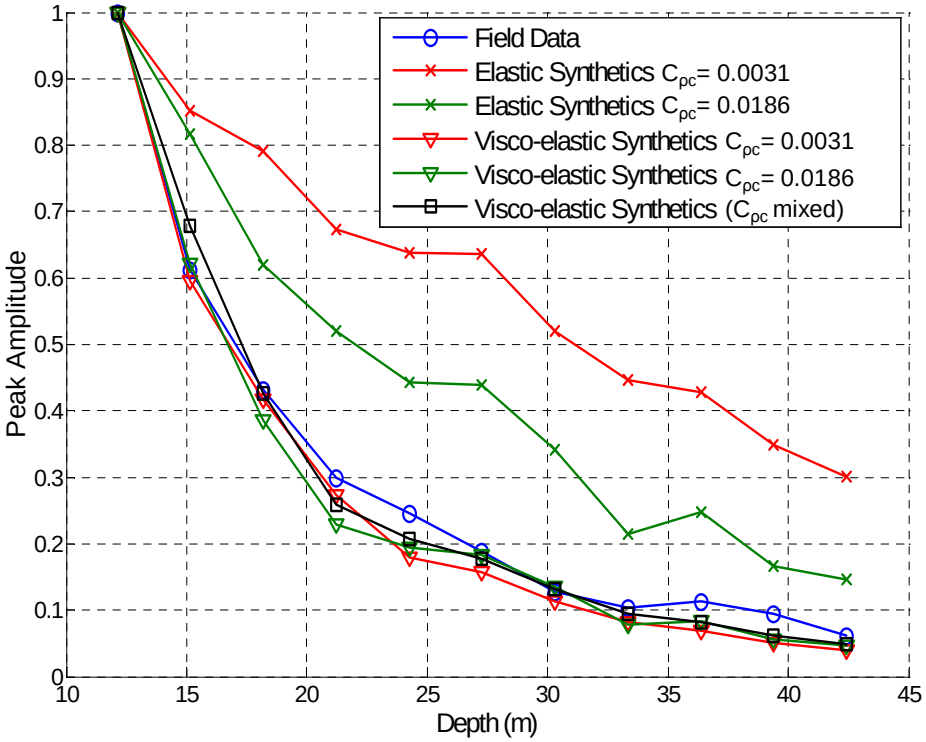


Figure 7.1 2 Peak amplitude decay of the first arrival versus depth, for the field data, elastic and visco-elastic finite-difference synthetics. Given that several visco-elastic models for can match the field curve, this suggests the non-uniqueness of our solution in terms of peak amplitude decay.

Another argument supporting the existence of intrinsic attenuation stems from the pulse broadening observed in the field data. Pulse broadening occurs because of dispersion caused both by scattering and intrinsic attenuation. Dispersion due to scattering occurs as a result of the frequency-dependent phase term in the expression for the transmissivity (equation 4.1.13). For a linear wave equation, absorption is a necessary and sufficient condition for the presence of dispersion (Futterman, 1962). The relationship between dispersion and Q is seen in expression (2.1.3.1).

To assess the pulse broadening caused by scattering and intrinsic attenuation, we compared the rise time at 12 m depth and 42 m depth in the field data, and the elastic and visco-elastic synthetics. As shown in Figure 7.1.3, for the elastic synthetics the rise times do not show a significant increase in rise time, both for the lowest and highest variance range considered. However, in the field data, the rise times increase by a factor > 1.5 over 30 m. The rise times in the visco-elastic data for the model with variance 0.0031 show a similar rise time increase as the field data. However, it is rather speculative to select a visco-elastic model on the basis of matching rise times, given that we do not know if the intrinsic attenuation mechanism should behave like the SLS model.

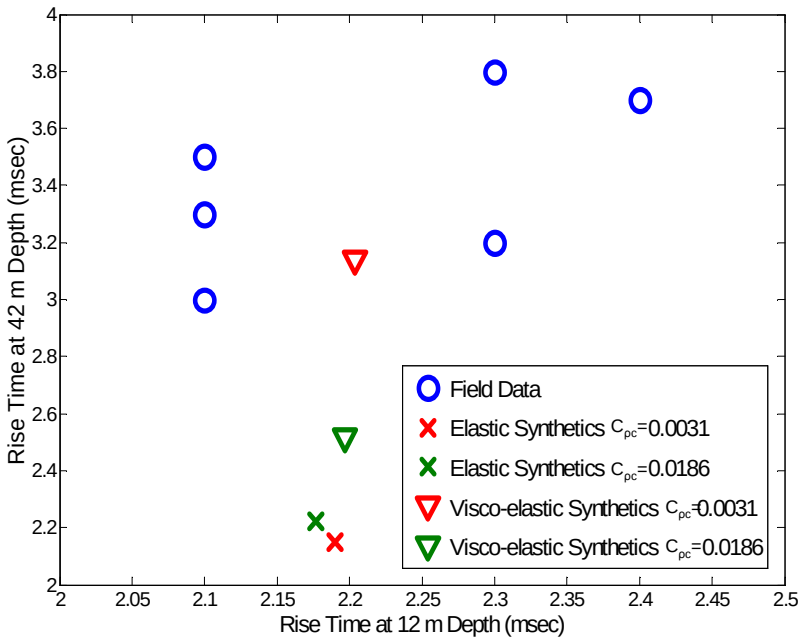


Figure 7.1 3 Comparison of rise times at 12 m depth and 42 m depth, between the field data for selected traces with high S/N ratio, the elastic synthetics and the visco-elastic synthetics. As shown, none of the elastic models considered can capture the pulse broadening evident in the field data. This implies the presence of an intrinsic attenuation mechanism which would cause additional dispersion.

## 7.2 The Effect of the Free Gas on $Q_P$

After finding low $Q_{intrinsic}$ values, the evident question was to identify its physical cause. To our knowledge, the only absorption mechanism that is non-negligible at

seismic frequencies is absorption due to the presence of free gas. White (1975), and Dutta and Seriff (1979) showed that segregated pockets of free gas cause high pressure gradients which cause fluid flow in response to the propagation of a compressional wave. This loss of energy at these local spots is averaged over the total volume and results in large attenuation of the compressional wave. On the other hand, this mechanism does not affect the energy of shear waves.

For a water-table at 48 m, we developed capillary pressure curves, and estimated that water saturation in the vadose zone at LLNL varies from 25-35% in the units predominantly containing sand, and 65-80% in the units predominantly containing clay. These saturation estimates are sensitive to water-table fluctuations in response to seasonal changes and the operation of pump-and-treat wells in the vicinity of the well. Modeling of the intrinsic attenuation due to the presence of free gas in the vadose zone is outside the scope of this dissertation. However, we consider it very worthwhile should future research, via analytical modeling and laboratory results, study the $Q_{intrinsic}$ behavior as a function of frequency in relation to saturation, porosity, pore size distribution and gas compressibility among many factors. Moreover, if the absorption mechanism is similar in the vadose zone as it is in reservoir environments, there may be an additional benefit to studying attenuation in the vadose zone which could be applicable to oil and gas exploration. Lastly, to verify the cause of absorption we suggest that $Q_S$ values are compared to $Q_P$ values in the vadose zone, given that the former is unaffected by the presence of free gas.

## 7.3 References

Dutta, NC, and Seriff, AJ. “On White’s model of attenuation in rocks with partial gas saturation,” *Geophysics*, Vol. 44, 1806-1812, 1979.

Larsen, S, Wiley, R, Roberts, P, and House, L. “Next-generation numerical modeling: incorporating elasticity, anisotropy and attenuation,” Society of Exploration Geophysicists Annual International Meeting, Expanded Abstracts, 1218-1221, 2001.

Futterman, WI. “Dispersive Body Waves,” Journal of Geophysical Research, Vol. 67, 13, 5279-5291, 1962.

Robertsson, JOA, Blanch, JO, and Symes, WW. “Viscoelastic finite-difference modeling,” Geophysics, Vol. 59, 9, 1444-1456, 1994.

Spencer, TW, Sonnad, JR, and Butler, TM. “Seismic Q-Stratigraphy or dissipation,” Geophysics, Vol. 47, 16-24, 1982.

White JE. “Computed seismic speeds and attenuation in rocks with partial gas saturation,” Geophysics., Vol. 40, 224-232, 1975.

# Chapter 8
# Conclusions and Future Work

## 8.1 Overview

A review of the experimental studies of near-surface Q reveals that the Q factor for P-waves ($Q_P$) is very low in the upper couple of hundred meters. As a result, shallow seismic studies offer suffer from low S/N due to energy loss, and signal distortion, which are both manifestations of the Q filtering effect. Whether the motivation is to restore the signal properties by designing an inverse Q filter which will compensate the Q effects, or to use Q as a geophysical parameter to enrich our knowledge of the subsurface properties, the key question is to measure Q accurately and to quantify the physical mechanisms that give rise to it. The interest in near-surface Q has primarily applications in both near-surface site characterization for earthquake engineering design, as well as for groundwater exploration. On the other hand, given that exploration of oil and gas deposits relies on near-surface seismic experiments, the near-surface attenuation phenomena are coupled to the imaging results and also affect the AVO inversion and simultaneous inversion of velocity and attenuation data targeted to the analysis of the deeper strata. Hence the near-surface Q problem is of great concern to the oil and gas industry.

To study attenuation, research efforts have been carried out in both field and laboratory environments. Given the fact that field and laboratory Q measurements are different in firstly scale, secondly experimental frequency band, and thirdly strain level, it is essential to establish Q as a function of frequency and strain level and to quantify the physical mechanisms that give rise to Q. Therefore, Q prediction requires separate modeling of the elastic and inelastic components of Q, which are $Q_{scattering}$ and $Q_{intrinsic}$. This dissertation study, which is based on a shallow VSP experiment at LLNL, offers two important contributions to the near-surface Q problem. Firstly, it provides estimates on the scattering component of attenuation based on a deterministic and probabilistic analysis of the elastic properties, and through comparison of these estimates with the field data, gives a range of expected intrinsic attenuation values. This analysis involves both field measurement, analytical and finite difference modeling. Aside from offering results for the particular case study, this methodology of Q separation can be applied to similar sites for $Q_P$ as well as $Q_S$ measurement. Secondly, given the short propagation pathlenghts, and small receiver spacing, which are inherent in a shallow VSP configuration, this dissertation quantifies the effects of the near-field, local impedance and interference phenomena, which bias Q measurement and are thus treated as pseudo-Q effects. Moreover, given the lack of previous documented research in near-field effects on shallow seismic studies, a significant portion of this dissertation deals with i) the effects of the near-field on parameter estimation in the near-surface, such as attenuation, migration and rotation of 3-component sensors, ii) the challenges in near-field removal and consequent requirements of near-field modeling to account for the near-field effects.

## 8.2 Conclusions for Attenuation

This dissertation study summarizes the attenuation results from a shallow VSP experiment conducted at the LLNL facility using permanent downhole receivers and a vertical impact source. Our efforts concentrated on separating scattering versus intrinsic mechanisms for the transmitted P-wave at vertical incidence, which is theoretically free of converted waves. The maximum receiver depth was 42 m, whereas the depth to the water table was approximately 48 m. Therefore, the medium sampled from the downgoing wave lied entirely within the vadose zone.

We expected high scattering attenuation losses due to the complex stratigraphy of the profile, characteristic of fluvial sedimentary deposits with pronounced 1D and 3D heterogeneity, and high intrinsic attenuation losses as a result of the interaction of the free gas with the compressional wave. Indeed, the measured effective $Q_P$ values (after correction for spherical divergence) were in the order of 3. The approach to separate the relative contributions from the two mechanisms was to consider the maximum and minimum scattering attenuation expected in this type of geologic environment and to deduce the minimum and maximum intrinsic attenuation values, respectively.

We considered 1D scattering for profiles with variance range $C_{\rho c}(0)$, 0.0031 to 0.0186. We verified that, in the absence of the near-field, local impedance and interference effects, the analytical results based on the Shapiro et al. (1994) theory agree with the attenuation measured in elastic synthetics. We showed that for the LLNL experimental geometry, where both the propagation pathlenghts and the receiver spacing are short, the effects of local impedance, interference and the presence of the near-field bias the attenuation measurements. Given that these factors are not related to the transmissivity of the medium between the receivers, they were treated as pseudo-Q factors. In the absence of an efficient pseudo-Q filter, a practical solution to compensate for these effects is to incorporate them in the scattering attenuation estimates and to deduce $Q_{intrinsic}$ values by comparing $Q_{field}$ to $Q_{apparent\text{-}scattering}$ from elastic finite-difference synthetics. With respect to the methods of Q measurement in the case of small receiver separation, we concluded that the amplitude decay method yields more stable Q results than frequency-domain methods such as spectral-ratio.

To conclude the modeling of scattering, we also considered 3D heterogeneity effects, which we found to be non-significant, both from our analytical and finite-difference results. This result was expected given that the vertical and horizontal correlation lengths, and the propagation pathlength were very short.

The results for $Q_{apparent\text{-}scattering}$ were in the order of 5 to 11, whereas the deduced $Q_{intrinsic}$ values were in the order of 5 to 15. From visco-elastic modeling using a single SLS mechanism, we matched the peak amplitude decay curve of the field data with both high-scattering low-intrinsic and low-scattering high-intrinsic attenuation models. Hence, from the perspective of peak amplitude decay, our solution is not unique. However, even this range of scattering and intrinsic attenuation estimates is sufficient to show that both scattering and intrinsic attenuation are equally important in the vadose zone. Moreover, from consideration of the rise times, which we used exclusively to quantify the effect of dispersion from the scattering and intrinsic attenuation mechanisms, we found that intrinsic attenuation is required to account for the pulse broadening observed in the field data.

Given that typical attenuation mechanisms of absorption, such as viscous flow,

matrix anelasticity and intergranular friction, do not cause significant absorption attenuation at seismic frequencies, we attributed the absorption present in the vadose zone to the interaction of the free gas with the compressional wave, which creates fluid flow resulting in energy loss. The effect of free gas was studied by White (1975) and Dutta and Seriff (1979) to describe the reservoir environment during production of a field, where gas may come out of solution and create distributed pockets of gas. It is also encouraging that for his numerical example for saturation equal to 80% and for arbitrary choice of geometry and medium properties, White (1975) obtains $Q_{intrinsic}$ values in the order of 10, which is in the same magnitude as the deduced $Q_{intrinsic}$ values found in this experiment. However, to apply his theory directly to the vadose zone conditions, it is necessary to assess the pore size distribution, gas compressibility, normal stress and fluid conditions, among many factors, to obtain the absorption filter characteristics in the vadoze zone.

## 8.3 Conclusions for the Near-Field Effects in Shallow Seismic Studies

Motivated by the fact that most seismic studies in the near-surface involve travel paths comparable to a seismic wavelength, we demonstrate that the presence of the near-field in shallow seismic studies is non-negligible. This is important as most investigators have extrapolated seismic reflection processing for deeper targets to the near surface, without, though, incorporating the near-field in their processing approaches.

It was shown that time-domain filtering and polarization filtering methods fail to remove the near-field in realistic media. Hence, we conclude that parameter estimation in shallow seismic studies has to account for the presence of the near-field. To this regard, it was shown that modeling of the near-field should be in 3D, and that, in addition, to include the effects of intrinsic attenuation, the modeling should be viscoelastic.

In terms of attenuation measurements in the near-surface, it was shown that, if not accounted for, the near-field underestimates the Q measurements and distorts the Q behavior as a function of frequency. Moreover, Q estimation with VSP geometry is more affected by the near-field, than it is in reflection studies, as it involves 1-way propagation. The current results from the VSO experiment at LLNL demonstrate the near-field bias in attenuation, where the near-field causes an apparent attenuation of an order comparable to the combined effects of scattering and intrinsic Q.

In addition, it was shown that the presence of the near-field measured in 3-component data produces an error in the rotation angles, which may be minimized through differentiation and low-cut filtering of the seismic data prior to rotation.

Finally, migration results presented for a shallow scatterer using Kirchhoff migration and show that the presence of the near-field causes a delay in the migrated sections. In light of this result, we suggest further study of migration in the near-surface with viscoelastic Reverse-Time migration methods.

## 8.4 Limitations and Future Work

The main limitation regarding the current analysis of near-surface Q, involves the modeling of the elastic profiles, which is linked to the $Q_{scattering}$ estimates. As discussed previously, the density and velocity series were unknown. Hence the modeling consisted of a deterministic low frequency component (interval values) computed from the density log and first-break times (for the velocity profile) and a high-frequency random

component. To establish more exact constraints in the elastic properties, which translates to a narrower range of $Q_{scattering}$ values, it is advisable to repeat a similar type of study in a borehole with better known properties, as would be the case, for example, of a borehole with an available sonic log, and neutron density log. In addition, it would be beneficial for near-surface Q studies to incorporate statistical information concerning the near-surface, which is sparse compared to studies of the statistical properties of deeper deposits. Such studies of the statistical properties would provide valuable information for both 1D and 3D structure, including critical constraints for the vertical and horizontal correlation lengths, and variance ranges typical of the near-surface. In the absence of both high-frequency log measurements and statistical analyses for near-surface materials, this study provided a 'reasonable' range of expected scattering attenuation estimates, which resulted in a range for the estimates of intrinsic attenuation.

The intrinsic component of attenuation was attributed to the presence of free gas interacting with the compressional wave. White (1975) and Dutta and Seriff (1979) provide a framework to model the attenuation due to the presence of a free gas, which includes several assumptions pertaining to the geometry of the pore space, the saturation, gas compressibility and stress conditions, among many factors. Should future studies apply this theory to the vadose zone conditions, it may be possible to obtain the absorption filter characteristics in the vadose zone, including the frequency-dependence of the attenuation and phase. Having the characteristics of the absorption filter, it may be possible to match the field data with a unique model, instead of estimating a range of scattering and intrinsic Q values. This analysis in turn, will also determine what visco-elastic mechanism is most appropriate to be implemented in visco-elastic finite difference modeling.

Moreover, it is expected that, should the presence of free gas be indeed responsible for absorption in the vadose zone, equivalent studies of $Q_S$ will show no evidence of an absorption mechanism. This hypothesis awaits validation. In addition, given that the scattering mechanisms are common between P- and S-waves and that the intrinsic mechanisms are most probably different for the two types of body waves, it may be possible to use correlation between $Q_P$ and $Q_S$ estimates to solve the separation of scattering and intrinsic attenuation as an over-determined problem.

Last, but not least, the current analysis of $Q_P$ was carried out for a particular geometry and source characteristics, i.e., for a source monopole in the z-direction, using vertical incidence, etc. It would be worthwhile for future studies to test Q results:

a) as a function of frequency. This could be accomplished for example by using strike plates of different diameter which would change the frequency content of the source.
b) as a function of strain level. To this end, the Q results can be compared from a hammer source vs. a larger weight drop source or even to strong-motion recordings where those are available.
c) in relation to the source directivity. Direct comparison between a source monopole in the z-direction and pressure source would show the near-field effect.
d) in relation to the location of the source, whether it is above or below the receiver array. This would result in a direct comparison of the interference effects, as those are different depending on the direction of propagation. Moreover, as pointed out by Spencer (1982), if a large reflector is present beneath the array, the

reflected wave can also be analyzed for Q estimation and interference effects may in fact be suppressed.

e) as a function of angle of incidence. This is indeed a challenging problem, given that the incident wave is converted to P- and S- transmitted waves at each interface, hence the $Q_{effective}$ value measured contains the characteristics of both $Q_P$ and $Q_S$. To this end, a comparison between acoustic, elastic and visco-elastic models to field measurements at non-vertical incidence would be a good starting point.

## 8.5 References

Dutta, NC, and Seriff, AJ. “On White’s model of attenuation in rocks with partial gas saturation,” *Geophysics*, Vol. 44, 1806-1812, 1979.

White JE. “Computed seismic speeds and attenuation in rocks with partial gas saturation,” Geophysics., Vol. 40, 224-232, 1975.